IVW - Schriftenreihe Band 102
Institut für Verbundwerkstoffe GmbH - Kaiserslautern

Angelos Miaris

Experimental and Simulative Analysis of the Impregnation Mechanics of Endless Fiber Rovings

Bibliografische Information Der Deutschen Bibliothek

Die Deutsche Bibliothek verzeichnet diese Publikation in der Deutschen Nationalbibliografie; detaillierte bibliografische Daten sind im Internet über <http://dnb.ddb.de> abrufbar.

Bibliographic information published by Die Deutsche Bibliothek

Die Deutsche Bibliothek lists this publication in the Deutsche Nationalbibliografie; detailed bibliographic data is available in the Internet at <http://dnb.ddb.de>.

Herausgeber: Institut für Verbundwerkstoffe GmbH
Prof. Dr.-Ing. Ulf Breuer
Erwin-Schrödinger-Straße
TU Kaiserslautern, Gebäude 58
67663 Kaiserslautern
http://www.ivw.uni-kl.de

Verlag: Institut für Verbundwerkstoffe GmbH

Druck: Technische Universität Kaiserslautern
ZBT – Abteilung Foto-Repro-Druck

D 386

Als Manuskript gedruckt. Printed in Germany.
ISSN 1615-021X
ISBN 978-3-934930-98-8

Experimental and Simulative Analysis of the Impregnation Mechanics of Endless Fiber Rovings

Dem Fachbereich für Maschinenbau und Verfahrenstechnik

der Technischen Universität Kaiserslautern

zur Verleihung des akademischen Grades

Doktor-Ingenieur (Dr.-Ing.)

genehmigte Dissertation

von

Angelos Miaris

aus Athen, Griechenland

Tag der mündlicher Prüfung:	01.06.2012
Prüfungsvorsitzener:	Prof. Dr.-Ing. Ulf Breuer
1. Berichterstatter:	Prof. Dr.-Ing. Peter Mitschang
2. Berichterstatter:	Univ.-Prof. Dr.-Ing. Ralf Schledjewski

D386

Preface

The following thesis contains the results of my work as research assistant at the Institut für Verbundwerkstoffe GmbH in the department of manufacturing science between 2007 and 2012.

I would like to specially thank my supervisor Prof. Dr.-Ing. Peter Mitschang for his trust, guidance and support over the last five years. Furthermore I would like to acknowledge Univ.-Prof. Dr.-Ing. Ralf Schledjewski for all the scientific discussions which allowed me to successfully cruise through the demands of this topic. I am also grateful to Prof. Dr.-Ing. Ulf Breuer for overtaking the chairmanship of the examination board.

My special thanks to all my colleagues at the IVW and particulary to those at the filament winding and tape placement group. Working with them had always been a pleasure and a great learning experience. I would like to affirm my gratitude to Michael Päßler and Torsten Weick for their valuable support and their fruitful ideas. Special thanks go to René Holschuh, Petros Karapappas, and Panagiota Tsotra for proofreading this thesis. I would also like to thank my former colleagues Jens Lichtner, and Muhammad Amir Khan for their advice during the development of the presented work. I am grateful to all my diploma thesis students and interns for their admirable performance and numerous working hours for the generation of the following results.

The European Community is acknowledged for the financial support under the framework of the project H2SusBuild (Grant Agreement No. NMP2-LA-2008-214395).

My parents are thanked for giving me the possibility to study and bringing me up to what I am today. Finally there are no words to thank my beloved Panagiota for her great encouragement, patience and support.

Kaiserslautern, June 2012

Μη είναι βασιλικήν ατραπόν επί γεωμετρίαν.
Ευκλείδης,4-3ος αιων π.Χ.,Αλεξανδρινός μαθηματικός.

There is no royal road to geometry. *Euclid of Alexandria 4-3 centutry BC.*

To my family and all my friends

.

Contents

Abbreviations

Short form	***Description***
FKV	*Faser-Kunststoff-Verbund*
PTFE	*Polytetrafluorethylen*
IVW	*Institut für Verbundwerkstoffe*
FRP	*Fiber Reinforced Polymer*
CF	*Carbon Fiber*
GF	*Glass Fiber*
UD	*Unidirectional*
Prepreg	*Pre impregnated*
CNC	*Computerized Numerical Control*
VOC	*Volatile Organic Compounds*
ODC	*Ozone Depleting Compounds*
EP	*Epoxy*
UP	*Polyester*
VE	*Vinyl ester*
PU	*Polyurethane*
PTFE	*Polytetrafluoroethylene*
2K	*2 components*
PAN	Polyacrylonitrile
SEM	Scanning Electron Microscope
RWF	*Resin Weight Fraction*
LCM	*Liquid Composite Molding*
RTM	*Resin Transfer Molding*

Symbols

Symbol	Unit	Description
η	*[Pa sec]*	*Viscosity*
τ	*[Pa]*	*Shear stress*
$\dot{\gamma}$	*[1/sec]*	*Velocity gradient, shear rate*
F_1	*[N]*	*Axial tension and*
σ_b	*[Pa]*	*Bulk compressive stress*
V_f	*[1]*	*Fiber volume fraction*
V_a	*[1]*	*Maximum compaction*
V_o	*[1]*	*Initial compaction ratio*
E	*[Pa]*	*Young modulus of the reinforcement.*
β	*[-]*	*Waviness parameter*
v	*[m/sec]*	*Superficial fluid velocity*
P	*[Pa]*	*Pressure*
K	*[m^2]*	*Permeability*
k	*[1]*	Kozeny constant
R_f	*[m]*	*Monofilament radius*
k_G	*[1]*	*Gebart permeability constant*
k_{zz}	*[1]*	*Gutowski permeability constant*
W	*[m]*	*Roving width*
R	*[m]*	*Impregnation unit curve radius*
T	*[N]*	*Roving tension force*
N	*[N]*	*Reaction force*
θ	*[rad]*	*Deflection angle*
γ_s	*[N/m]*	*Surface tension between fiber*
θ_{ca}	*[°]*	*Contact angle*
R_c	*[m]*	*Capillary radius*
μ	*[1]*	*Friction coefficient*
T_f	*[N]*	*Roving tension force due to friction*
T_s	*[N]*	*Roving tension force due to shear*
U	*[m/sec]*	*Roving speed*
δ	*[m]*	*Resin film thickness*
f	*[1]*	*Friction factor*
$F_{\deg r}$	*[1]*	*Roving filling degree*

Re	*[1]*	*Reynolds number*
τ	*[1]*	*Flow tortuosity*
ρ	*[Kg/m^3]*	*Fluid density*
g	*[m/sec^2]*	*Gravity acceleration*
z	*[m]*	*Flow front position in Capillary experiment*
x	*[m]*	*Flow front position during impregnation*
F_N	*[N]*	*Viscous drag in Capillary experiment*
λ	*[m]*	*Arc length*
P_c	*[Pa]*	*Capillary pressure*
ε	*[1]*	*Capillary radius constant*
a	*[1]*	*Tortuosity constant*
B	*[1]*	*Tortuosity constant*
C_f	*[1]*	*Friction constant*

Kurzfassung

Unidirektionale (UD) faserverstärkte Kunststoffe eignen sich hervorragend für die Herstellung von extrem leichten und sehr steifen Strukturen. Die Faserverbundwerkstoffe finden ihren hauptsächlichen Einsatz in der Luft- und Raumfahrt, in der Automobil- sowie auch in der Maschinenbauindustrie. Hochbelastete Bauteile wie beispielsweise Antriebswellen, Druckbehälter für die Speicherung von Wasserstoff oder Raketenmotorgehäuse werden heutzutage aus unidirektionalen Faser-kunststoffverbunden (FKV) gefertigt. Die Wickeltechnik, die Pultrusion und das automatisierte Ablegen sind die geeigneten Prozesse für die Fertigung von Bauteilen aus unidirektionalen faserverstärkten Halbzeugen. In den letzten Jahrzehnten steigt die Nachfrage für Bauteile aus UD Verbundwerkstoffen kontinuierlich an; dadurch bedingt nimmt die Forderung nach höheren Produktionsraten und niedrigeren Herstellungskosten kontinuierlich an Bedeutung zu.

Die Imprägnierung der trockenen Verstärkungsfasern mit dem flüssigen Matrixwerkstoff ist eine der wichtigsten Prozessschritte bei der Herstellung von Halbzeugen und Bauteilen aus Faserverbundwerkstoffen. Ein ideales Halbzeug zeichnet sich dadurch aus, dass die Rovings vollständig mit Harz getränkt sind, es einen möglichst geringen Porengehalt aufweist und einen definierten Faservolumenanteil besitzt. Die Imprägniergüte im Halbzeug ist von großer Bedeutung für die Qualität des Bauteils. Wenn diese Imprägnierung mit entsprechend hoher Geschwindigkeit erfolgt, kann dies einen gravierenden Einfluss auf die Wirtschaftlichkeit des gesamten Prozesses haben.

Im Rahmen dieser Arbeit wurde ein Konzept für eine Imprägniereinheit mit einer sinusförmigen, geschlossenen Kavität für den Einsatz im duromeren Nasswickelverfahren entwickelt (Siphon-Imprägniereinheit), die dadurch gekennzeichnet ist, dass Fasern und Harz kontinuierlich in Abhängigkeit einer definierten Prozessgeschwindigkeit diesem Imprägniermodul zugeführt werden. Im Gegensatz zu herkömmlichen Harzbädern ist die entwickelte Imprägniereinheit ein geschlossenes System ohne bewegliche Teile. Innerhalb der Imprägnierungskavität existieren keine Stellen, an denen sich das Harz im Prozess ansammeln kann und dort über die Zeit ungewollt reagiert. Dadurch können konstante Prozessbedingungen unabhängig von der Materialtopfzeit gewährleistet werden. Darüber hinaus ist der Aufwand für die Vorberei-

tung und die Reinigung durch den Einsatz von Einwegartikeln (Polytetrafluorethylen (PTFE)-Schläuche) minimiert. Die entwickelte Imprägniereinheit besteht aus der Imprägnierungskavität und dem Harzeinspritzblock. Die spezielle Ausformung des Harzeinspritzblockes ermöglicht die Ausbildung der Harzschicht zwischen Fasern und Kavität. Der Hauptteil der Einheit besteht aus der sinusförmigen Imprägnierkavität, in die die PTFE-Schläuche eingesetzt werden.

Das Prinzip des Imprägniervorgangs innerhalb der Einheit kann auf drei unterschiedliche Zonen physikalisch-mathematisch diskretisiert werden:

1. Eintrittszone: Rovings und Harz werden kontinuierlich der Einheit zugefördert. Es bildet sich eine Harzschicht zwischen der Kavitätswand und dem Roving aus. Die Dicke der Harzschicht ist abhängig von allem von der Harzdosierung.

2. Imprägnierungszone: Der Roving wird entlang der gekrümmten Kavität gezogen und es bilden sich Scherkräfte zwischen dem Roving und der Harzschicht aus. Ein Anstieg der Zugkräfte bewirkt einen Druckanstieg an den Krümmungen. Dieser Überdruck impliziert einen Harzfluss quer durch das poröse Faserbündel. Dies führt zu einer Durchtränkung des Rovings.

3. Kontaktzone: Abhängig von der Prozessgeschwindigkeit ergeben sich entlang den Krümmungen unterschiedliche Harzschichtdicken, welche in Prozessrichtung abnehmen und ein Minimum erreichen. Kommen die Filamente in Kontakt mit der Kavitätswand, führt dies zu einem weiteren Anstieg der Druckkräfte durch auftretende Kontaktreibung. Hierbei wird eingeschlossene Luft aus dem imprägnierten Faserbündel herauspresst.

Für die Betrachtung der Imprägniermechanismen in der sinusförmigen Kavität wurde ein mathematisches Modell aufgestellt. Dieses Modell implementiert alle wesentlichen physikalischen Phänomene, die während des Prozesses auftreten. Grundlegende Untersuchungen wurden durchgeführt, um ein tieferes Verständnis der Parameter Faserkompaktierung, Kapillarwirkung und Fadenspannungssteigerung zu gewinnen. Die Lösung des Imprägnierungsmodels erfolgte mit Hilfe der Programmiersprache MATLAB. Vier unterschiedliche Imprägnierungskavitäten wurden in einem breiten Prozessfenster simuliert. Versuche auf einem Imprägnierungsprüfstand zeigten, dass das Simulationsprogramm den Imprägnierungsverlauf präzise nachbilden

kann. Basierend auf den Ergebnissen der Modellierung wurde eine neue und optimierte Imprägniereinheit konstruiert und gefertigt. Die Ergebnisse der Funktionstests mit dieser Einheit zeigten, dass hiermit eine sehr gute Tränkung von 24k Kohlenstofffaser-Rovings mit einem Epoxidharz unter industriellen Prozessbedienungen erreicht wird.

Die Einheit wurde mit einer 2 Komponenten (2K) -Harzdosieranlage gekoppelt, die in Abhängigkeit der Prozessgeschwindigkeit kontinuierlich Harz und Härter mischt und zudosiert. Zudem bietet ein solches System die Möglichkeit aktiv und präzise den Faser-Harz-Anteil zu beeinflussen. Dadurch können auch Harzsysteme mit einer sehr kurzen Topfzeit verarbeitet werden. Das entwickelte Imprägnierungssystem wurde auf dem vom Institut für Verbundwerkstoffe (IVW) entwickeltem Ringwickelkopf eingesetzt. Hiermit wurden Typ III Druckbehälter hergestellt. Die Ergebnisse der Behälterprüfung haben gezeigt, dass die gesetzlichen Anforderungen bezüglich Berstdruck erreicht wurden. Dabei konnte eine sehr gute Impägniergüte nachgewiesen werden.

Durch den Einsatz des entwickelten Imprägnierungssystems ist sowohl ein effizienter Einsatz des Matrixwerkstoffs, eine Minimierung der Nutzung von Lösungsmitteln als auch eine Reduzierung des Arbeitaufwands für Vorbereitung und Reinigung im Vergleich zu einem traditionellen Harzbad festzustellen. Um die Auswirkung der Nutzung der Imprägniereinheit auf die Herstellungskosten eines konkreten Bauteils zu zeigen, wurde eine techno-ökonomische Analyse durchgeführt. Die Studie hat gezeigt, dass durch die Verwendung des entwickelten Systems die Herstellungskosten für Wickelbauteile reduziert werden können und gleichzeitig die Produktivität gesteigert wird.

Der entwickelte Imprägnierprozess ist geeignet für kontinuierliche Verarbeitungsprozesse, wie beispielsweise die Wickeltechnik, die Pultrusion oder die Herstellung von Prepregs. Die Umsetzung eines Simulationstools für den Imprägnierverlauf ermöglicht die Auslegung von Imprägniereinheiten basierend auf den jeweiligen Prozessanforderungen. Damit ist es möglich für gegebene Materialparameter, wie Garnfeinheit und Harzviskosität, die optimale Geometrie der Imprägniereinheit festzulegen und wichtige Prozessparameter, beispielsweise die maximale Prozessgeschwindigkeit, vorherzubestimmen.

Abstract

Unidirectional (UD) composites are the most competitive materials for the production of high-end structures. Their field of application spreads from the aerospace up to automotive and general industry sector. Typical examples of components made of unidirectional reinforced composite materials are rocket motor cases, drive shafts or pressure vessels for hydrogen storage. The filament winding technology, the pultrusion process and the tape placement are processes suitable for the manufacturing using UD semi-finished products. The demand for parts made of UD composites is constantly increasing over the last years. A key feature for the success of this technology is the improvement of the manufacturing procedure.

Impregnation is one of the most important steps in the manufacturing process. During this step the dry continuous fibers are combined with the liquid matrix in order to create a fully impregnated semi-finished product. The properties of the impregnated roving have a major effect on the laminate quality, and the efficient processing of the liquid matrix has a big influence on the manufacturing costs.

The present work is related to the development of a new method for the impregnation of carbon fiber rovings with thermoset resin. The developed impregnation unit consists of a sinusoidal cavity without any moving parts. The unit in combination with an automated resin mixing-dosing system allows complete wet-out of the fibers, precise calibration of the resin fraction, and stable processing conditions.

The thesis focuses on the modeling of the impregnation process. Mathematical expressions for the fiber compaction, the gradual increase of the roving tension, the static pressure, the capillarity inside the filaments of the roving, and the fiber permeation are presented, discussed, and experimentally verified. These expressions were implemented in a modeling algorithm. The model takes into account all the relevant material and process parameters. An experimental set-up based on the filament winding process was used for the validation of the model. Trials under different conditions have been performed. The results proved that the model can accurately simulate the impregnation process. The good impregnation degree of the wound samples confirmed the efficiency of the developed impregnation unit. A techno economical analysis has proved that the developed system will result to the reduction of the manufacturing costs and to the increase of the productivity.

1. Introduction

The increasing demand for stronger and lighter structures has provoked the development of novel lightweight materials. The major characteristic of these materials is the high strength to density ratio. The use of such materials results to significant savings of valuable natural and human resources. These new materials are used in a broad range of applications in the aerospace, automotive, marine, sport, and civil industry. [1]

Beside metallic materials like aluminium or titanium, some of the most promising lightweight materials are the Fiber Reinforced Polymers (FRPs) so called Composites. The development of composite materials is based on the physical intermixture, at a macroscopic level, of at least two distinct materials and the production of a new material with advanced final properties. Although the working principle of a composite material is known since the early historic ages, the idea of combining technical fibers (e.g. carbon-, glass-, aramid fibers) with a polymeric matrix was initially developed in the late 50's.

The modern polymer composite materials are made of different types of reinforcing semi finished products. These can be categorized according to the length of the reinforcing phase. In this way the composite materials are divided to the nano-reinforced, short fiber reinforced, long fiber reinforced and endless fiber reinforced composite materials. The "endless" fiber reinforced composites are the ones with the highest strength and stiffness and are made of either single rovings or textile semi finished products.

The rovings, commonly referred as tows, are bundles of continuous, untwisted aligned fibers. Carbon fiber (CF) rovings can include from 1,000 up to 50,000 individual filaments. The FRPs made of endless unidirectional fiber rovings are considered to be the most technically advanced composites. Because of the very high strength and stiffness of their reinforcement, components build from these materials are used as load carrying structures and therefore have high quality requirements. Typical examples of these parts are pressure vessels, rocket motor cases, shafts, cantilever beams and tension rods made from composite materials.

Filament winding, tape placement and pultrusion are processes suitable to produce parts directly from endless rovings. The production of glass reinforced composites with these processes exceeded the 120 kt in Europe in 2010 and the total turnover of carbon reinforced parts has reached the 4.5 bn €. Generally speaking these three processes represent more than 30% of the total world production of long fiber composites [2].

Impregnation is the common processing step in the production of composite materials by endless rovings e.g. in filament winding, pultrusion, tow prepreging. In this processing step, the dry fibers are combined with the liquid resin in order to produce a fully wetted semi finished product. [3]. Fiber impregnation is considered as a unique operation as it does combine the fundamentals of fluid flow (matrix) and fiber elasticity.

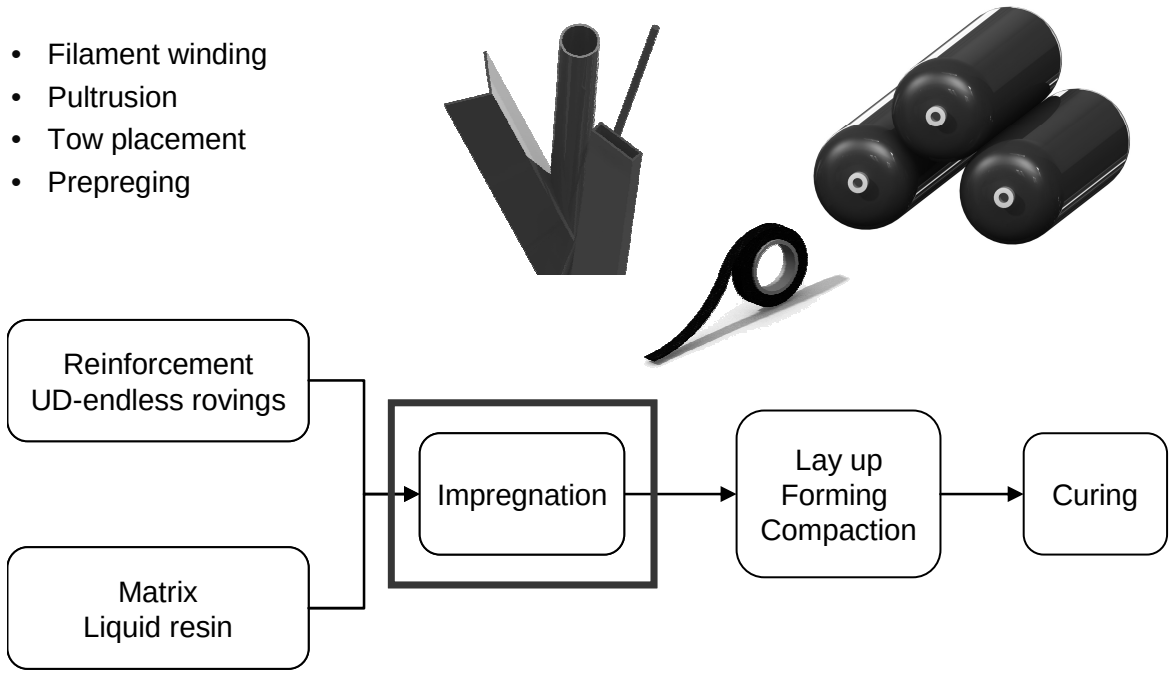

Figure 1.1: Continuous composite manufacturing processes, characteristic parts and process flow chart.

The impregnation can strongly influence the efficiency of a process. Properties like resin and fiber content, or quality criteria like void fraction are controlled by the impregnation process and have a strong impact on the mechanical properties of the final product. On the other hand impregnation also affects the processing costs. Ma-

jor cost factors such as process speed and temperature, material characteristics like resin viscosity and roving tex and even production method (e.g. continuous or batch wise production) are chosen according to the impregnation process.

1.1. Motivation

The introduction of endless reinforced composites in new applications has increased the demand for higher production rates, lower costs and better quality assurance. Since impregnation is a key-factor in the production of endless unidirectional FRPs the development of advanced impregnation techniques has become essential. The existing impregnation techniques are associated with unstable processing conditions, variation in the part quality, extensive material waste and high labor demands. These problems derive mainly from the equipment which is used for the realization of the fiber impregnation. A deeper analysis of this equipment follows in chapter 2.

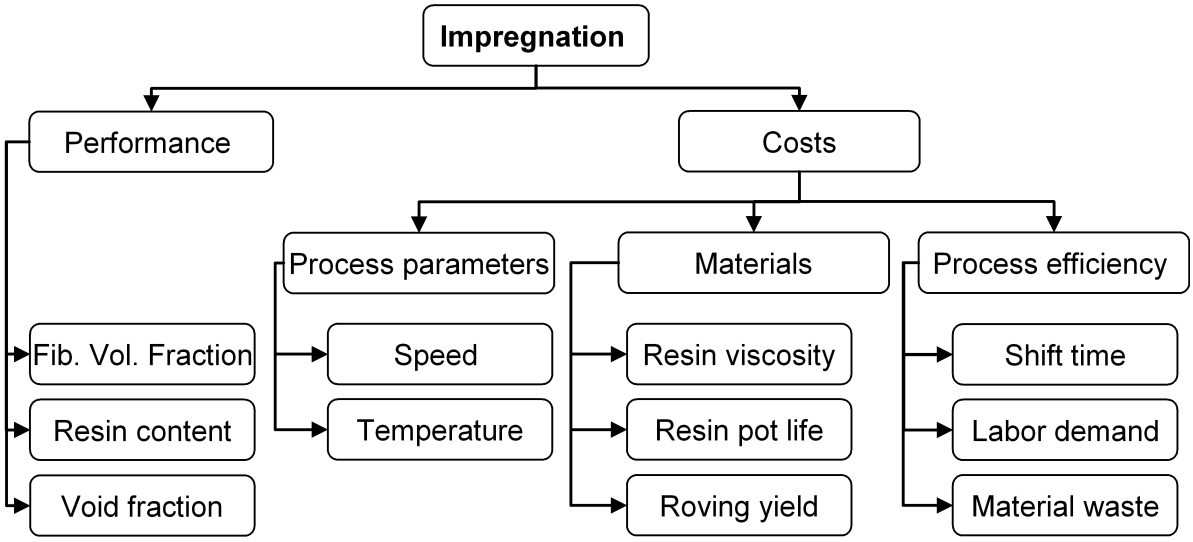

Figure 1.2: Parameters affected by the impregnation.

In order to overcome these difficulties and to fulfill the new production standards one has two options to follow. The first option is to develop new fiber and resin systems which will cooperate better with the existing equipment. Although this could be possible it would mean that the investment in know-how concerning the mechanical properties, the qualification and the environmental impact of the state of the art materials would become useless. The second option, which also sets the motivation for the present work, is the development of new impregnation techniques which will over-

come the current problems. These techniques have to be compatible with the state of the art materials and easy to implement in existing processes. Moreover the new impregnation techniques have to be suitable for material systems which will be developed over the next years and allow the design of revolutionary composite manufacturing methods.

The development of a new impregnation system through a trial and error process would not cover the industry demands. Such an approach could possible lead to the development of a system which would perform optimal at a certain process window but would be almost impossible to be implemented in another application. The optimum solution is the development of a new concept incorporating the deep understanding of the impregnation mechanics, the mathematical modeling of the system and finally the design of an impregnation device according to the process specifications. In this way not only the development of a single apparatus is secured but also the development of the overall know-how. The aforementioned developed know-how could face the industry needs for the manufacturing of high performance composite materials from endless fiber rovings.

1.2. Objectives

In previous studies of Schledjewski and Paessler (IVW) [4, 5] it was found that the use of an impregnation unit with a closed sinusoidal cavity has adequate advantages in comparison to state of the art impregnation systems used in the filament winding. Although these preliminary studies have revealed the potential of this concept, there was a lack of deeper understanding which could lead to widespread of this technology.

The primary objective of this work is the deeper understanding of the impregnation of fiber rovings in an impregnation unit with a closed sinusoidal cavity. The accomplishment of this target is associated with the following milestones:

1. Conceptual development of the impregnation device. Analysis of the process and discretization of the various process stages.

2. Theoretical and experimental investigation of the physical phenomena occurring during the process.

3. Development of a mathematical algorithm for the simulation of the impregnation process, and validation of the model.

4. Parameter study concerning the determination of the optimal working window, insight to further improvements of the equipment.

5. Adaptation of the developed impregnation system in existing processes and demonstration of the functionality.

1.3. Approach

Chapter 2 describes the state of the art devices used for the impregnation of endless rovings. The functionality of these devices is analyzed and the advantages and disadvantages of every method are discussed.

Chapter 3 presents the concept of the impregnation unit developed under the framework of this study.

Chapter 4 deals with the physical mechanisms that act during the process. Every physical phenomenon is discussed and the corresponding physical laws are presented.

Chapter 5 shows the experimental validation of the physical laws presented in Chapter 4 and their modifications in order to describe the specific materials used in this study.

Chapter 6 deals with the process modeling of the impregnation in the developed impregnation unit. The mathematical algorithm of the model is presented and the simulation tool is analyzed.

Chapter 7 analyzes and validates the results of the impregnation model. Furthermore a parameter study and a sensitivity analyses is given.

Chapter 8 presents the industrial implementation of the developed impregnation method.

Chapter 9 lists the main achievements of this study and presents the outlook for the developed impregnation process.

2. State of the art

Filament winding and pultrusion are two of the most established composite manufacturing processes dealing with the processing of endless fibers. The first winding machines were developed on the late 60's and had as major task the production of rocket frames. During 90's the production of pressure vessels with the filament winding technique had been further industrialized. Over the last 30 years the filament winding machines have been equipped with modern Computer Numeric Controlled (CNC) controllers, improved machine frames, automatic start stop modules and robotic systems for the feed of the liners and the demounting of the finished cylinder. Although these developments have increased the lay up accuracy and allowed higher winding speeds the process efficiency is still not satisfactory. The main drawbacks are associated with the use of conventional resin bath impregnators for the fiber impregnation.

The resin bath systems are also widely used in the pultrusion process as well as in the production of semi finished products (prepregs). In all cases the use of these systems is associated with some major disadvantages.

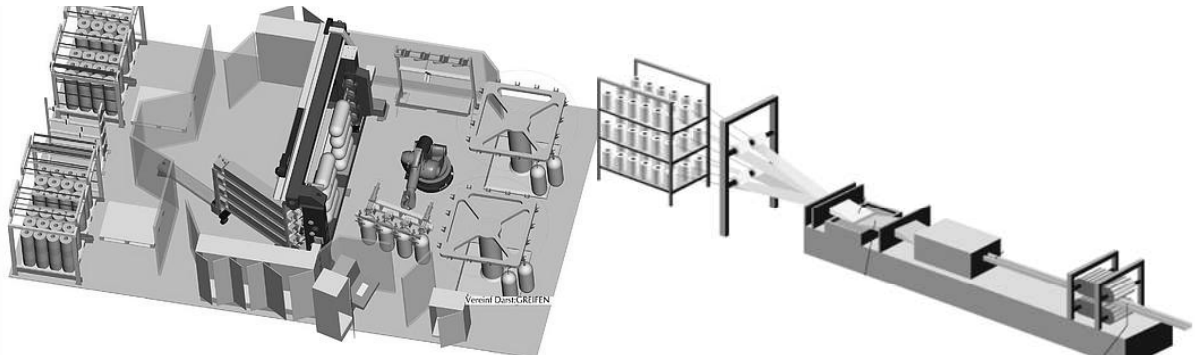

Figure 2.1: Left: Automated pressure vessel winding cell [6]. Right: State of the art pultrusion line [7].

2.1. Resin bath impregnation systems

The resin bath impregnators have been initially developed in the 60's. Although some minor improvements have taken place, the basic concept of these devices remained the same over the last 40 years. The resin baths can be divided in two main categories. These are the dip type baths and the drum type baths.

2.1.1. Dip type bath impregnation systems

The dip type resin baths are the simplest type of impregnators. They are mainly used in the pultrusion process where a large number of usually low cost rovings (e.g. glass) has to be impregnated. The impregnator consists of a resin container and an arrangement of rollers or pins. During process, the reinforcements dip into the resin and run through the roller arrangement. The resin is absorbed as the fibers dip inside the container. The air which is entrapped between the filaments is squeezed out by the pins.

The complex pin arrangement results to high friction and roving tension. Moreover the pins used by the dip baths have a small radius which in combination with the high enlacement can result to filament breakage and fuzzle. The dip baths do not allow a control of the fiber ratio. The fibers usually absorb and uptake a high amount of resin which can be scrapped out only later on.

Figure 2.2: Left: basic concept of a dip resin baths [8, 9]. Middle, right: Commercial available dip type resin baths [6, 10].

2.1.2. Drum type bath impregnation systems

The drum type baths are a further development of the dip type impregnators. They are mainly used in the filament winding process and are also applicable for fibers with lower shear strength (e.g. carbon). In this type of impregnators a drum rotates according to the fiber speed inside the resin container. Due to this rotation, a resin film is formulated on the drum surface. The thickness of the resin film is controlled by a doctor blade. The fibers are guided over the drum and absorb the resin from the resin film. A secondary system of rollers and blades ensures the fully impregnation of the fibers and strips out any excess resin.

The drum type baths are relatively complex assemblies which implement a lot of rotating parts. The use of bearings that come in contact with the reacting resin encloses the danger of an unexpected clamping of the rotating parts. The adjustment of the resin content though the doctor blade is a complex trial and error procedure with low accuracy. The system is characterized by poor repeatability and is extreme difficult to achieve the same resin weight fraction among to different production intervals.

Figure 2.3: Left: basic concept of the drum type resin baths [11, 12]. Middle, right: commercial available drum type resin baths [6,10].

2.1.3. Roller Impregnators

Another impregnator type is the roller impregnator. The working principle is very similar to that of a drum type bath. In this case a film is created with the help of a doctor blade on a roller which will come in contact with the reinforcement. Resin film and reinforcement are guided through a roller system with a calibrated distance. As the material runs through the slot between the rollers the resin is forced to flow through the reinforcement and in this way impregnates the fibers.

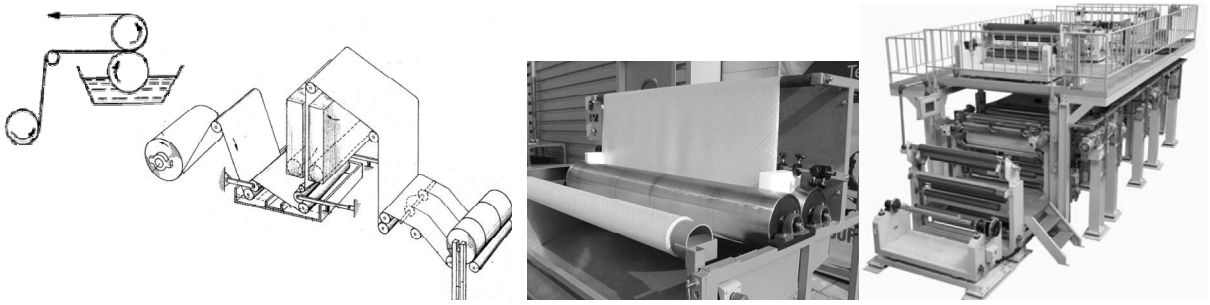

Figure 2.4: Left: roller impregnators systems [13, 14]. Middle, right: roller impregnators in the prepreg industry [15, 16].

The roller impregnators are mainly used for resin systems with very high viscosity or for very thick reinforcements e.g. prepreg production. Another variation of the roller impregnation is the film impregnation method which is mainly used in the prepreg industry. The technique is based on the creation of a resin film on a traveling release film and the application of the fibers over the resin film.

2.1.4. Application experience

The above described impregnation devices are the most widespread among the filament winding, the pultrusion, and the UD-Prepreg (film impregnation) industry. Despite the fact that they are capable of impregnating every available roving with a wide spectrum of resins they are associated with some of the most important technical problems in the production of endless reinforced composites.

The main drawback of the resin bath systems is that the resin, which is mixed with the hardener, is stored in the resin container. During the process the resin tends to polymerize causing an increase of the viscosity. This fact has a negative impact on the quality of the impregnation and influences other process parameters such as the roving tension. By the time that the resin exothermic reaction reaches a certain rate, the process has to stop and the bath has to be replaced, get cleaned and prepared again with fresh resin. Furthermore the calibration of the matrix weight fraction is a complicated trial and error procedure which demands exclusive experience. A further and important disadvantage is the large surface area of resin which is exposed to the air and causes the emission of Volatile Organic Compounds (VOC's) and Ozone Depleting Compounds (ODC's) in the work environment. These emissions raise health concerns and demand special health and safety measures.

All the above can lead to periodic stops of the production, decreased output, and low automation level. Additionally such impregnators are incompatible with fast reacting resins and with systems that are sensitive to moisture absorption. Moreover the high amount of scraped resin, the use of solvents and the high labor demand increase significantly the production costs.

2.2. Closed type systems

Over the last years several research and development efforts have focused on the

design of novel impregnation units. Main aim of these developments was to overcome the drawbacks of the bath impregnators.

The solution which is proposed by most of these concepts is the controlled resin injection that takes place inside a closed cavity. The constant flow of “fresh” resin can provide stable processing conditions and eliminates the possibility of resin cure inside the impregnation unit. The restricted volume of the cavity guaranties that there are no deadspots where the resin can stagnate and start polymerizing. In order to implement this concept various working groups have followed two different designs. These can be discretized according to the resin injection pressure either as high or low pressure impregnation systems.

2.2.1. High pressure impregnation systems

The high pressure systems, often referred as injection boxes, were initially developed in the early 90’s. Based on that approach, the impregnation unit is a straight cavity with a slight taper angle. The injection point of the resin is located at the middle of the cavity and the impregnation of the fibers is forced by the high injection pressure. During the process the fiber pack is constantly under compaction and the fiber volume fraction is determined by the final cavity cross section [17–19].

The injection boxes are able to impregnate thick fiber preforms with high viscosity resins (>300 mPa sec). They don’t have any moving parts and are relative simple and compact designs.

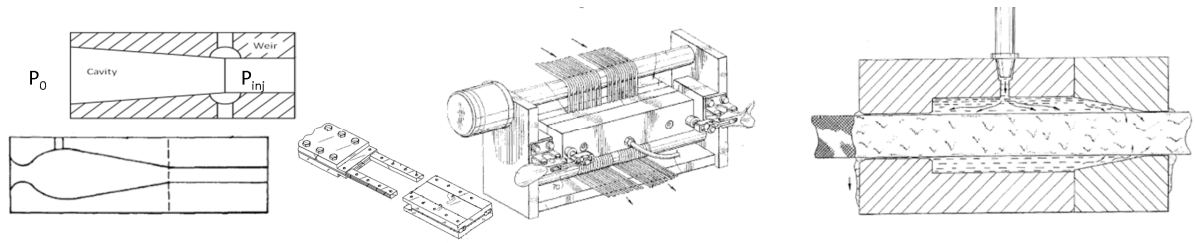

Figure 2.5: Various designs of high pressure impregnation systems [20–22].

2.2.2. Low pressure systems

The second design approach is the low pressure systems. In these designs a resin film is formulated in a first stage on the reinforcement. This film can be applied either

by a spraying technique or, by a low pressure injection through an orifice. The impregnation process is driven by the capillary forces and by a hydrostatic pressure which is caused by the deflection of the fibers inside the cavity.

The low pressure impregnation units are generally more complex designs compared to the high pressure ones. They also do not include any moving parts and because of the low fiber compaction they are also suitable for sensitive fibers.

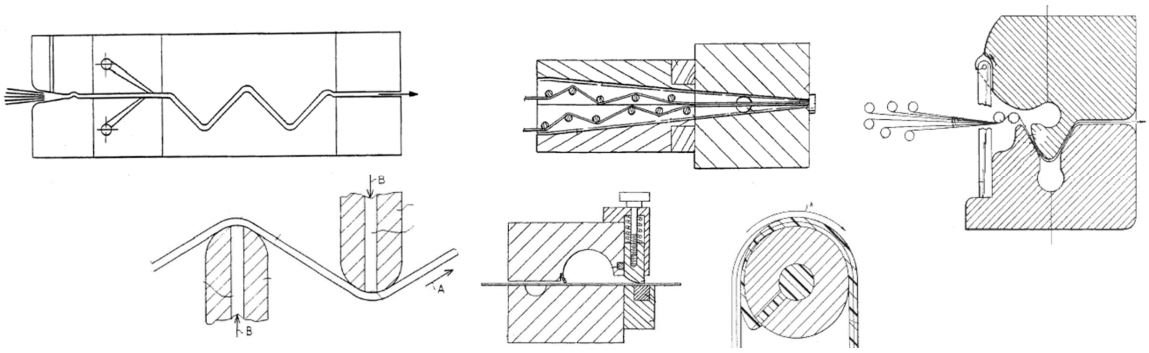

Figure 2.6: Various designs of low pressure impregnation systems [23–28].

2.2.3. Application experience

Different prototype impregnation units have been built and tested. Various injection boxes have been already implemented in industrial pultrusion applications. The positive performance of these designs had allowed the introduction of new reactive resins (e.g. polyurethane) in the pultrusion industry [29]. Nevertheless the high pressure designs have some major disadvantages. The main problem is the uncontrolled resin backflow. Due to the tapered cavity the fibers are non-uniformly compacted. On the entrance region the fiber volume fraction is lower compared to the exit region. As the resin is injected in the cavity, it tends to flow easier towards the entrance (opposite to the process direction) creating a strong backflow. The backflow cannot be effectively controlled always and often leads to undesired flow of matrix material out of the fiber entrance. This phenomenon restricts the processing window and makes the equipment suitable for limited processing speed. Another disadvantage of the high pressure designs is the possible fiber damage. As already mentioned, the fiber pack has to pass through a die which has a cross-section that corresponds to the set fiber volume fraction. In a lot of applications the desired fiber volume fraction can be up to 55-60%. This can lead to high compaction forces and high friction phenomena. This lo-

cal loading of the fiber package could lead to extensive filament damage. Furthermore the injection boxes are calibrated only for a certain fiber volume faction. A resin ratio different from the set value would lead to resin back-flow or void creation. The use of a fiber pack with a different yield would lead to extreme friction phenomena and fiber damage.

The low pressure designs are mainly used in applications were a single roving or a thin fiber pack has to be impregnated. The length and the geometry of the cavity are very important. The hydrostatic pressure which is needed for the impregnation is created by the form of the cavity. The pressure is generated by the cavity curvature or by the deflection of the roving over an arrangement of pins. If the radii of these deflection points have a critical value, they could lead to a filament breakage especially for fibers with high stiffness (e.g. CF). Since the impregnation is not driven by any externally applied pressure, the design of the cavity can lead to a restriction concerning the viscosity of the resin. The low pressure designs do not face back flow problems since the cross section of the cavity is bigger than the fiber pack. An important advantage is that the low pressure systems are capable to adjust different fiber volume fractions.

Table 2.1 presents an overview of the analyzed impregnation methods. The table associates every impregnation method with the three most important processes of unidirectional composites. The symbols +/0/- indicate the suitability of the method to the chosen process. Furthermore the compatibility of the impregnation method with the very basic material properties like resin viscosity and tow thickness is given. The roving thickness in this way is a variable that depends on the roving tex, material density and filament diameter. In this case the same density and filament diameter is taken into account for all cases. The roving thickness is in this way is a variable of the roving’s tex. More specifically for the case of carbon fibers the rovings with less than 6000 filaments are considered as low thickness, these with 12000 and 24000 filaments are taken into account as medium thickness and all these with more than 48000 filaments are though as high thickness. Respectively the margin for the low viscosity resin is set at 100 mPa sec whereas this for the high viscosity at 500 mPa sec.

Table 2.1: Basic impregnation methods and their compatibility to unidirectional composites manufacturing processes and basic material properties.

	Process			Materials	
	Fil. Winding	Pultrusion	Prepreging	Resin Visc.	Roving Thick.
Drum bath	+	0	0	Low /Middle	Low/Middle
Dip bath	0	+	-	Low/Middle	Low /Middle
Roller impregnator	-	-	+	Middle/High	Middle/High
High pres. closed type	0	+	+	Middle/High	Middle/High
Low pres. closed type	+	+	+	Low/Middle	Low /Middle

3. Siphon impregnation unit

The Institute für Verbundwerkstoffe (IVW) has developed the Siphon impregnation unit. Aim of the development was to design a device for the continuous impregnation of single rovings in a closed cavity that works under the low pressure principle. The unit is designed in order to comply with the modern industry demands. During the concept development high priority was given to the aspects of excellent impregnation quality, constant processing conditions and user friendly design.

3.1. Impregnation process

The developed unit is based on a low pressure impregnation concept. The process starts with the formation of a resin film between the cavity wall and moving roving (Figure 3.1). The resin is metered according to the roving speed and the thickness of the film is proportional to the matrix weight ratio. In this way, resin and matrix enter the impregnation unit under predefined conditions. In order for the impregnation to proceed, hydrostatic pressure on the resin film is essential, besides the capillary phenomenon. This is provided by the roving deflection over the curved surface. The roving which is under tension, bends over the curve and applies hydrostatic pressure on the resin. This pressure in combination with the capillary phenomenon are the driving phenomena of the impregnation process.

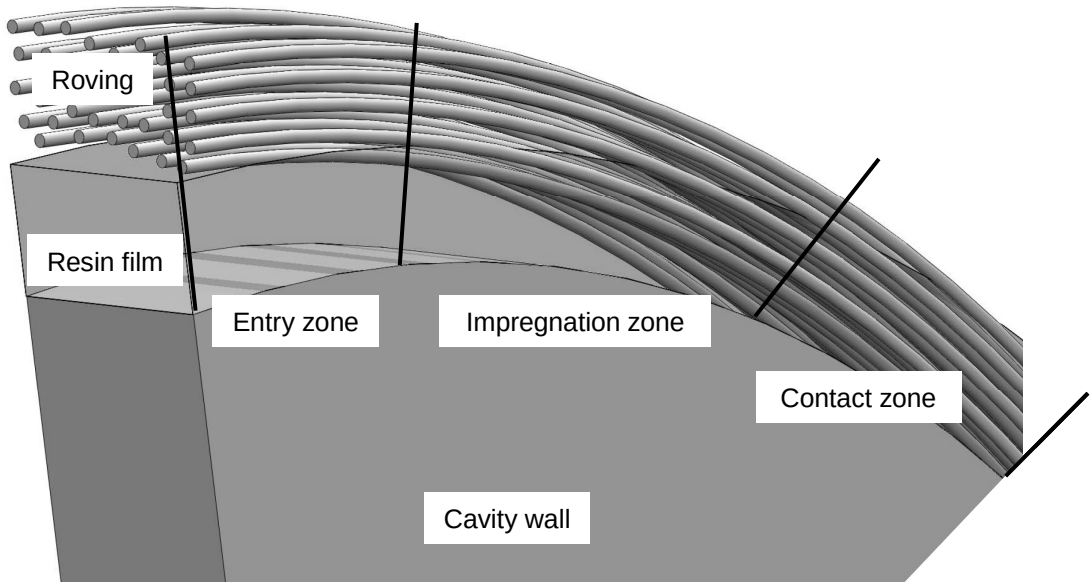

Figure 3.1: Schematic representation of the impregnation process.

The roving passes gradually during the process duration from the dry state to the fully impregnated state. As reported in [30] the process can be divided into 3 main regions. These are schematically represented in Figure 3.2 :

1. Entry zone: The materials enter the unit. The resin film is formulated between the cavity wall and the roving. The thickness of the film is mainly controlled by the resin dosing rate.

2. Impregnation zone: The roving runs over the curve and shear tension develops on the resin film. The roving tension generates a pressure field on the resin film which results to the transverse flow of the resin through the roving.

3. Contact zone: The resin layer tends to zero thickness and the roving is in contact with the cavity wall maximizing the friction phenomena. A further compaction of the fiber bed takes place and the entrapped air is forced out.

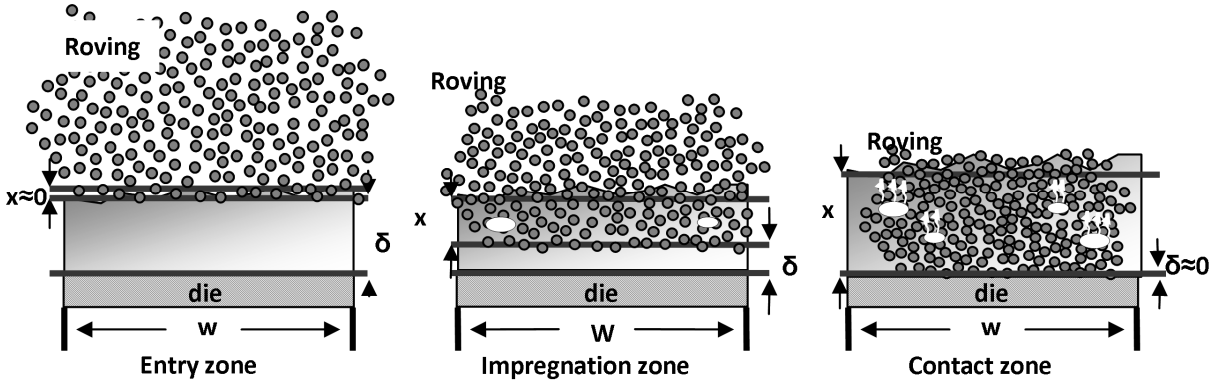

Figure 3.2: Schematic diagram of the threes discrete zones during impregnation (w indicates the cavity width, x the impregnation depth, and δ the resin film thickness).

3.2. Cavity design

In the developed unit the impregnation cavity has a sinusoidal shape with multiple recurrent curves. Every curve results into a pressure development region which further advances the impregnation. Depending on the number and the design of the curves the roving can enter and exit the unit with or without any directional change. In order to minimize the work load for cleaning and preparation, the solution of a disposable cavity has been preferred. So as to have constant processing conditions

among parallel processed rovings it has been specified that every single roving should be processed in a separate cavity. These two conditions are fulfilled by the use of a PTFE tube as an impregnation cavity. The tube is placed inside a metallic mold. The distance between the upper and lower part of the mold is smaller than the outside diameter of the PTFE tube in order to compress the tube to a flat-oval shape. In contrary to a cyrcular cross section, a cavity formed out of a flat pressed tube gives constant pressure and compaction conditions over the roving width and does not lead to an increase of the roving's thickness.

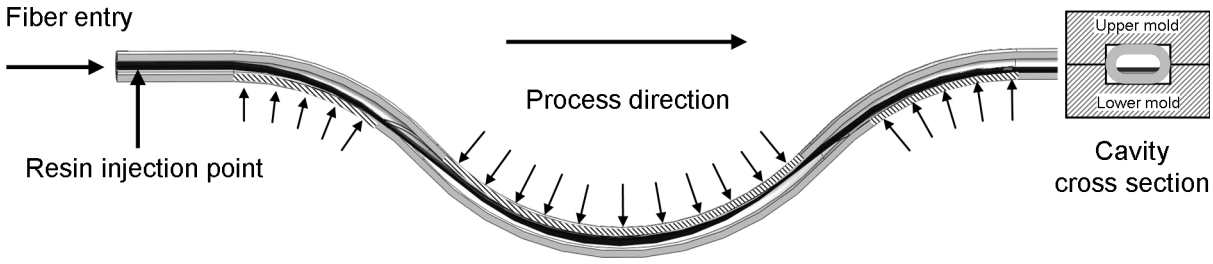

Figure 3.3: Schematic diagram of the sinusoidal cavity formed out of a PTFE tube. The roving is indicated as black continuous line. The areas where the roving has contact with the cavity (pressure areas) are indicated by the dashed lines.

3.3. Resin injection block

The impregnation unit consists of the resin injection block and the impregnation cavity. Fibers and resin enter the impregnation unit under a predefined flow rate through the resin injection block. The resin is not injected directly on the roving but is initially supplied in a small cavity. The injection cavity acts as a buffer and reduces the injection pressure to a lower pressure. The cavity design is asymmetric with the exit edge on a slight lower level than the entrance. In this way the resin tends to flow in the process direction preventing any possible resin back-flow. Furthermore due to this design a homogenous resin film is formulated under the roving. The uniformity of the resin film is very important because it determines the impregnation process.

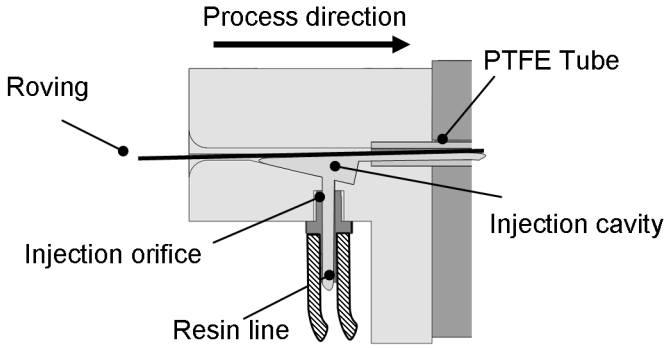

Figure 3.4: Schematic diagram of the resin injection box.

4. Impregnation physics – theory

In order to analyze the impregnation of compressible porous media, the flow of the fluid cannot be separated from the bulk of the porous mass. During processing the porous medium is undergoing finite deformations and at the same time the fluid is being displaced. Taking that into account it can be concluded that the examination of the impregnation is a twofold problem [3, 31]. The physical laws that treat the impregnation problem are analyzed in the following sections.

4.1. Resin viscosity

The resin during the impregnation phase is a liquid. It is considered to be a continuous medium meaning, that the motion of every point of the fluid can be described by mathematical equations. In order to formulate these mathematical expressions one has to consider three physical conditions. These are the continuity condition, the rheological condition, and the Newton's law of motion. The continuity equation and the Newton's law are easily explained and well known. The rheological condition is the connection between the stresses and the strains in the fluid. This condition is expressed by the physical quantity of the viscosity. Viscosity can be interpreted as the quantity that describes a fluid's resistance to flow. Fluids resist the relative motion of immersed objects through them as well as to the motion of layers with differing velocities within them. Formally, viscosity (represented by the symbol η) is the ratio of the shearing stress (τ) to the velocity gradient ($\dot{\gamma}$) in a fluid. Equation (4.1) gives the mathematical expression of the viscosity [31].

$$\eta = \frac{\tau}{\dot{\gamma}} \tag{4.1}$$

4.2. Elastic deformation of the roving

During the impregnation process, mechanical loads are applied on the roving. These loads can be either axial (tension) or transverse (compaction). During processing the axial tension is initially applied by the spool brake and increased by viscous and cou-

lomb friction phenomena inside the impregnation unit. The through the thickness compaction is generated by the pressure that develops on the curves of the impregnation unit.

As suggested by Gutowski in [32, 33] the fibers inside the roving are neither perfectly aligned nor perfectly straight. According to the abovementioned theory the fibers have a slight waviness of a sinusoidal character (Figure 4.1).

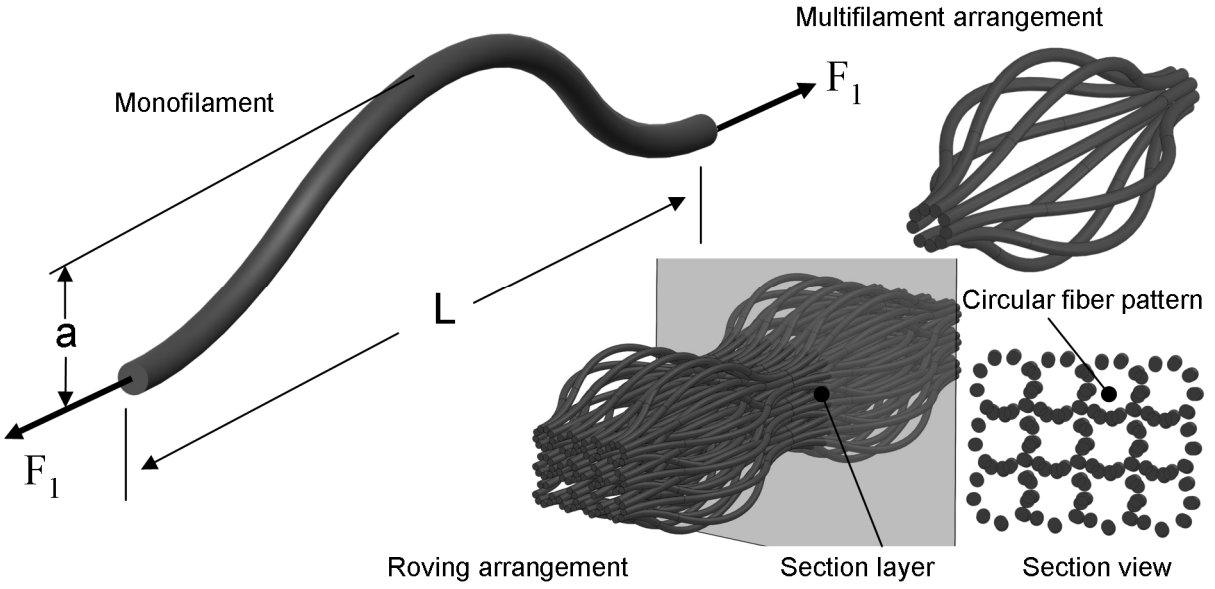

Figure 4.1: Left: Schematic diagram of a single filament. Right: Representative cells of multiple filaments.

This disorientation creates multiple fiber-fiber contacts and inter-fiber gaps. According to that theory any action of stress on the roving will result to a reduction of the gaps and therefore to a corresponding increase of the fiber volume fraction of the roving. Gutowski created two semi empirical models. The first one (Equation (4.2)) calculates the axial load (F_1) that has to be applied on a roving in order to reach a certain fiber volume fraction (V_f).The model takes into account the maximum compaction ratio (V_a), the initial compaction (V_o) and to the elastic modulus (*E*) of the reinforcement. The parameter (β) expresses the waviness of the filaments and is defined as the ratio between *L* and *a* (Figure 4.1). The second model (Equation (4.3)) describes the correlation between bulk compressive stress σ_b and fiber volume fraction V_f taking into account the same parameters as Equation (4.2).

$$F_1 = \frac{A_0 V_0}{V_f} \frac{1 - \sqrt{\frac{V_f}{V_0}}}{\frac{16}{\pi^3}\frac{\beta^2}{E}\sqrt{\frac{V_a}{V_f}\left(\sqrt{\frac{V_a}{V_f}} - 1\right)^3}} \tag{4.2}$$

$$\sigma_b = \frac{3\pi E}{\beta^4} \frac{\left(1 - \sqrt{\frac{V_f}{V_o}}\right)}{\left(\sqrt{\frac{V_a}{V_f}} - 1\right)^4} \tag{4.3}$$

4.3. Darcy's law and permeability

The filaments inside the roving form a porous structure. The most established modeling procedure for the calculation of the flow through a fiber bed is based on Darcy's law [34]. According to Equation (4.4), which presents the mathematic expression of the Darcy's law, the superficial fluid velocity vector (v) is analogue to the pressure gradient (∇P) and the permeability of the porous medium (K) and reverse analogue to the fluid viscosity (η). The Darcy's law is valid only for incompressible Newtonian viscous laminar flows.

$$v = -\frac{K \nabla P}{\eta} \tag{4.4}$$

The permeability tensor lumps all the complicated interactions that take place between fluid and fibre bed. As stated in the Darcy's law the permeability can be directly measured in an experiment. Nevertheless in order to study a certain composite manufacturing process it is necessary to predict the permeability of the roving (*K*) perpendicular to the fiber direction at different fiber volume fractions. Carman has developed a relation (Equation (4.5)) for the calculation of the permeability values in dependence to the compaction grade [35]. According to this relation the permeability depends on the volume fraction (V_f) and on the so-called Kozeny constant (*k*) and to the radius of the fiber (R_f).

$$K = \frac{R_f^2}{4k} \frac{(1-V_f)^3}{V_f^2} \tag{4.5}$$

The Carman relation which is based on the hydraulic radius was initially developed for granular beds consisting of ellipsoids. Later studies have proved that the relation can be valid for fibrous porous media. Also Gutowski et al. used the Equation (4.5) and approximated the longitudinal and transversal fibre tow by setting the value of parameter *k* at 0.5-0.7 and 11-18 respectively [36]. However as reported by Skartzis et al. [37] this constant is not suitable to describe the flow through aligned fibre beds. The theory does not take into account the non-uniformity of real fiber beds. Gutowski et al. and Gebart proposed some modified expressions for the more accurate calculation of the transverse flow in unidirectional fiber beds [38, 39]. Gutowski proposed the Equation (4.6) where he relates the permeability with the volume fraction value at which the flow stops V_a and with the empirical parameter k_{zz}. The value of V_a is proposed to be between 0.7 and 0.85 and k_{zz} at 0.2. Gebart in Equation (4.7) calculates the theoretical value of the permeability based on an analytic approach. $V_{f\max}$ stands for the highest possible compaction degree and k_G takes the value of $16/\left(9\pi\sqrt{6}\right)$ if the fibers are in hexagonal arrangement or respectively $16/\left(9\pi\sqrt{2}\right)$ if the fibers are in a quadratic arrangement.

$$K = \frac{R_f^2}{4k_{zz}^{'}} \left(\frac{\sqrt{\frac{V_a^{'}}{V_f} - 1}}{\frac{V_a^{'}}{V_f} + 1} \right) \tag{4.6}$$

$$K = k_G \left(\sqrt{\frac{V_{f\max}}{V_f}} - 1 \right)^{5/2} R_f^2 \tag{4.7}$$

Chapter 4.3 highlighted the importance of the permeability for the determination of the fluid flow. In order to prove the validity of the theoretical models for the materials that were used in the present study experimental data have been taken into account.

Due to the unidirectional orientation of the fibers, the roving has orthotropic symmetry conditions. As shown in Figure 4.2 in the case of a roving that is made of endless unidirectional fibers, the inter-fiber porosity in the y direction should have the same geometrical aspects with the inter-fiber porosity in the z direction. Based on this symmetry the permeability in the through the thickness direction is considered to be equal with the permeability perpendicular to the fibers in the in-plain direction.

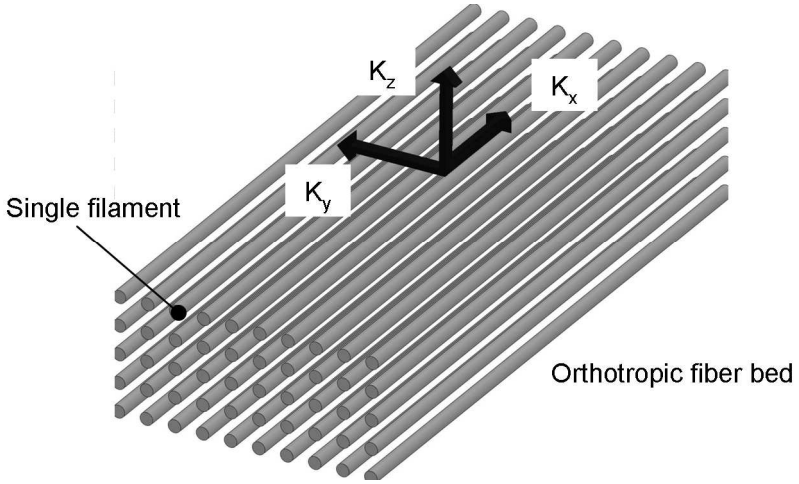

Figure 4.2: Schematic diagram of the ideal unidirectional fiber orientation inside a roving structure.

Kissinger et al. have developed a cell for the measurement of the in-plain permeability of flat textile performs (s. Figure 4.3). The work principle is based on the continuous detection of the flow front position during the infiltration of a flat laminate. The flow front detection is carried out by linear capacity sensors which are implemented on the surface of a closed mould. The permeability measurement cell has been validated in different studies. The results have proven that the permeability of different textiles can be measured accurately and with high repeatability [52–54].

The measurement of the permeability on performs built exclusively from single rovings was proven to not be possible with the above described equipment. In order to get an estimation of the fiber permeability in unidirectional fiber structures preforms made out of non crimp fabrics were measured. The Unidirectional non crimp reinforcements are built from rovings that are held together with a stitch pattern and are considered as a fiber bed that has a very similar structure with this of a roving. In order to measure the roving permeability preforms from UD non crimp CF reinforce-

ments were tested in the permeability measurement cell.

Figure 4.4 shows representative permeability values of CF-UD non crimp reinforcements. The tested performs were made of 6 layers of UD non crimp carbon fiber with a surface weight of 300 g/m^2 As expected, it was found that the permeability decreases with the increase of the fiber volume fraction. The values of the permeability perpendicular to the fiber direction are about 5 times lower than the permeability along the fibers.

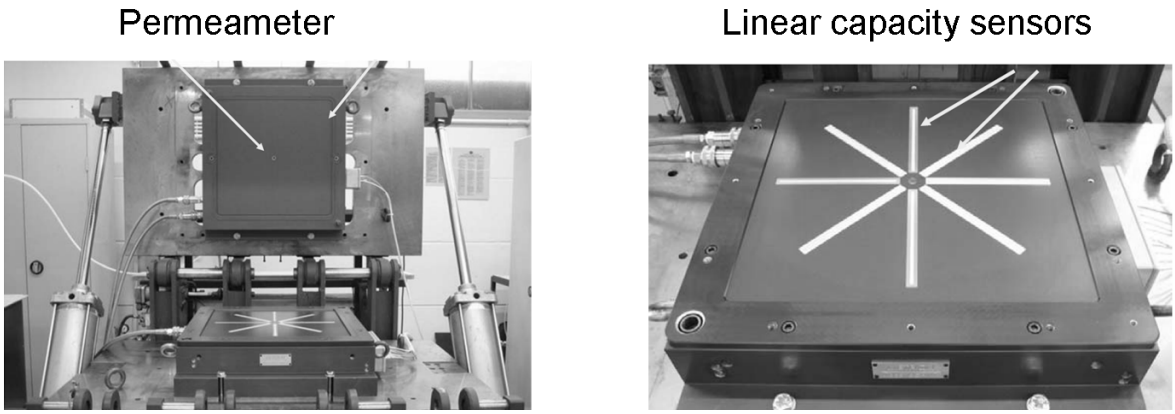

Figure 4.3: Set-up for the measurement of permeability of a unidirectional preform.

In order to extract data which can be used for the study of the impregnation mechanics of single rovings, the Carman model (Equation (4.5)) was fitted on the experimental results of Figure 4.4. Concerning the flow parallel to the fiber direction, the stitching pattern of the CF-UD non-crimp reinforcements is not expected to have any significant influence on the perform permeability. Taking that into account, the theoretical curve of the Carman model was fitted exactly on the experimental data and the Kozeny constant was set at 0.02. On the other hand, for the case of resin flow perpendicular to the fiber direction, the stitching pattern of non-crimp reinforcements is expected to have a significant influence over the preform permeability. Since the focus of the present study is the impregnation of single rovings, the effect of the stitching should be excluded for the theoretical predictions. In order to do so the curve of the Carman model was shifted to an order of magnetite lower than the experimental results by setting the Kozeny constant at 0.4.

The values of the Kozeny constant as calculated above will be used in the following

chapters of the study for the solution of the Darcy's law and for the calculation of the resin flow inside an endless unidirectional carbon fiber roving.

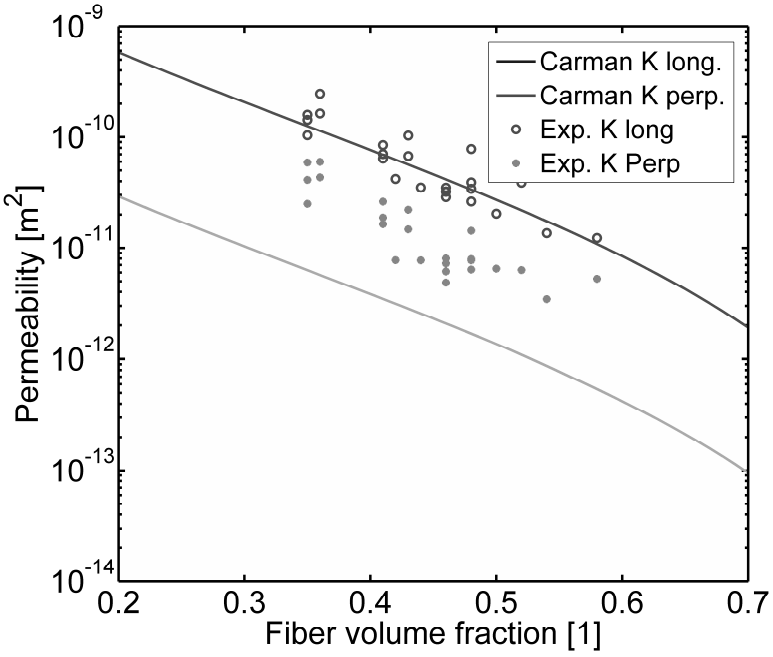

Figure 4.4: Comparison of measured permeability values in UD non crimp CF reinforcements (6 layer preform 300 g/m^2/layer) with the Carman model for a single roving.

4.4. Pressure

Pressure is the driving force of the impregnation process. The total effective pressure which is applied on the resin during the process is influenced by the hydrostatic pressure, imposed by the fiber tension, as well as by the capillary pressure which is generated by the differences between the surface tension of the resin, fiber and atmospheric air [3].

4.4.1. Hydrostatic pressure

The roving tension generates a pressure field on the resin film between roving and cavity surface. Figure 4.5 presents the free body diagram of a roving that runs over a curve of the impregnation unit. The radial force acting upon a roving element with width *W* is $dN = PWRd\theta$ where P is the pressure, R is the curve radius and θ is the deflection angle. Resolving the roving tension forces in the vertical direction we

get $dN = (T + T + dT)\sin(d\theta/2)$. For small deflection angles it is considered that $d\theta dT \approx 0$ and $\sin\theta \approx \theta$. Therefore we get $dN = Td\theta$ and by substituting the dN we get the Equation (4.8) which expresses the hydrostatic pressure that acts on the resin during the impregnation process.

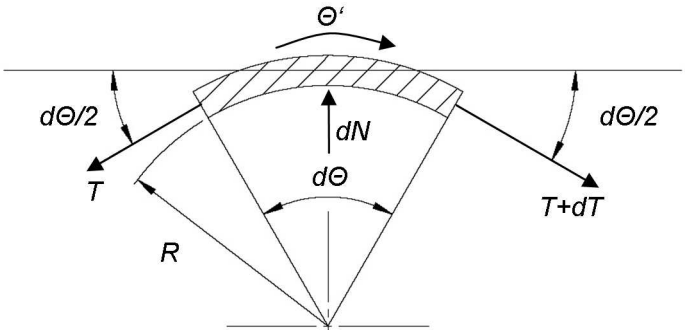

Figure 4.5: Free body diagram of the roving.

Equation (4.8) expresses the developed resin pressure under the roving taking into account the geometrical characteristics of the die and the roving tension. Gutowski et. al. and Springer et. al. in [40, 41] used the Equation (4.8) to simulate the impregnation process on the mandrel surface during filament winding.

$$P = \frac{T}{WR} \tag{4.8}$$

Bates et. al. and Gaymans et. al. in [42, 43] have used the same relation for the calculation of the resin pressure in the pin assisted impregnation process. They proposed that the pressure increases along the impregnation unit proportionally with the increase of the roving tension (Figure 4.6).

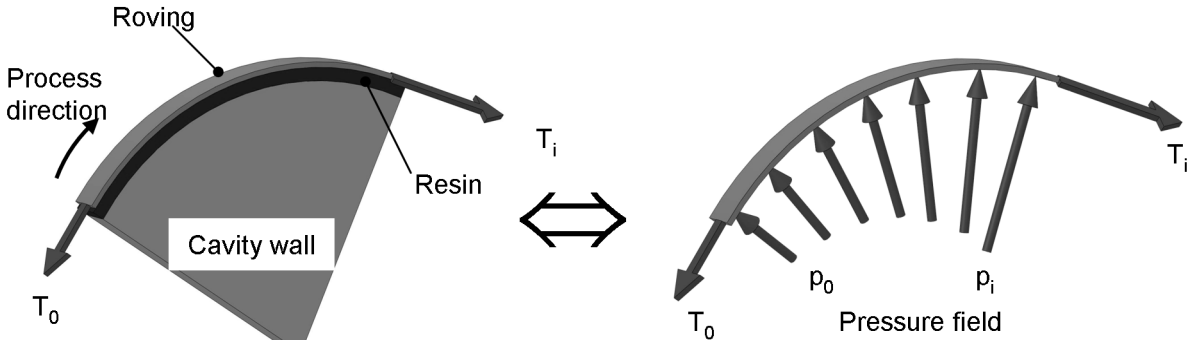

Figure 4.6: Schematic diagram of the pressure build up on the surface of the impreg-

nation cavity.

The above assumption will be used for the calculation of the resin pressure in the modeling of the impregnation unit. Furthermore it will be considered that the pressure in the resin is preserved over the entire arc length even if the resin film has reached its minimum value.

4.4.2. Capillary pressure

The roving is a porous structure consisting of multiple aligned endless filaments. During processing the roving is guided through the impregnation cavity in which the liquid resin flows and fills-in the space between the filaments. As the resin comes in contact with the fibers and the atmospheric air, due to the differences in the surface tensions, a pressure is developed at the three phase interface.

Although the capillary pressure is present only in the unsaturated flow and is relatively low compared to the injection pressures used in LCM-RTM techniques, it should be taken into account for the modeling of the continuous impregnation. The reason is that in contrary to the LCM-RTM, the resin pressure that is applied by the curves of the impregnation cavity is in the same order of magnitude with the capillary pressure.

The capillary pressure can be expressed by the Young-Laplace equation (Equation (4.9)) in which γ_s and θ_{ca} are the wetting parameters expressing the surface tension of the resin and the contact angle between fiber and resin respectively. The capillary radius R_c is a geometrical factor that depends on the distance between the single filaments [56-58].

$$P_c = \frac{2\gamma_s \cos\theta_{ca}}{R_c} \tag{4.9}$$

The contact angle *γ* is a quantitative measure of the wetting of a solid by a liquid. The lower the contact angle the better the wetting. Under the framework of this study, in order to experimentally define the contact angle between resin and fiber the method proposed by Rebouillat et. al. in [44] was followed.. Therefore, resin droplets were

deposited on single filaments and the shape of these was observed under the REM microscope. According to Rebouillat et. al.[44] tanθ is defined as the slope at the drop foot at the point where the filament start to be wetted (s. Figure 4.7).

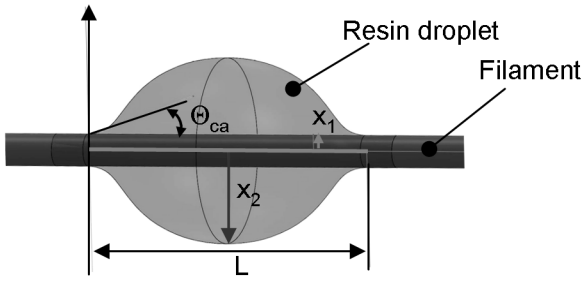

Figure 4.7: Schematic diagram of the contact angle measurement as described in [44].

4.5. Tension development

The roving tension force is one of the most important parameters in the processing of unidirectional composite materials. As explained in the previous chapters the tension influences the fiber compaction and the roving permeability, adjusts the impregnation pressure and affects the capillary phenomenon. In the filament winding process the roving tension plays an even more global role as it not only influences the impregnation but also defines the consolidation pressure, the compaction of the filament wound laminate, and thus the overall part quality.

The roving tension is initially applied at the spool creel through a brake system. Nevertheless the tension does not remain constant during the impregnation process. As the roving runs thought the impregnation unit the tension force gradually increases. A number of studies [30, 42, 45–47] have proven that the increase of the tension is generated by two physical phenomena.

The first phenomenon is the contact of the fibers with the impregnation unit. Although a resin film is formulated between roving and cavity wall (Figure 3.1) during the process some monofilaments come in contact with the cavity wall. This phenomenon is getting more frequent by the time that the resin is absorbed by the roving and the resin film thickness reaches it minimum value (contact zone Figure 3.2). The contact of monofilaments with the cavity wall generates Coulomb friction which causes an

increase of the roving tension. Equation (4.10) gives the relation for the differential increase of the roving tension due to Coulomb friction.

$$dT_f = \mu dN \tag{4.10}$$

Taking into account the free body diagram of Figure 4.5 and for small $d\theta$ the Equation (4.10) can be written in the form of Equation (4.11).

$$dT_f = \mu T d\theta \tag{4.11}$$

The second phenomenon which causes the increase of the roving tension is the shear of the resin film. The roving moves inside the impregnation unit with a linear speed U. Between roving and cavity wall the resin film exists which has a viscosity value η. Since the epoxy resin behaves as a Newtonian fluid the differential tension increase due to the shearing of the resin film over a differential arc length is described by the Equation (4.12).

$$dT_s = \eta \frac{U}{\delta} WRd\theta \tag{4.12}$$

Where δ is the resin film thickness W, *the* roving width, and R the cavity curve radius.

The above Equations (4.11) and (4.12) can be added in a common expression (Equation (4.13)) that describes the development of the roving tension over the curve length of the impregnation unit. At this point it should be mentioned that the resin film thickness δ can not decrease infinitely and never takes the value 0. The minimum physically possible value of the resin film thickness is analyzed in the following chapter.

$$\frac{dT}{d\theta} = f\mu T + \eta \frac{U}{\delta} WRd\theta \tag{4.13}$$

The term f correlates the magnitude of the Coulomb friction with the thickness of the resin film. The variable f can take values between 0 and 1. A f value equal to 0 indicates that there is no contact between fibers and cavity wall and thus no friction.

On the other hand a f value equal to 1 indicates full contact between fibers and cavity wall. In order to link the term f with the processing parameters the following relation is proposed. The above expression was used in [42] for the modeling of the roving tension development in a pin assisted impregnation process.

$$f = F_{\deg r}^2 \tag{4.14}$$

The term $F_{\deg r}$ stands for the felling degree which is percentage of the resin penetration inside the roving as it will be explained later in Chapter 8.

4.6. Resin film thickness

Inside the impregnation unit the roving runs over a resin film that is formulated on a curved surface. Such a flow situation can be described by the Tailor-Couette flow. Nevertheless since the resin film thickness is low, the curve radius much higher than the resin film and considering the fact that the aim of the present work is to set the basics for the development of a new impregnation module and not the detailed analysis of the resin flow, the shearing of the resin will be modeled as a plain Couette flow.

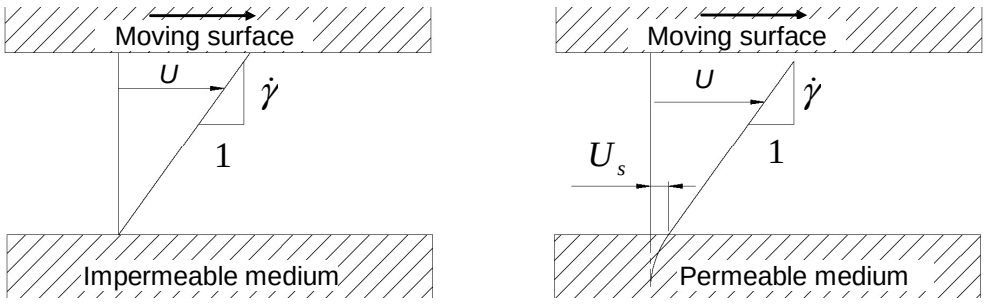

Figure 4.8: Velocity profile for a shear driven flow over an impermeable and over and through a permeable porous medium.

Figure 4.8 (left sketch) represents the velocity profile of a liquid film between two moving surfaces in a plain shear driven flow (Couette flow). The velocity profile is linear and decreases proportionally to shear rate $\dot{\gamma}$. The local fluid velocity on the impermeable surface is considered to be zero which is known as no slip condition. The right sketch in Figure 4.8 illustrates the velocity profile of a shear driven flow over a

permeable porous surface. The profile is again linear in the channel and decays to zero inside the porous medium. Nevertheless for this particular case it should be pointed out that the fluid velocity at the interface has a higher than zero value (U_s) (slip velocity) and the flow penetrates the porous medium [48].

In order to determine the shear forces that act on the roving, the shear profile of the film thickness has to be fully defined. Taking into account the slip condition it can be understood that the film thickness that contributes to the development of the roving tension expands inside the roving. Figure 4.9 illustrates the velocity profile in two different stages of the impregnation process. In the left sketch the process is in the initial stage where a relative thick resin film is present. The right sketch shows the velocity profile by the time that the resin is fully absorbed and the fibers come in contact with the cavity wall. In this case it can be seen that the resin film thickness cannot be directly defined by the distance between cavity wall and the slip condition has to be taken into account in order to predict the shear forces accurately.

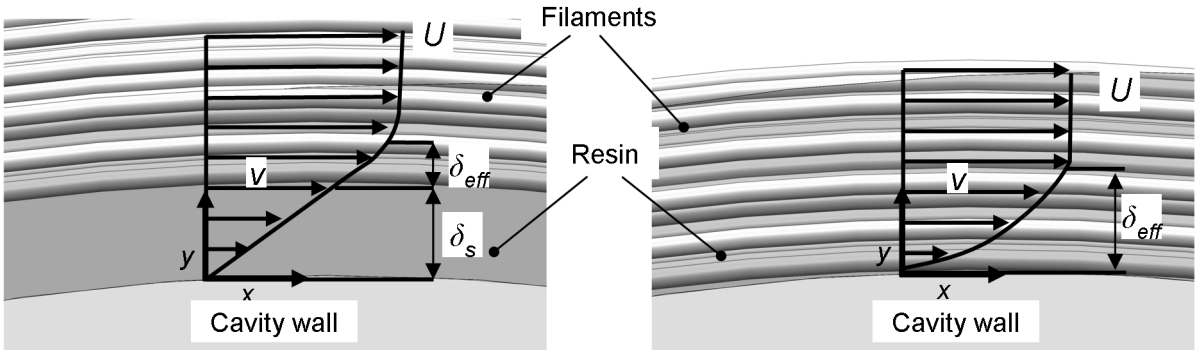

Figure 4.9: Schematic representation of the resin velocity profile in the film thickness left in the initial stage of the process (entry and impregnation zone) and right in the final stage of the process (contact zone).

Gibson in [49] analyzed the resin velocity profile at the cavity wall interface for a continuous composites manufacturing process. According to the analysis of Gibson the Darcy equation should be combined with the creeping flow version of the Navier – Stokes equations in order to get the pressure profile (Equation (4.15)).

$$\nabla P = \eta(\nabla^2 v - K^{-1} v) \tag{4.15}$$

Gibson assumed that the resin velocity (v) relative to the fiber bed does not vary

along *y* or *z* axis (Figure 4.9) and that the pressure gradient remains constant in the y-direction. He expanded the Equation (4.15) in *x* direction and applied the boundary conditions $v = 0$ at $y = 0$ and $v = U$ at $y = \infty$ where U in this case is the fiber speed. The Equation (4.16) describes the resin velocity relative to the cavity in *x*-direction υ_{xdie}.

$$v_{xdie} = U(1 - \exp(-y / \sqrt{K_x})) \tag{4.16}$$

$$\delta_{eff} = \sqrt{K_x} \tag{4.17}$$

The differentiation of Equation (4.16) gives the effective film thickness (Equation (4.24)).The similar analysis for isotropic porous materials was followed by [48, 50, 51] and all authors concluded that the thickness of the viscous transition zone is in the $\sqrt{K}$ order of magnitude.

Combining Equation (4.17) with Equation (4.13) the roving tension development can be directly calculated. This is valid in case of a laminar flow. The Reynolds number (Equation (4.18)) is a dimensionless number that gives a measure of the ratio of inertial forces to viscous forces. At low Reynolds numbers the flow is characterized as laminar meaning that the viscous forces are dominant, and is characterized by smooth, constant fluid motion. Over a critical Reynolds number the flow is characterized as turbulent and is dominated by inertial forces, which tend to produce chaotic eddies, vortices and other flow instabilities. The critical Reynolds number for Coquette flow cases is set over 360.

$$\mathrm{Re} = \frac{\rho U \delta}{\eta} \tag{4.18}$$

For the case of the impregnation process where the resin viscosity η varies between 50 and 1000 mPas, the resin density ρ is between 1000 and 1200 kg/m^3, the processing speed U ranges from 0 to 100 m/min and the resin film takes values in the order of magnitude between 10^{-3} to 10^{-12} m, the value of the Reynolds number stays under the critical value.

5. Impregnation physics – experimental validation

5.1. Materials

The fibers and resin used in the present study were chosen according to their ability to represent the industry standards and highlight the perspectives of the developed process according to the latest material trends.

5.1.1. Fibers

The high strength Polyacrylonitrile (PAN) -based carbon fiber 34-700 from the company Grafil Inc., USA was chosen as reinforcement. The fibers were supplied in endless continuous rovings treated with an epoxy based sizing. The high strength PAN-based carbon fibers are a common material choice for the production of high-end components like Type III & IV pressure vessels. Although for most of the filament winding applications the 12k rovings are the standard choice, the 24k was chosen in order to highlight the ability of the process to work efficiently with heavier tows. The heavier tows increase the productivity and reduce the costs. The roving was supplied in the WD type that has the form of a flat tow with a width of 7.2 mm and a thickness of 0.2 mm.

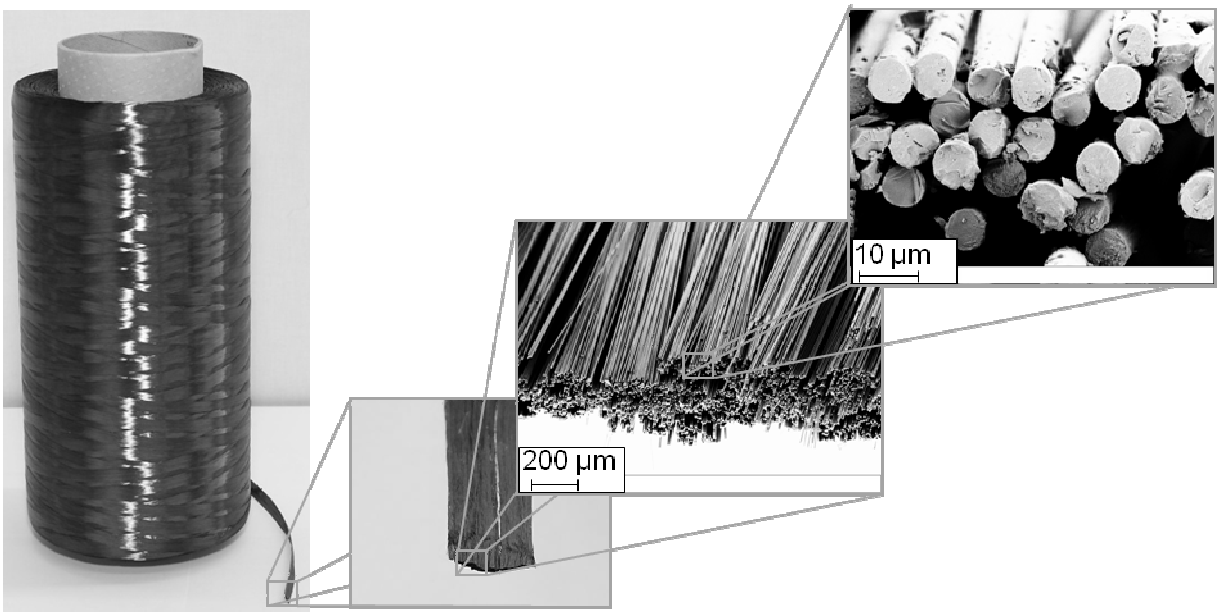

Figure 5.1: Illustration of the 24k CF roving used in the study.

Table 5.1: Basic physical and mechanical properties of the Grafil 34-700 WD carbon fiber roving [80].

Fiber type	Number of filaments	Filament diameter (μm)	Density (g/cm^3)	Tensile strength (MPa)	Tensile modulus (GPa)	Yield (mg/m)
34-700 WD	24.000	7	1.80	4830	234 GPa	1600

5.1.2. Resin

The warm curing epoxy resin system Araldite LY 564 / Hardener XB-3486 from, Huntsman Advanced Materials GmbH, CH was chosen as matrix system. The epoxy resin Araldite LY 564 is a state of the art general industry resin with a wide range of applications. The formulated amine hardener XB 3486 gives to the system long pot life which makes it suitable for the production of very large components. According to the producer the system is applicable for the filament winding, wet lay up and LCM processes.

Table 5.2: Basic physical properties of the Araldite LY 564/ Hardener XB 3486 epoxy resin system (mixing ratio: 100 / 34) [81].

Epoxy system	Initial viscosity (mPas)	Density (g/cm^3)
Araldite LY 564 / HardenerXB 3486	200-300 (at 25 ℃)	1.0-1.1 (at 25 ℃)

The rheological characteristics of the resin were examined in a plate-plate rheometer. The resin viscosity remains stable only for the first 150 sec. After that point, the reaction starts and the viscosity increases with an exponential trend (Figure 5.2 - left). Nevertheless, since in the developed impregnation system the resin is continuously mixed and dosed, for the investigation of the developed impregnation process the viscosity will be considered stable and equal to the initial value. A steady state shear experiment that was performed directly after resin mixing and had a duration of 100 sec showed that the resin behaves as a Newtonian fluid since the viscosity values

remain constant independent to the applied shear rate (Figure 5.2 – right).

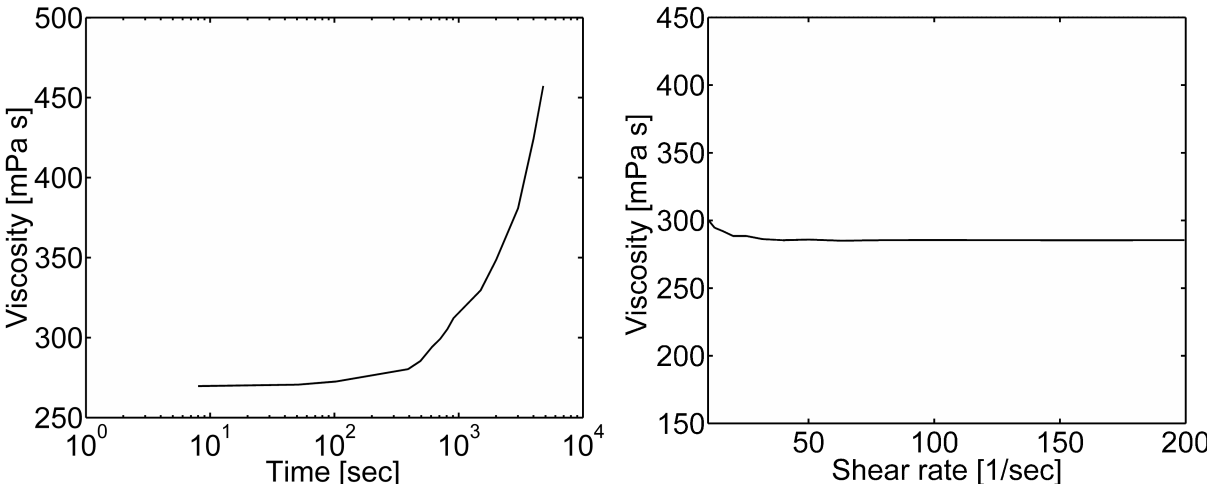

Figure 5.2: Left: Resin mix viscosity over time. Right: Resin mix viscosity over shear rate.

5.2. Elastic deformation of the roving

As shown in Chapter 4.2 the fiber rovings deform under the application on load. In order to verify the compaction behavior (s. Equations (4.2) and (4.3)) of the materials that were used in this study, a testing device was build. The apparatus (Figure 5.3) consisted of a clamp, a resin reservoir, two guiding rollers and a static load. The rovings were lubricated with resin in order to simulate the processing conditions and to avoid any inter-fiber friction phenomena. The aim of the first experimental set-up was to test the compaction behavior of the roving during the loading with axial tension. In this case the roving was fixed on the jig and was guided through the resin vat. Defined static loads were applied and the vat was filled with epoxy resin. The resin was left to cure in room temperature and samples were cut out of the rovings. After polishing, the samples were examined under a light microscope and the fiber volume fraction was calculated according to the area method. A similar set-up was followed in order to examine the bulk compaction behavior of the roving. In this case the rovings were guided over a curved surface instead through a straight resin vat. The curvature of the surface had a radius of 42.5 mm which gives the same through the thickness compaction conditions as in the case of the siphon unit. In order to better approximate the actual processing conditions a groove with a width of 4.5 mm was machined into the curve's surface. The groove restricts the spreading of the fi-

bers whereas the width of the groove corresponds to the width of the flat compressed PTFE-tube that forms the cavity of the impregnation unit. The tension loads for both experimental set ups were chosen according to the typical roving tensions that are applied during the filament winding process. In this way the load applied during the experiments ranged between 1 and 50 N.

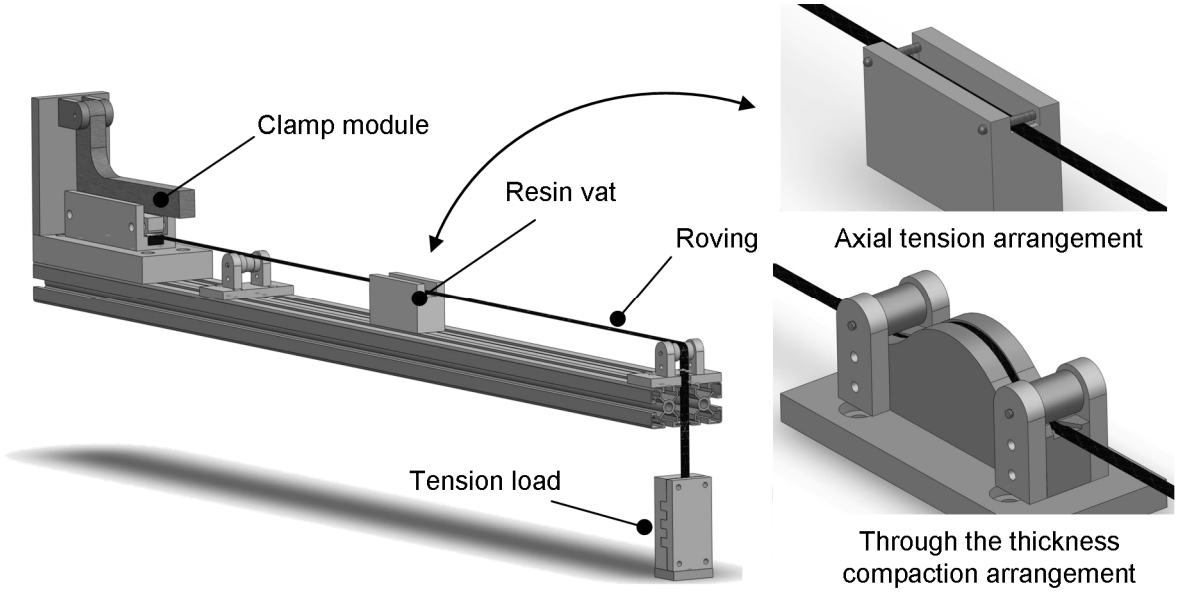

Figure 5.3: Schematic representation of the axial tension – roving compaction experimental set up.

The diagram in Figure 5.4 presents the testing results together with the predictions of the Gutowski models. In Equations (4.2) and (4.3) the initial compaction (V_o) was set to 0.1 and the maximum possible compaction (V_a) to 0.65. In the case of the axial tension arrangement the parameter β was found to be 130. This value is significantly lower compared to the one reported by Gutowski (350) in [33]. This leads to the conclusion that the 24k rovings that have been used in the current study have higher filament waviness than the 3k carbon fiber rovings that were used in the reference.

In order to fit the bulk compaction experiments with the Equation (4.3) the value of the parameter β was set at 300. According to the theory the parameter β should be common for both compaction cases. Nevertheless in the experimental procedure that was followed in the current study the fibers were not loaded by a pure bulk compaction load but they were tensioned in a mixed axial tension- through the thickness

compaction loading condition. The deflection of the fibers over the curved surface combined with the application of an axial load (Figure 5.3) resulted to a slight pretensioning and realignment of the fibers which balanced the fiber waviness. This combined loading condition explains the higher value of the parameter β compared to the pure axial tension experimental set-up. The disagreement between experimental data and model predictions for the case of 10 N cannot be theoretically explained.

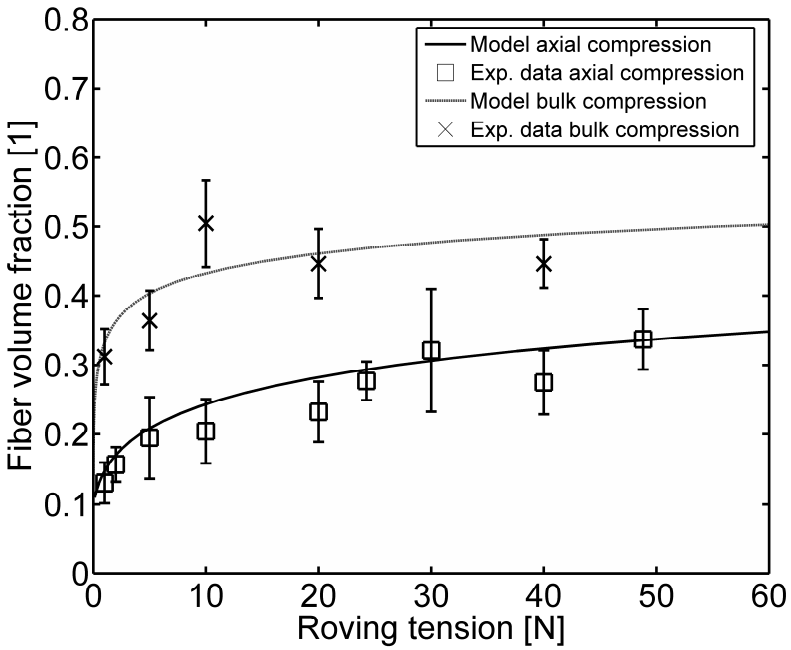

Figure 5.4: Experimental data and model predictions for the axial and bulk compression of the 34-700 24k carbon fiber roving.

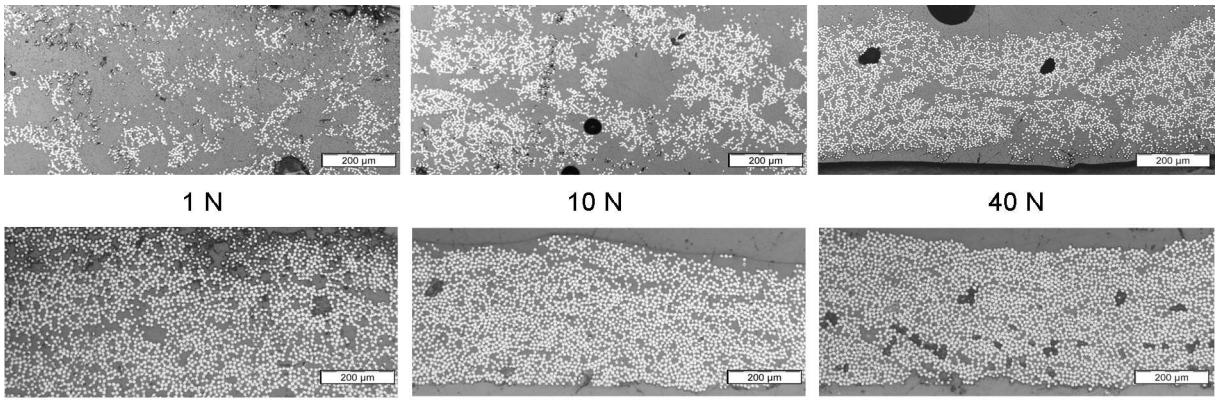

Figure 5.5: Micrographs of the roving cross section. In the upper row the samples for the case of pure axial tension are presented and in the bottom row for the case of axial tension-bulk compaction.

Figure 5.5 presents the micrographs of the tested samples for both set ups and for different loading conditions. In both cases it can be seen that as the tension increased, the fibers come closer to each other resulting on higher fiber volume fraction. In the low compaction cases it is observed that the filaments tend to have an uneven distribution. A more careful examination reveals that the fibers are arranged on circular patterns. The radius of the circular patterns reduces as the tension load increases and disappears for values of V_f higher than 0.3. This circular fiber arrangement is assumed to be a result of the filament waviness as shown in Figure 4.1.

5.3. Capillary pressure

Chapter 4.4.2 highlighted the presence of the capillary pressure in porous materials. The understanding of this phenomenon is necessary since it accelerates the resin flow thought and it is believed to have a drastic influence on the impregnation process. The following Chapter deals with the analysis of the capillary phenomenon inside a single carbon fiber roving and with the calculation of the exact magnitude of the developed pressure.

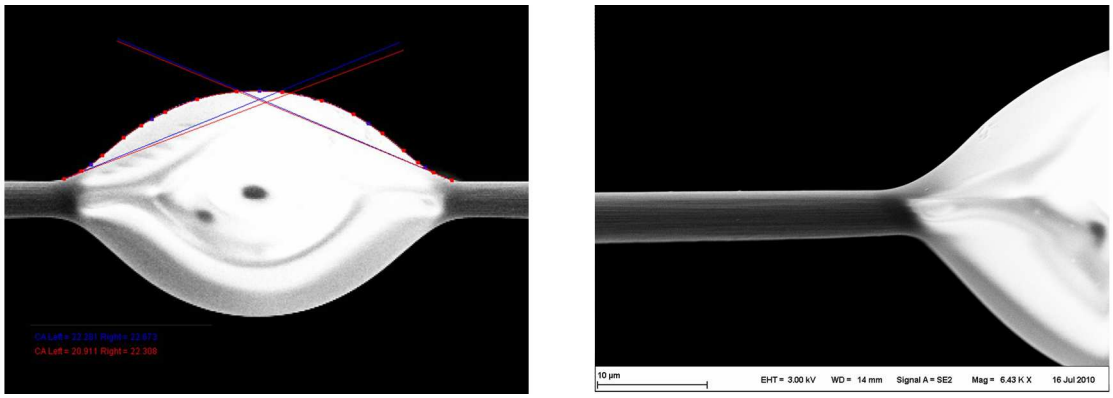

Figure 5.6: Measurement of the contact angle between resin and a single carbon roving filament.

The contact angle between single filaments and epoxy resin was measured as droplets were deposited on single filaments and observed under a Scanning Electron Microscope (SEM) microscope. The contact angle software DropSnake [55] was used in order to measure the contact angle (Figure 5.6). The average contact angle between the carbon fiber Grafil 34-700 and the resin system Araldite LY564- Hardener XB3486 was found to be 17.35° with a standard deviation of 4.25°. The resin surface

tension was measured according to the pendant drop method (DIN 55660-3) and was found to be 35.03 mN/m.

In order to calculate the exact magnitude of the capillary pressure for a certain fiber compaction the only unknown term of the Equation (4.9) is the capillary radius $R_{c.}$ The capillary radius would be easy to determine in the case on a porous structure with a 2D symmetry. Nevertheless as it can be seen in Figure 5.7 in the case of a real roving, in which the fibers are chaotically distributed, the determination of the parameter $R_{c.}$ is not a straightforward procedure. Under the framework of the present work an experimental set up for the measurement of the capillary radius and thus the capillary pressure under different compaction grades has been developed.

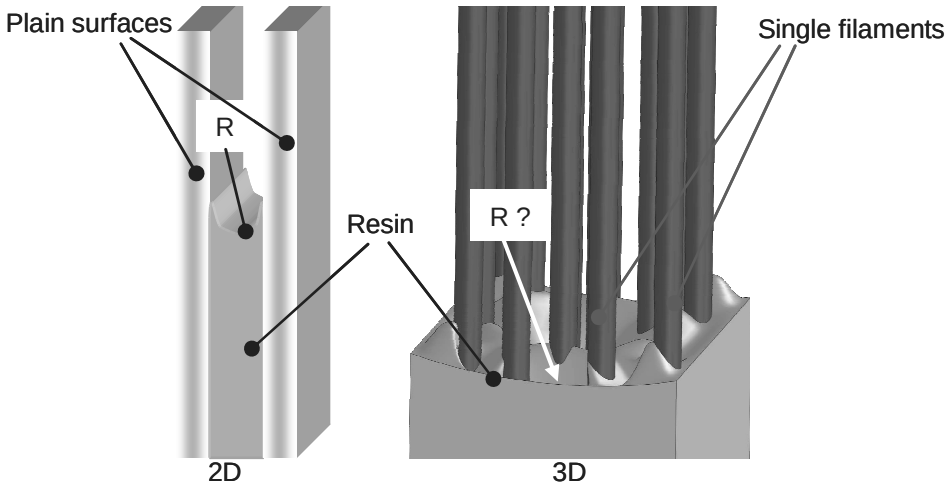

Figure 5.7: Schematic representation of the definition of the capillary radius in a porous structure with a 2D symmetry and in a roving.

The capillary flow along parallel filaments can be modeled as flow through parallel tubes of uniform radii. In this case, the internal viscous forces, the gravity forces and the surface tension acts simultaneously on the flow front. The force balance for this case is given by the Equation (5.1) where R_c is the capillary radius, z is the flow front position as described in Figure 5.8, τ the flow tortuosity and ρ and η the fluid density and the fluid viscosity [56].

$$\pi R_C^2 z\rho \frac{d^2 z}{dt^2} = \pi R_C^2 P_c - 8\pi\eta\tau \frac{dz}{dt} - \pi R_c^2 \rho g z \qquad (5.1)$$

The left hand side of the Equation (5.1) can be set to zero since the inertial forces are not significant [57]. Based on that, the force balance for the front of the capillary flow can be written as follows where *F* is the capillary force, *W* is the gravity force, and F_n is the viscous drag.

$$F - W = F_n \tag{5.2}$$

$$F = 2\pi R_c \gamma \cos\theta \tag{5.3}$$

$$W = \pi R_c^2 \rho g z \tag{5.4}$$

$$F_n = 8\pi\eta\tau \frac{dz}{dt} \tag{5.5}$$

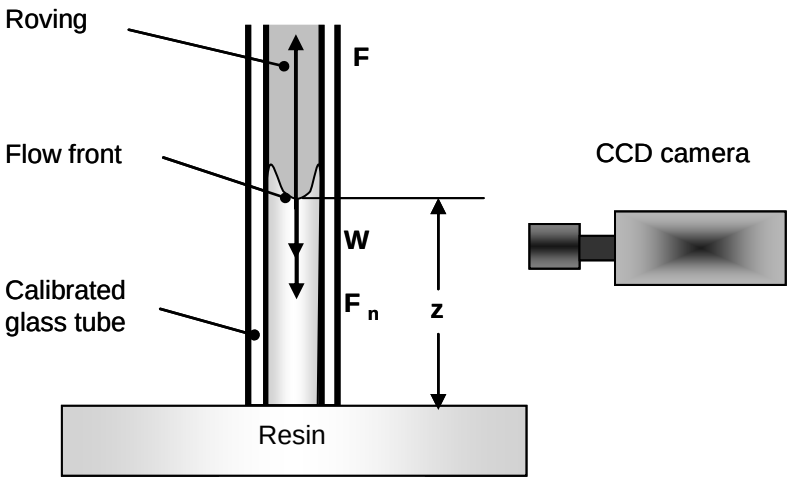

Figure 5.8: Schematic diagram of the capillary rise experimental set-up.

Aim of the capillary rise experimental set up (Figure 5.8) was to measure and analyze the capillary flow under defined processing parameters. Under the framework of this study 24k carbon fiber rovings (Grafil 34-700 WD) were placed in calibrated glass tubes with internal diameters of 2.5, 2.0, and 1.6 mm resulting in a fiber volume fraction of 19, 30, and 46 % respectively. Figure 5.9 illustrates the cross sections of the rovings for the 3 different compaction set ups. The micrographs present the effect of the radii of the glass tubes on the fiber compaction and on the fiber distribution of the samples. The figure. During the experiment, the samples were placed in contact with the epoxy resin system and the flow front position was recorded using a CCD camera. The experiments were terminated after 900 sec and the height of the

flow front was measured by means of image analysis software. For simplicity reasons it was considered that the viscosity of the resin due to the small volume does not change significantly over the experiment duration.

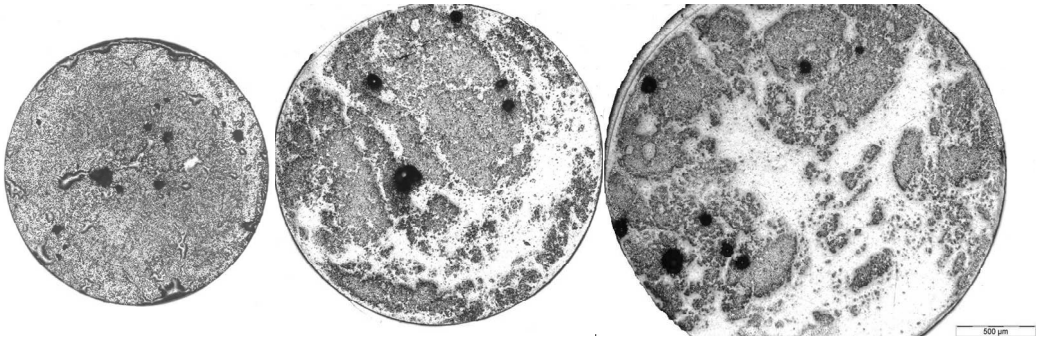

Figure 5.9: Micrograph of the cross section of the samples. From left to the right 1.6 mm, 2.00 mm, and 2.5 mm.

Figure 5.10 presents the flow front in three different snap shots during the experiments. The test results show that the wicking effect is maximized when using 30 % fiber volume fraction (V_f). In the case of the 19 % V_f during the early stage of the experiment a high flow front speed was observed but a low final height. On the contrary for the high compaction case 46 % V_f the flow front advanced at a very low rate without reaching its final height until the end of the experiment. The above behavior can be explained and predicted using Equation (5.2). It should be taken into account that as the compaction increases the parameter R_c in Equation (4.9) will decrease as the filaments are coming closer into contact resulting in higher capillary pressure. On the other hand under higher compaction grades the viscous forces will increase causing a decrease of the flow front speed.

In order to mathematically describe the experimental results the Equation (5.2) can be transformed into the Equation (5.6) which is called the Washburn's law [58].

$$\frac{dz}{dt} = \frac{R_c^2}{8\tau\eta z}\left(\frac{2\gamma\cos\vartheta}{R_c} - pgz\right) \tag{5.6}$$

The capillary radius and the tortuosity are the only unknown terms in Equation (5.6). The value of the capillary radius can be obtained from the final height of the flow front

from the case of V_f 30 % and 19 %. An expression depending on the volume fraction and similar to the Kozeny equation was used. In Equation (5.7) D expresses the fiber diameter and the ε is a constant set at 6 in order to feet the experimental results.

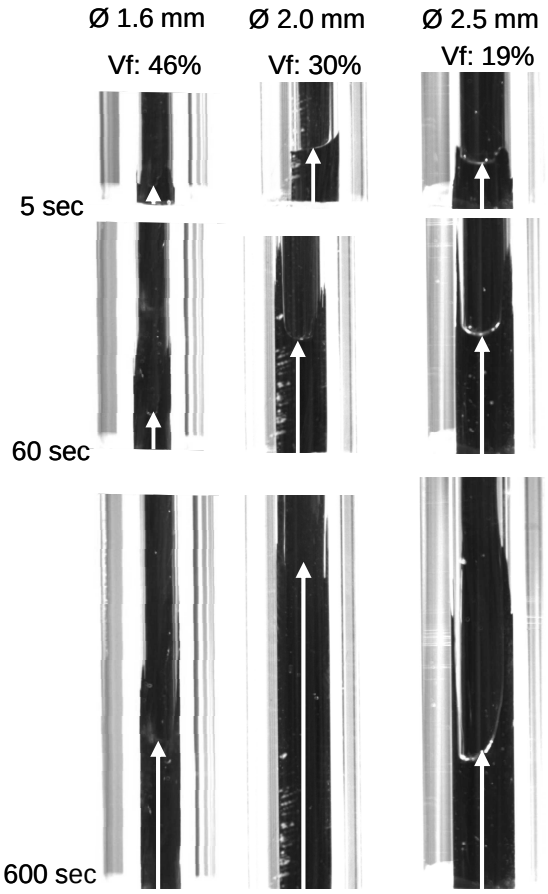

Figure 5.10: The flow front position for the 3 compaction grades during the capillary rise experiment.

$$Rc = \varepsilon D \frac{(1-V_f)^3}{V_f^2} \tag{5.7}$$

The second parameter to be defined was the parameter τ expressing the tortuosity. Tortuosity expresses the ratio between the length of a true flow path for the fluid and the straight line distance between inflow and outflow. The above is a kinematic definition but as reported elsewhere it should be a geometric quantity [31]. The parameter was defined by consideration of the flow front speed during the experiments. The τ is again expressed in terms of V_f as shown in Equation (5.8) where α was set at 2

and *B* was set at 14 in order to feet the experimental results.

$$\tau = \alpha + \mathrm{B}\,\frac{V_f^{\,2}}{(1-V_f)^3} \tag{5.8}$$

Figure 5.11 shows the numerical solution of Equation (5.6) taking in account Equation (5.7) and Equation (5.8). The comparison between experimental data and model shows that the model predicts accurately the flow front movement over the entire experiment duration.

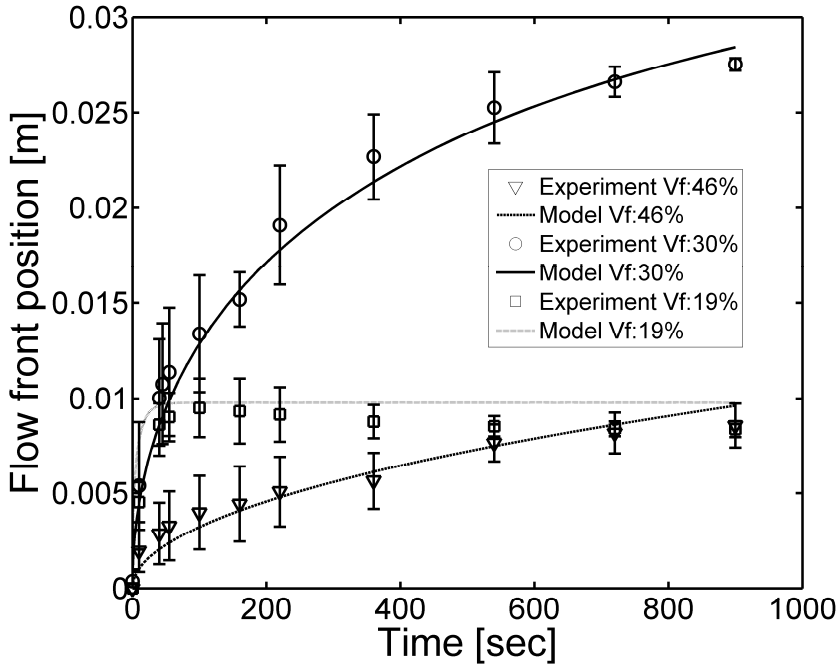

Figure 5.11: Model prediction and experimental results for the capillary rise experiment.

Equation (5.6) can be expressed in the terms of the Darcy's law. In that case the term $R^2/8\tau$ expresses the permeability of the roving and the term inside the parenthesis the applied pressure. The apparent permeability of Equation (5.6) is plotted together with the capillary pressure in the logarithmic diagram of Figure 5.12. it can be seen that with increasing fiber volume fraction the permeability of the fiber structure drops whereas the capillary pressure increases. By normalizing the permeability and the capillary pressure relative to the maximum and by multiplying their logarithmic values as shown in Equation (5.9) a criterion concerning the magnitude of the capillary effect has been created. Figure 5.13 presents the values of the Equation (5.9)

over the fiber volume fraction. The diagram shows the spontaneous impregnation phenomenon is maximized for the middle compaction grades (30-40 %) as it was found out in the experiments.

$$Ca_{eff} = \log P_{cNORM} \cdot \log K_{Norm} \tag{5.9}$$

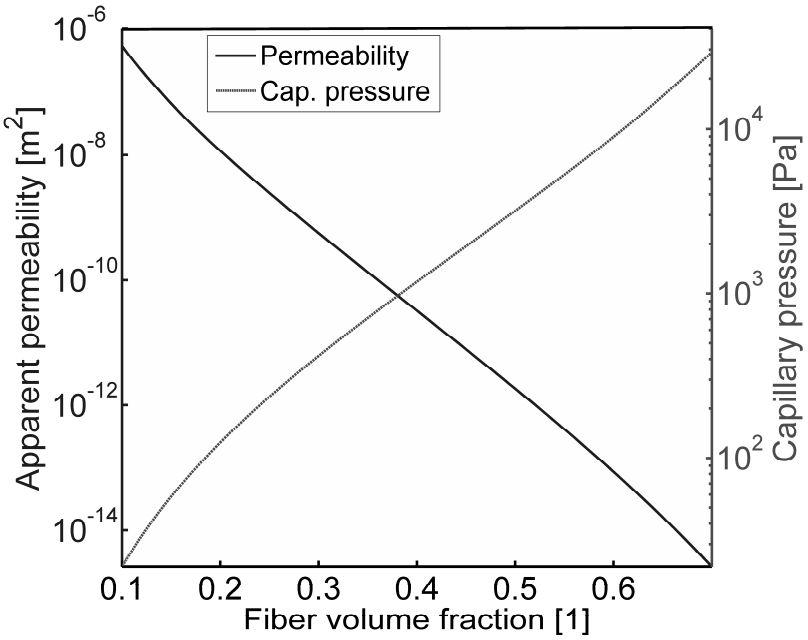

Figure 5.12: Apparent permeability vs capillary pressure.

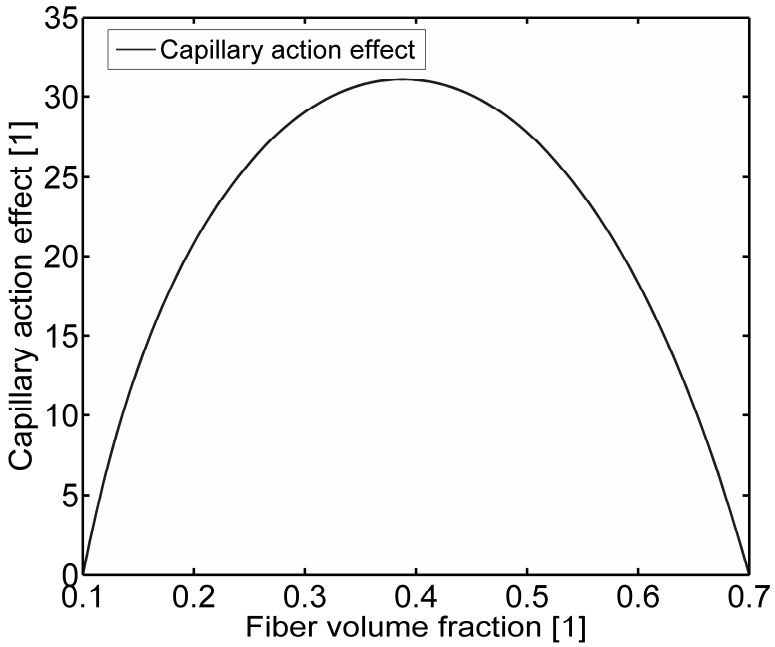

Figure 5.13: Capillary action effect vs fiber volume fraction.

5.3.1. Hydrostatic-capillary pressure relation

Figure 5.14 presents the development of the hydrostatic and capillary pressure in dependence to the roving tension. Equations (4.8) and (4.9) give the magnitude of the hydrostatic and capillary pressure respectively. For the case of the hydrostatic pressure a curve radius of 42.5 mm and a roving width of 4.5 mm were taken into account. For the calculation of the capillary pressure the roving fiber volume fraction was calculated by using the Equation (4.3) and the capillary radius by using the Equation (5.7). According to the diagram in Figure 5.14 the capillary pressure is between 5 and 10 % of the magnitude of hydrostatic pressure and the effect of the capillary pressure is more significant for the low tension values. Based on that and considering the low thickness of the carbon fiber roving it can be stated that the capillary pressure should be taken into account in the modeling of the impregnation process.

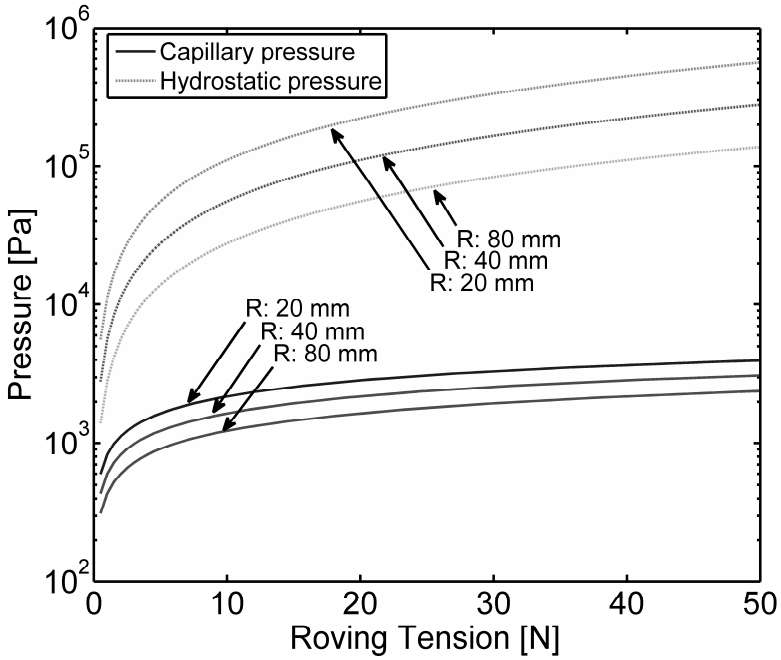

Figure 5.14: Hydrostatic pressure and capillary pressure for given roving tension (impregnation cavity radius 42.5 mm).

Darcy‘s law (Equation (4.4)) does not implement directly the capillary pressure. The capillary pressure is only present in the three phase interface (flow front) and tents to zero for the saturated areas. Amico et. al. in [59] and Ahn et. al. in [60] have proposed the implementation of a capillary pressure term in the Darcy’s law expression Equation (5.10). Since in the case of the continuous impregnation of a fiber roving

the flow path is relatively small, the following equation will be used for the modeling of the impregnation process.

$$v = -\frac{K\nabla(P + P_c)}{\eta} \tag{5.10}$$

5.4. Resin film thickness

In Chapter 4.6 it was shown that according to the theory, once the filaments of the roving come in contact with the cavity wall, the effective resin film thickness will take the value of $\sqrt{K}$ (Equation (4.17)). A test set-up (Figure 5.15) was build in order to validate this theoretical prediction and prove its applicability for the modeling of the continuous impregnation of fiber rovings. The concept of the experimental set up was to monitor the increase of the tension of a single impregnated roving that runs though a straight die. According to the Equations (4.13) and (4.17) the increase of the roving's tension is proportional to the thickness of the resin film which should be on the $\sqrt{K}$ order of magnitude. Main element of the set-up was a straight die made of PMMA (Plexiglas). Three different dies were built in order to extract the equivalent resin film thickness under three different compaction grades. The die length was 300 mm for all the set ups, whereas the cavities cross section was 7.2 x 0.3, 7.2 x 0.4, and 7.2 x 0.6 mm respectively. Every different cross section resulted in a nominal fiber volume fraction of 41, 31 and 21%. Two tension measurement devices were mounted on the experimental rack and in line with the die.

During the experiment a carbon fiber roving (Grafil 34-700WD) fully impregnated with epoxy resin (Araldite LY 564/ Hardener XB 3486) was guided through the die and pulled at a defined speed by a filament winding machine. The roving tension was measured by the tension measurement devices before entering and after the exiting of die. The signal was continuously logged by a data logger connected to a computer.

Two types of tests were performed. In the first test campaign the pretension on the rovings was kept constant while the roving speed was increased step-wise from 0 up to 20 m/min. In the second test campaign the speed was kept constant and the roving pretension was gradually increased. Every test was repeated 3 times and an av-

erage tension was extracted for every parameter set.

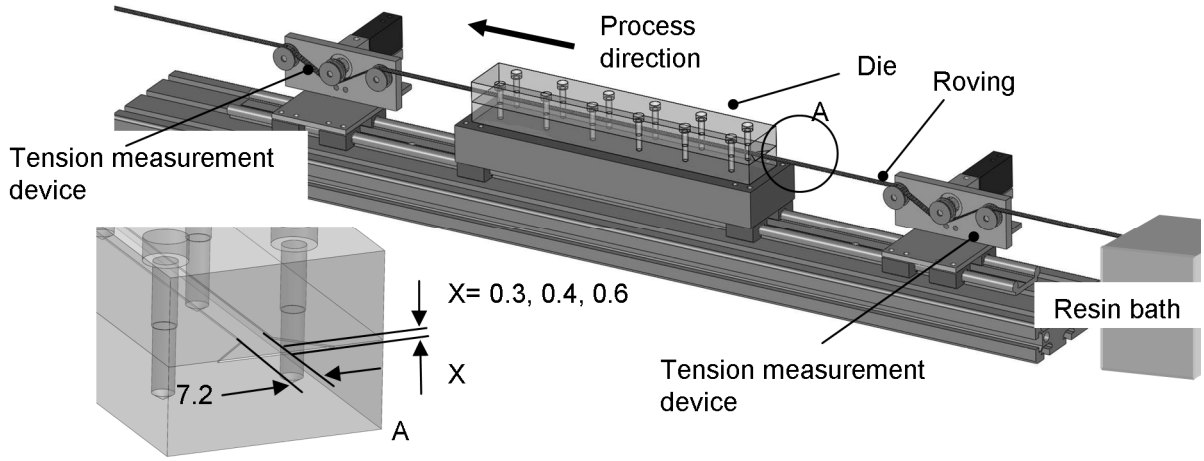

Figure 5.15: Experimental set-up for the validation of the viscous drag.

Figure 5.16 illustrates exemplary a raw data set collected by the experimental set up. On the left diagram it can be seen that the roving speed was increased in steps of 20 sec. The instability of the tension signal measured by pulling speeds higher than 8 m/min can be attributed to the fiber slip on the spool during unwinding, to the absence of tension damper on the creel and to the presence of twists in the roving. In order to further process the results the average tension value for every velocity step was calculated and plotted in a speed-tension diagram. The same procedure was followed for the tests where the pretension was gradually increased whereas the speed was kept at constant level.

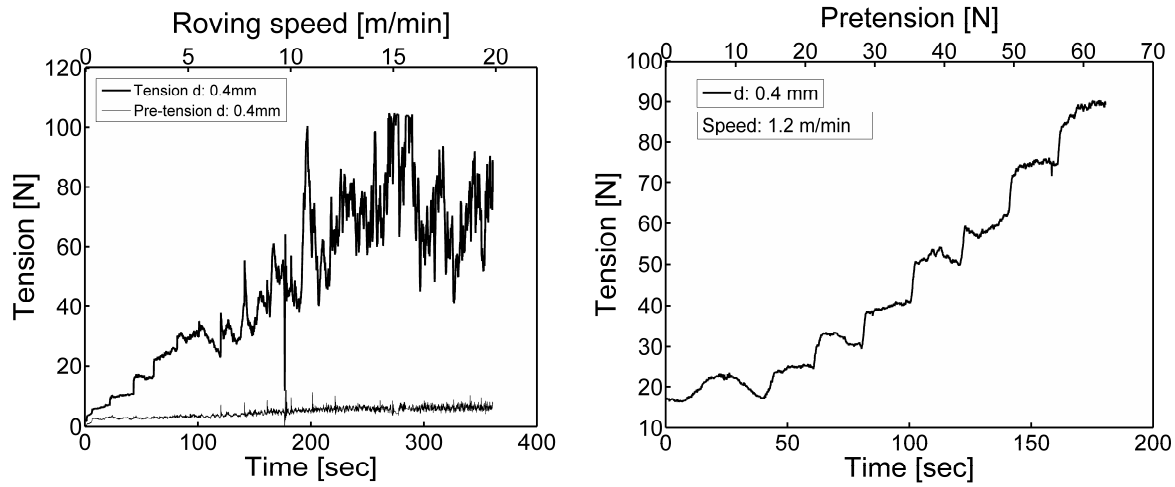

Figure 5.16: Raw experimental data Left: Tension signal during step wise increase of the roving speed. Right: Tension signal during step wise increase of the pretension.

In order to extract the right conclusions from the experimental results, the increase of the roving tension had to be analyzed in correlation with the tension-compaction behavior of the roving. During the experiment the pulling speed increases causing higher shear rate and thus higher fiber tension. On the other hand, as shown in Chapter 5.2 the increase of the roving tension leads to a higher compaction of the fibers. As the fibers are getting more compacted, the overall dimensions of the roving decrease leading to an increase of the film thickness. This trade off between pulling speed, tension and shear rate had to be taken into account during the analysis of the experimental results. Figure 5.17 shows a schematic representation of the effective resin film thickness is given for the case where the roving is separated for the die wall as well as for the case is in contact with the cavity.

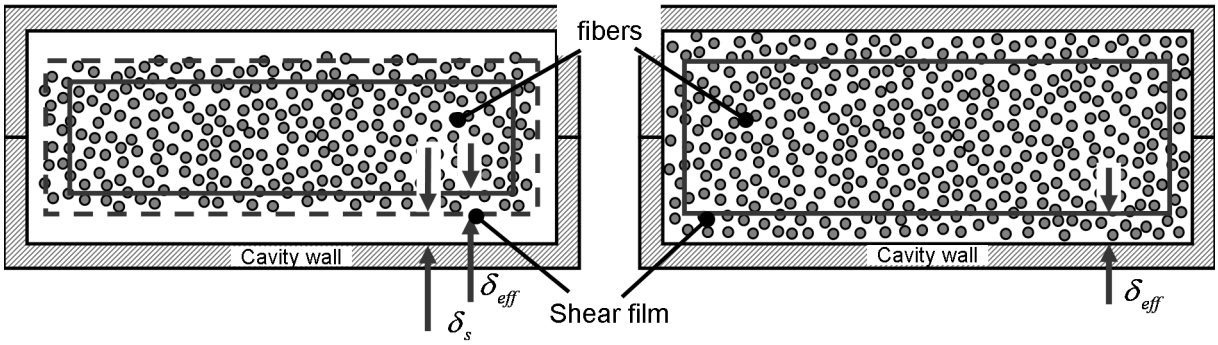

Figure 5.17: Schematic representation of the cross section of the roving inside the experimental set up. On the left side a case where the roving is not in contact with the wall. On the right side a case where the roving is in contact with the cavity wall.

A numerical simulation of the experiment that incorporates the different phenomena was developed. The differential increase of the tension over the length l of the die was calculated according to Equation (5.11). In the present study only the resin shearing between roving and top and bottom die surface was taken into account. Due to the great aspect ratio of the die cross section, the resin shearing with the vertical walls was not taken into account. The term C_f was used in order to couple the Coulomb friction phenomena that occur inside the die due to the contact of single filaments with the die wall. The term was defined through experiments with dry rovings. The value of C_f was kept constant for all processing speeds. Equation (5.12) expresses the total shear film thickness. The shear film inside the roving is given by the

term δ_{eff} and was set to $\sqrt{K}$ according to the Equation (4.17). The term δ_s expresses the shear film created by the distance between roving and cavity wall. The value of δ_s was calculated by taking into account the die cross section and the fiber volume fraction of the roving.

$$\frac{dT}{dl} = 2\eta \frac{U}{\delta_{tot}} W + C_f \tag{5.11}$$

$$\delta_{tot} = \delta_s + \delta_{eff} \tag{5.12}$$

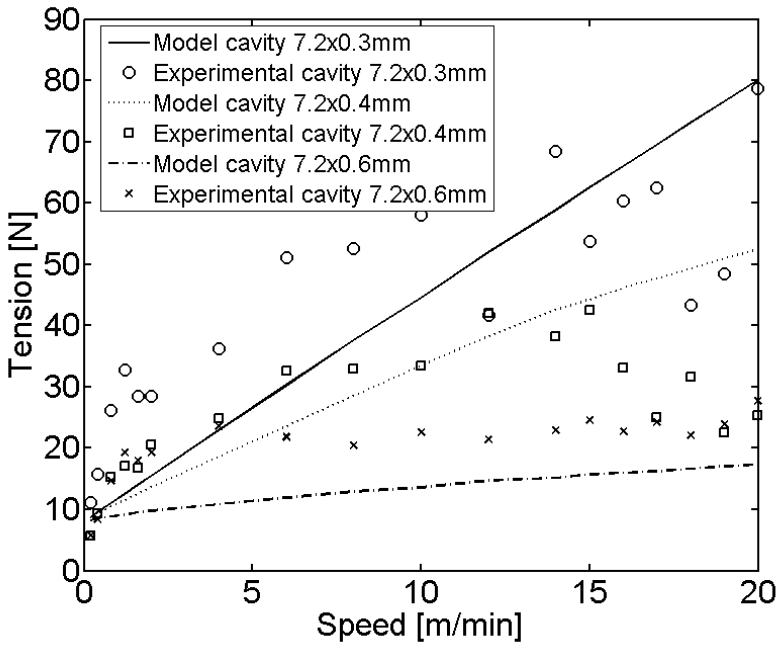

Figure 5.18: Comparison between experimental and modeling results for the validation of the viscous drag.

Equation (5.11) was solved numerically using the explicit Runge-Kutta solver ode23 of the MATLAB® computing environment. The pretension acting on the roving during the experiment was given as initial condition. Within every step of the solution the fiber volume fraction of the roving was calculated according to the Equation (4.2). A logical evaluation has controlled if the roving has separated from the die wall due to the fiber compaction. The logical evaluation was based on the comparison of the die‘s cross section area with the theoretical cross section area of the roving. The ar-

ea of the roving was calculated by taking into account the fiber volume fraction. In the case of a separation the distance between roving surface and die wall (δ_s) was calculated. The total film thickness (δ_{tot}) was calculated according to Equation (5.12).

Figure 5.18 presents the experimental results of the first test compared with the developed model. It can be seen that the theoretical lines follow the trend of the experimental data points. Both model predictions and experimental results are in the same order of magnitude.

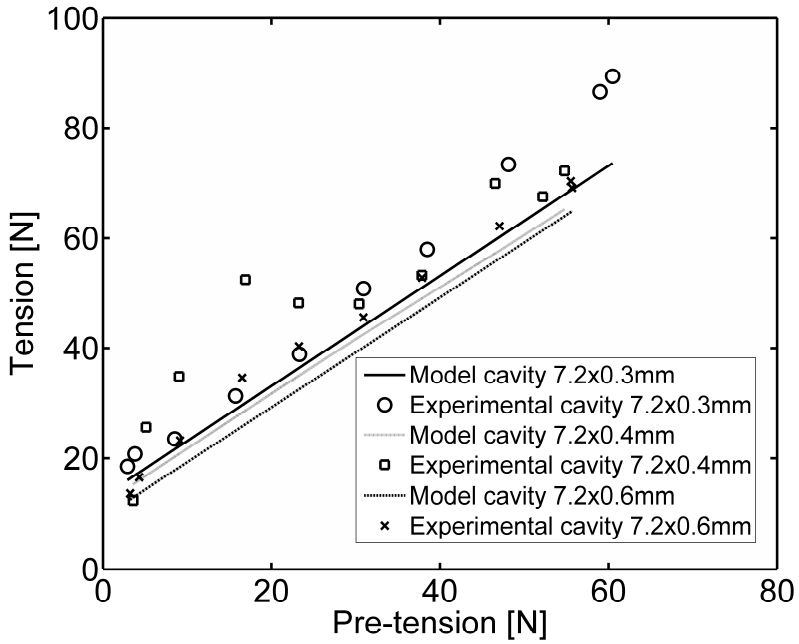

Figure 5.19: Comparison between experimental and modeling results for the validation of the viscous drag. Roving speed was set at 1.2 m/min.

The results reveal that the smaller the cross-section of die the higher the roving tension will be. This can be explained from the fact that for a smaller cross-section the fiber volume fraction is higher resulting to a lower permeability and thus to a smaller film thickness and higher shear rate. The constant value of C_f that was used for all cross sections can explain the slight mismatch between experimental values and model results for case of the 7.2 x 0.3 mm^2 cross-section. In higher degree of compaction, the fibers are expected to come more often in contact with the die wall producing higher Coulomb friction which was not taken into account in the present anal-

ysis since the term C_f in Equation (5.11) was kept for all cases constant. In the case of the 7.2 x 0.6 mm^2 cavity it was found that the tension does not increase significantly relevant to the pulling speed. This can be attributed to the separation of the roving from the die wall. The trade-off between tension, compaction and shear rate leads to a balancing of the developed tension. The same phenomenon can be noticed for the 7.2 x 0.4 mm^2 cavity for speeds and tension values higher than 15 m/min and 40 N respectively.

Figure 5.19 presents the comparison between experimental results and model predictions for the experimental set-up with constant pulling speed and gradually increased pre-tension (spool brake). Model and experiment come into agreement and according to the results there is a linear relation between tension and pretension. In order to highlight the effect of the spool brake on the further tension development, Figure 5.20 presents the increase of the tension (tension minus pre-tension) in dependence on the pre-tension.

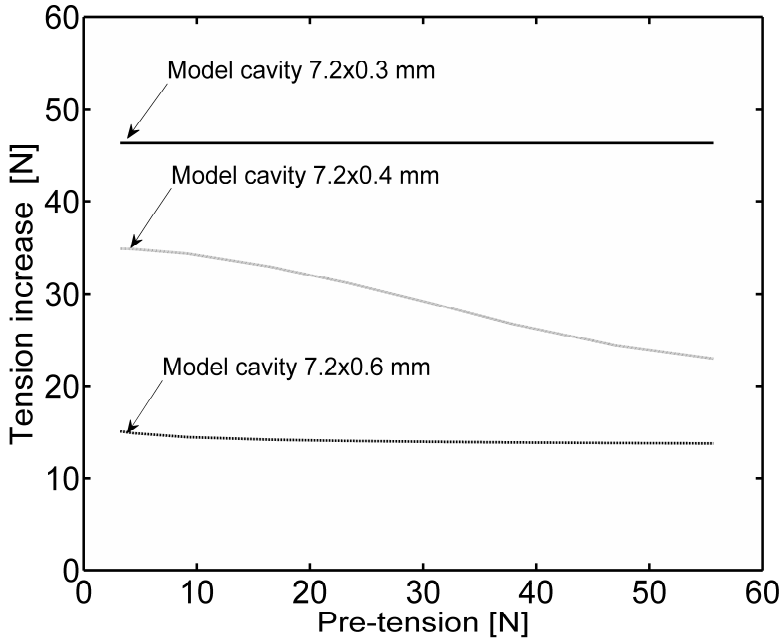

Figure 5.20: Model predictions for the increase of the tension due to the viscous drag in dependence to the pretension.

According to the model predictions for the cases of the 7.2 x 0.3 mm^2 and 7.2 x 0.6 mm^2 cross-section and a roving pulling speed of 10 m/min the tension increase remains constant and independent from the pretension. In the case of the 7.2 x 0.3

mm^2 the roving is so highly compacted that the pretension increase has no influence on the permeability. On the other hand, in the case of 7.2 x 0.6 mm^2 die the roving separates from the die wall due to the tension. According to the results, as long as the roving separates for the die the influence of the compaction degree has not any drastic effect on the magnitude of the tension increase since $\delta_s >> \delta_{eff}$. In the case of 7.2 x 0.3 mm^2 die the influence of the pre-tension on the tension increase is clearer. The increase of the roving pretension has an influence on the compaction grade of the roving which results to a slow separation from the die wall. The separation from the die wall leads to the increase of the film thickness and to a reduction of the tension increase.

Based on the above results and due to the agreement of the model with the experimental results it can be concluded that the effective thickness of the shear film δ_{eff} inside the roving as described in Chapter 4.6 and in Figure 5.17 is in the $\sqrt{K}$ order of magnitude as suggested by Gibson in [49]. This relation will be used for the further modeling of the impregnation process under the framework of the present study.

6. Impregnation model

Chapters 4 and 5 presented the main physical phenomena that take place during the impregnation process. Moreover in order to analyze the impregnation process and extract conclusions about the efficiency of the process a global impregnation model is essential. The impregnation model has to incorporate all the physical interactions, has to take into account all process relevant variables and has to give output data that can help the user to fully understand and improve the process.

Figure 6.1 illustrates the correlation between the different process parameters and variables. As shown, the input parameters have a direct impact on the “primary parameters” and an indirect impact on the output parameter which is the resin flow. The diagram reveals the complex relation between the single parameters. As shown a lot of parameters have a retrospective behavior making it very difficult to find a clear one way correlation between the actions of every parameter.

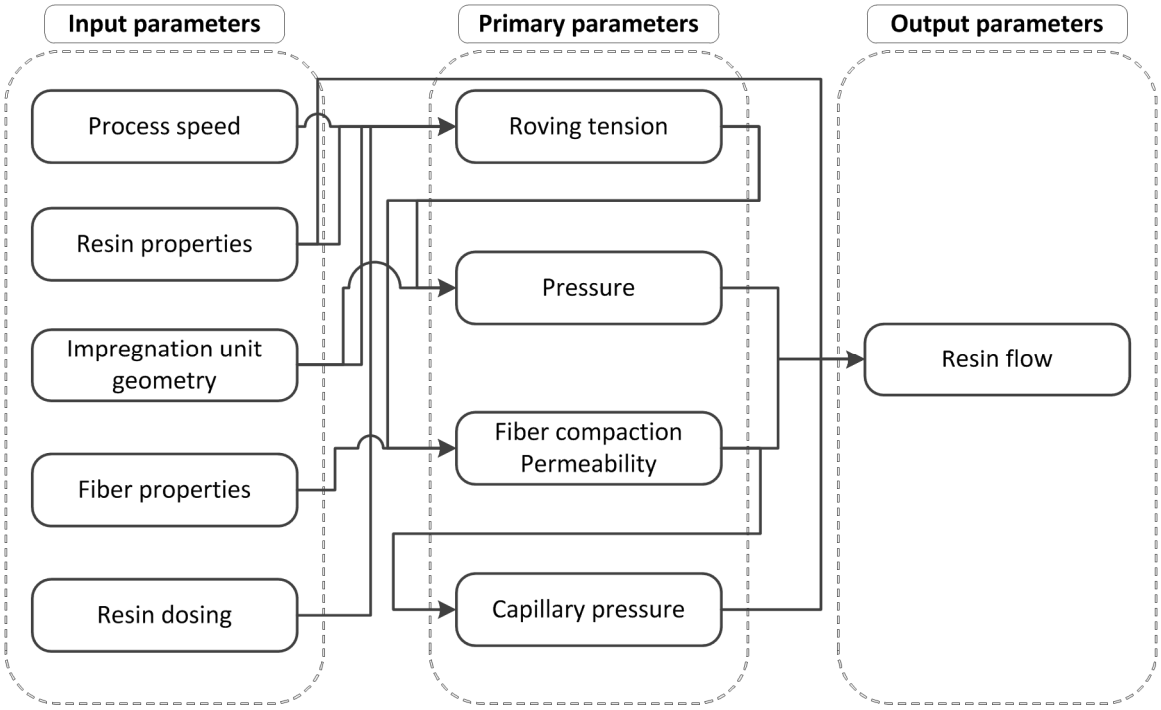

Figure 6.1: Interactions between the different parameters of the impregnation process.

6.1. Numerical formulation and computer simulation

The roving tension plays a major role since it couples most of the process parameters. In order to calculate the roving tension the Equation (4.13) has to be solved. This can be done by a numerical solution algorithm and by applying the correct boundary conditions.

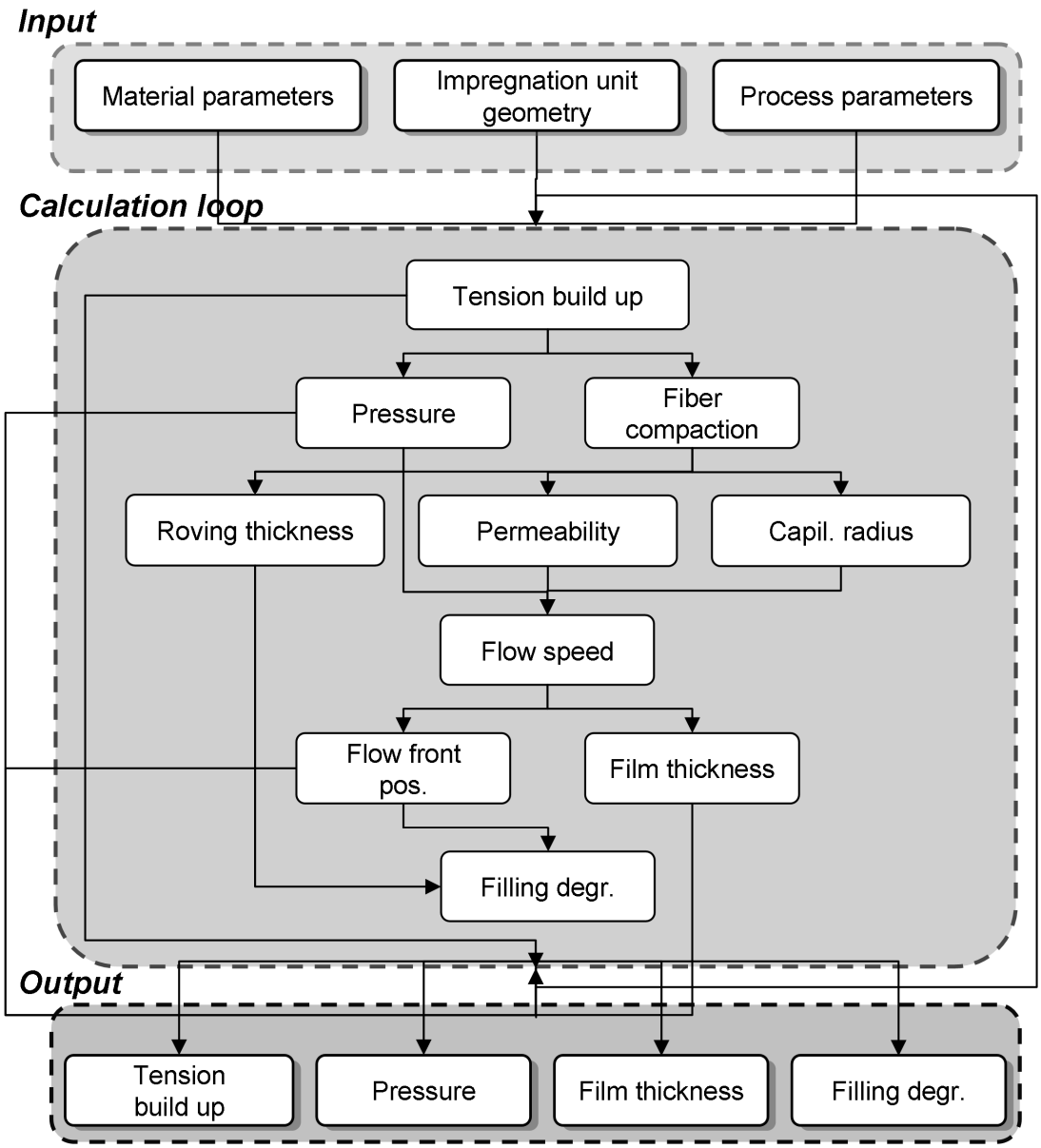

Figure 6.2: Calculation scheme of the impregnation process.

Under the framework of the present study the Equation (4.13) was solved by using the explicit Runge-Kutta (4,5) algorithm *ode45* of the MATLAB® computing environ-

ment. The boundary conditions for the initial tension and the total roving deflection were set according to the winding process set up and the impregnation unit geometry. The time step of the solution was chosen in order to achieve the necessary accuracy. After every solution iteration the values of the primary and secondary parameters were calculated and the Darcy equation (Equation (4.4)) was solved. After updating the parameter values and setting the new boundary conditions the solution proceeded to the next time step. The exact code of the simulation tool is given at the appendix.

Figure 6.2 presents the flow chart of the solution algorithm. The calculation starts with all the necessary inputs for the solution parameters followed by the calculation loop. In the end the results are exported for further analysis. Since the impregnation unit consists of more than one curve the Equation (4.13) has to be solved for every curve of the impregnation unit. The equation is solved independently and the output data is used as input for the boundary conditions of the next curve. Moreover since the curvature of the cavity alternates the coordinate system that is used for the calculation of the flow front position has to be respectively reversed.

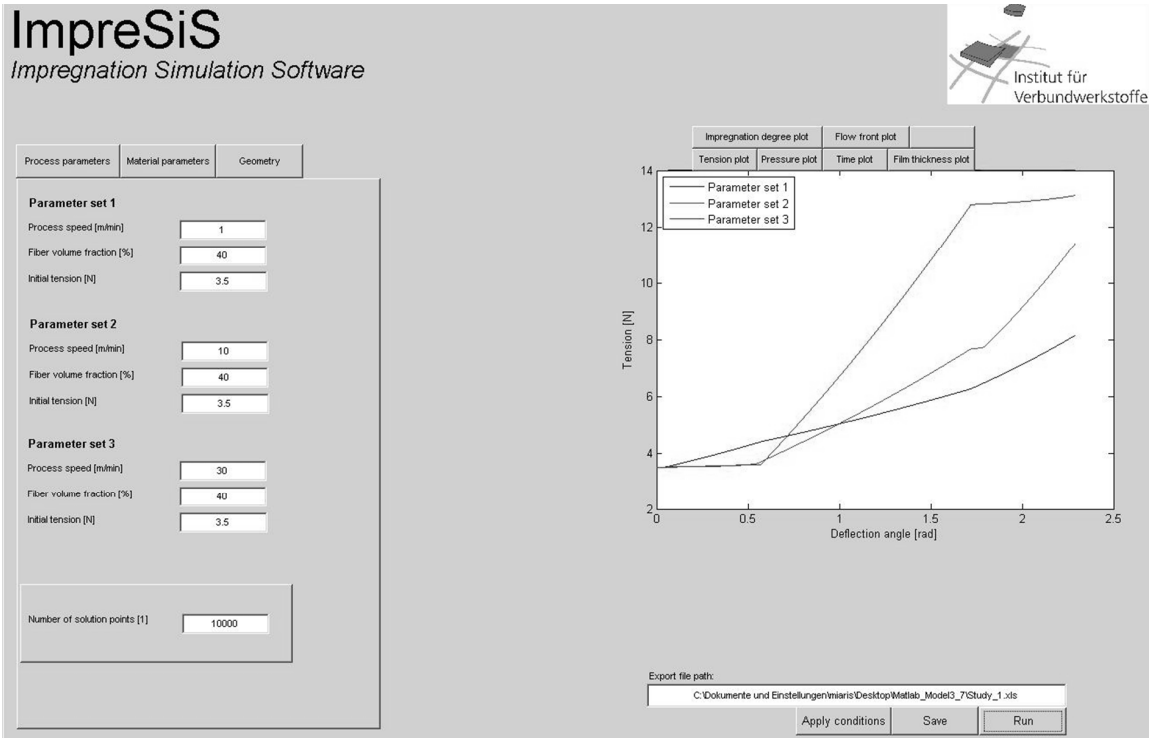

Figure 6.3: Main input menu (Graphical User Interface - GUI) of the developed impregnation simulation software.

Figure 6.3 illustrates the main input interface of the developed simulation software. The interface incorporates all the functionalities of the software in a single panel with multiple tabs. The input fields are placed in the left side of the panel whereas the output on the right side. The input is organized in three sub-menu tabs (Figure 6.4). Through the process parameter tab the user can define three different set values as process speed, fiber volume fraction and initial tension. The material constants and the material properties as described in Chapter 4 are set in the material parameters tab. Through the geometry tab the user can define the radius and the arc length of every curve of the impregnation unit.

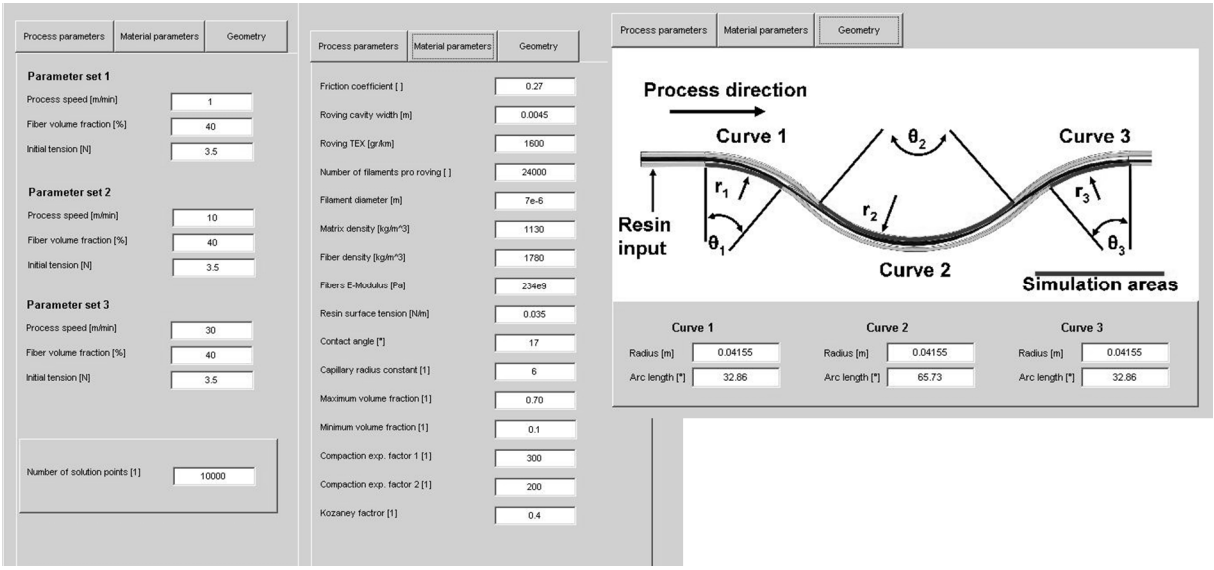

Figure 6.4: Graphical user interface input tabs.

After applying the material parameters and the boundary conditions thought the apply conditions button, the user can choose the path to save the results and run the solution. The time for the solution can vary between 1 and 15 min depending on the chosen number of solution data points and the available computer power. Once the simulation problem is solved the user is able to choose the results he wants to plot on the right side of the panel. For a further analysis the complete results together with the input parameters are exported into a spread sheet format file (e.g. MS Excel) at the previously chosen path.

7. Model validation

The comparison between experimental results and simulation predictions is essential for the validation of the calculation module. In order to extract plausible conclusions about the accuracy of the model it is important to choose the right validating parameters. The importance of the roving tension force has been extensively analyzed in the previous chapters. The roving tension couples the major processing parameters and acts as the driving force of the impregnation. During the process the tension can be easily measured before and after the impregnation unit. The degree of impregnation is another very important parameter. The impregnation degree can be defined as the percentage of the roving volume which is filled with resin. It can be easily understood that for every impregnation process the goal is to reach an impregnation degree of 1.0 that is equal to 100%. Nevertheless the measurement of the impregnation degree is not a straight forward procedure with the state of the art equipment. The easiest way to measure the impregnation degree is to examine impregnated rovings after resin curing.

7.1. Experimental Set-up

The experimental set-up for the validation of the impregnation model is based on a filament winding process. Figure 7.1 illustrates the basic components of the set-up. During the winding process the roving pulling speed (winding speed) was set by the CNC control of the winding machine. The resin was dosed under predefined conditions and the dosing rate was continuously logged. In order to do so, the resin was premixed in a pot which was placed inside a pressurized vessel. The metering rate was controlled by a pressure regulator. In order to log the resin flow, the system was placed on an electronic balance. The pretension of the roving was adjusted by the mechanical brake of the creel and it was also continuously logged by a tension measurement device. The tension force that was generated by the impregnation process was measured by a second tension measurement device that was placed directly after the exit of the impregnation unit.

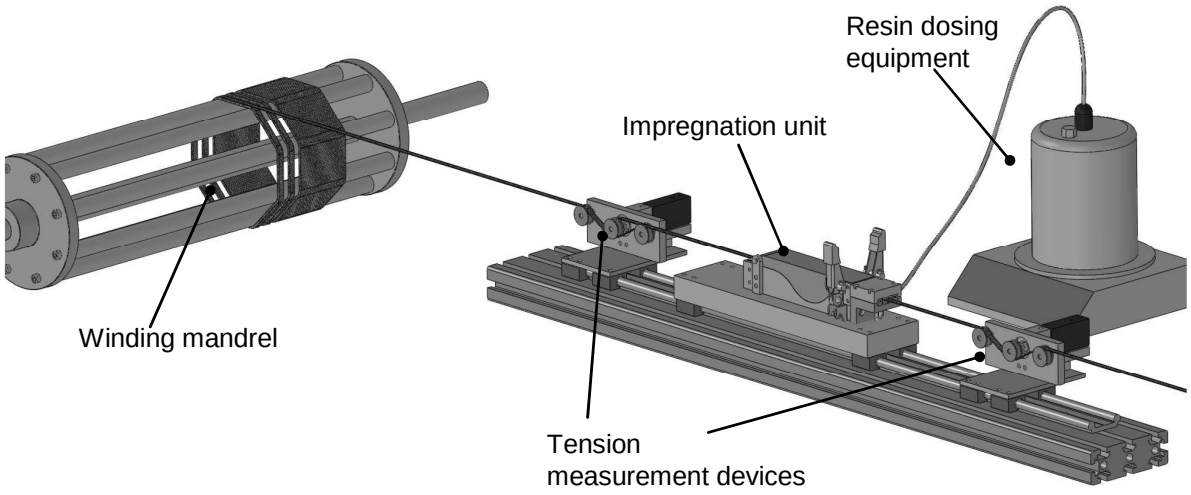

Figure 7.1: Schematic diagram of the experimental set-up for the validation of the impregnation simulation software.

In order to examine the impregnation quality and the impregnation degree an octagonal modular winding mandrel was used (Figure 7.2). This type of mandrel prevents any through the thickness compaction of the rovings which would have an influence on the impregnation state while it keeps the fluctuation of the roving speed on a low order of magnitude. So as to produce the needed samples, a start-up laminate was initially wound and by the time that the steady state situation was reached a spiral path was wound in order to produce the actual sample. During winding of the impregnation quality samples the tension measuring devices were demounted from the rack in order not to influence the impregnation state of the roving. After curing the straight samples between the rods of the mandrel were prepared for microscopical analysis.

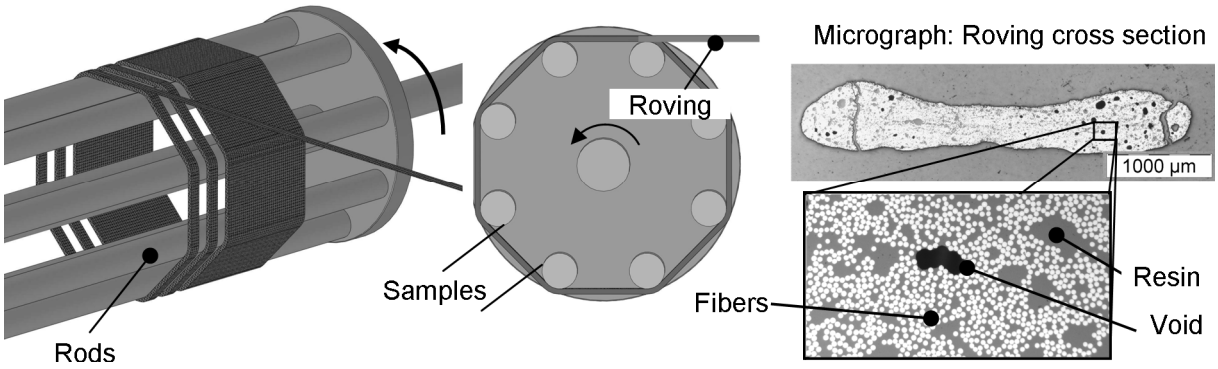

Figure 7.2: Schematic diagram of the octagonal mandrel used for the validation of the impregnation quality.

7.2. Parameter study

A parameter study has been performed in order to evaluate the validity of the model in different processing conditions. The parameters that systematically varied were:

- Roving speed
- Resin weight fraction
- Roving pretension

Except the above mentioned parameters four different impregnation unit geometries were tested. Every unit implemented a PTFE tube for the formation of the impregnation cavity with identical cross section for all the designs. Two units had a single curve with a radius of 42.5 and 85 mm respectively. The choice of these radii values was based on preliminary test campaigns which have shown that impregnation units with curves radii between 40 and 90 mm are suitable for the processing of 24k CF rovings. The units with only one curve were chosen in order to highlight the influence of the radius on the processing parameters under clear defined conditions. One unit was designed with two curves of a 42.5 mm radius. This unit was chosen in order to explore the transition between alternate curves. The fourth impregnation unit had the typical siphon lay out identical to the one presented in chapter 3 and was chosen in order to highlight the ideal working window of the process.

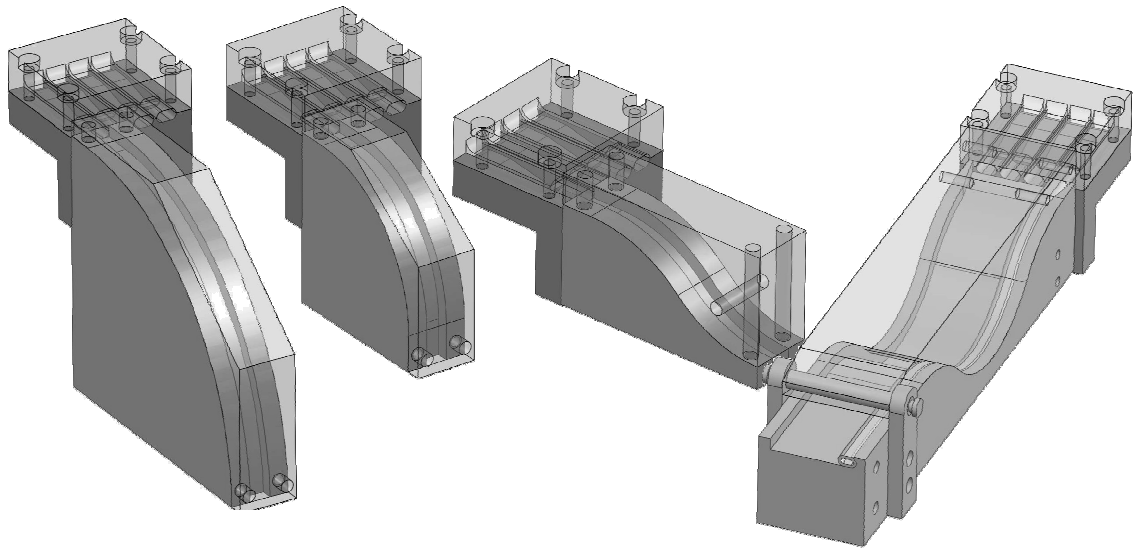

Figure 7.3: Schematic representation of the four impregnation units which were used for the validation of the impregnation model.

The diagram of Figure 7.4 presents the calculated resin flow for different resin weight fractions (RWF) and different roving speeds. The values are calculated for a single CF-24k roving having 1600 tex. The metering equipment which was used for the parameter study was found to have a precision of ±2 %.

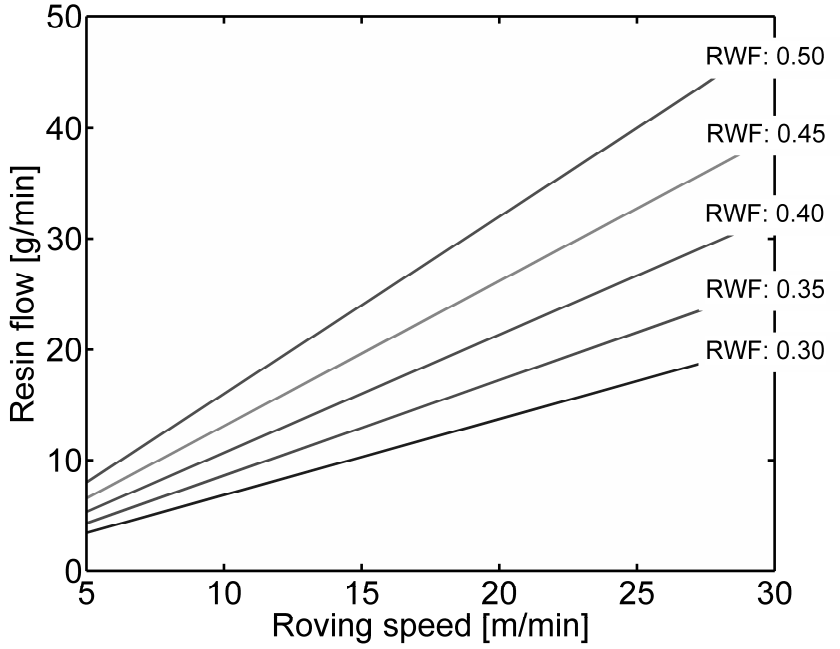

Figure 7.4: Resin flow according to roving speed and resin weight fraction set up.

In order to avoid the influence of the environment on the viscosity of the resin, all tests took place in a controlled working environment with temperature of 23℃±2℃. The same test procedure was followed for the complete parameters study concerning the preparation of the impregnation units the adjustment of the measuring equipment and the mixing of the epoxy resin.

8. Model results and discussion

8.1. Single curve impregnation unit geometry

Two impregnation units with a single curve were chosen for the initial validation of the impregnation model. The exact dimensions of the units are given in Figure 8.1. The test rig described in Chapter 6 was slightly modified in order to comply with the 90° shifted exit of the roving and used for the parameter study. The model results were generated with the software presented in Chapter 5.

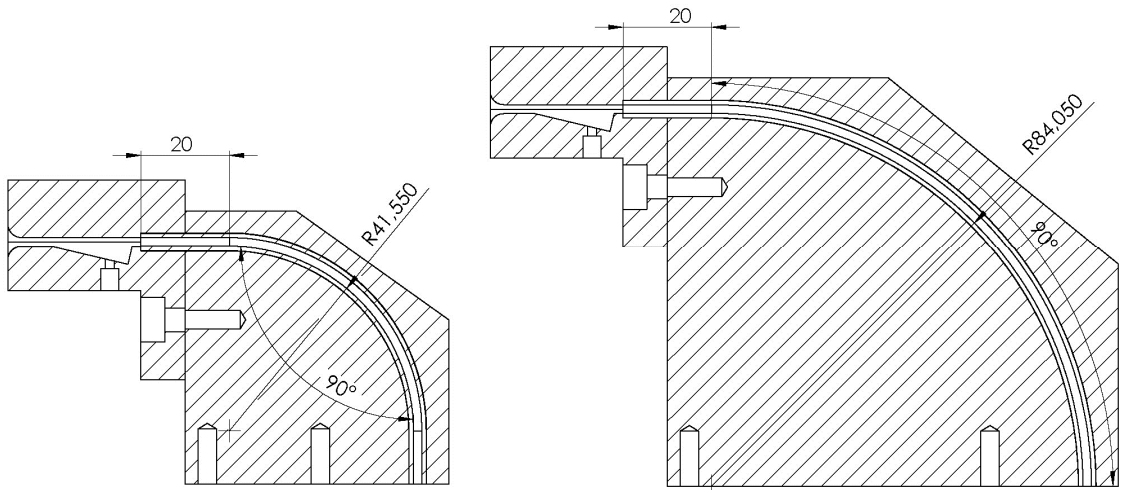

Figure 8.1: Left: Impregnation unit A1. Right: Impregnation unit A2.

8.1.1. Impregnation unit A1

Figure 8.2 illustrates the roving tension versus the roving speed for the case of the impregnation unit A1. The diagram presents the results for three different initial tension (pre-tension) set-ups. According to the diagram the model predictions come in agreement with the experimental results. As expected it was found that the pre-tension has a major influence on the order of magnitude of the generated tension. The slight mismatch between model and experimental results can be attributed to the fact that the resin injection box and the straight inlet of 20 mm were not taken into account in the model geometry. According to the model the tension does not increase monotonically over the roving pulling speed. In the case of the lowest pre-tension (1 N) it was found that the tension increases for speeds up to 15 m/min. After that point and for higher roving speeds the tension starts to gradually decrease. Simi-

larly for pre-tension of 5 N the roving tension reaches the maximum for a speed of 20 m/min and then starts slightly to decrease. On the other hand for the maximum pretension value (13 N) the model predicts a constant tension increase over the complete roving speed window.

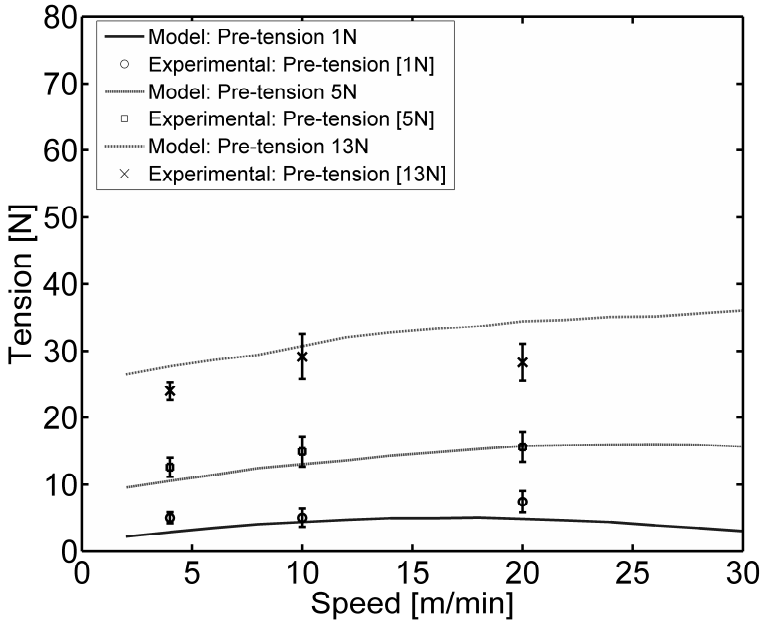

Figure 8.2: Roving tension vs. roving speed vs. Comparison between experimental and modeling results. Target value of the resin weight fraction was set at 45 % (s. Figure 7.4).

In order to explain the above described behavior one has to take into account the development of the tension and the absorption of the resin film over the length of the impregnation unit. Figure 8.3 presents the development of the tension along the cavity of the impregnation unit for three different processing speeds. The roving enters the impregnation unit with a pre-tension of 1 N. After an initial phase where the tension force increases on a very low rate follows a transition zone with a more gradual increase of the tension and finally a region where the tension increases almost linear. This behavior is common among the three speed set-ups. The difference lies on the position of the transition zone over the length of the impregnation unit. For the lower speed (4 m/min) the transition zone is located at an angle of 0.18 rad whereas for the case of 16 and 28 m/min is located further inside the impregnation unit at about 0.7 and 1.3 rads respectively.

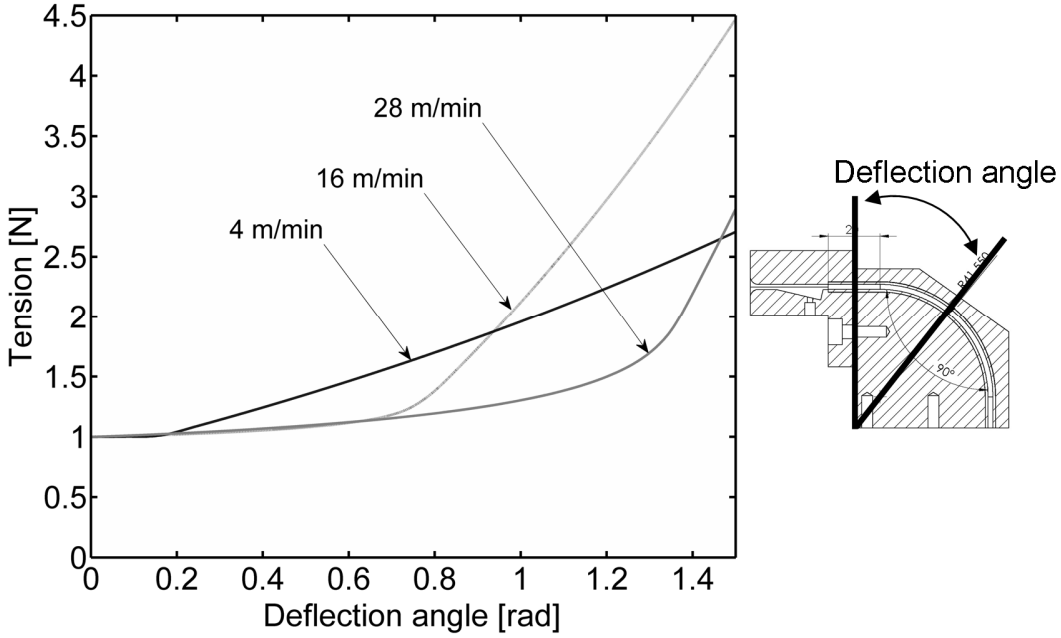

Figure 8.3: Roving tension vs. deflection angle. Target value of the resin weight fraction was set at 45 %. Initial tension was set at 1 N.

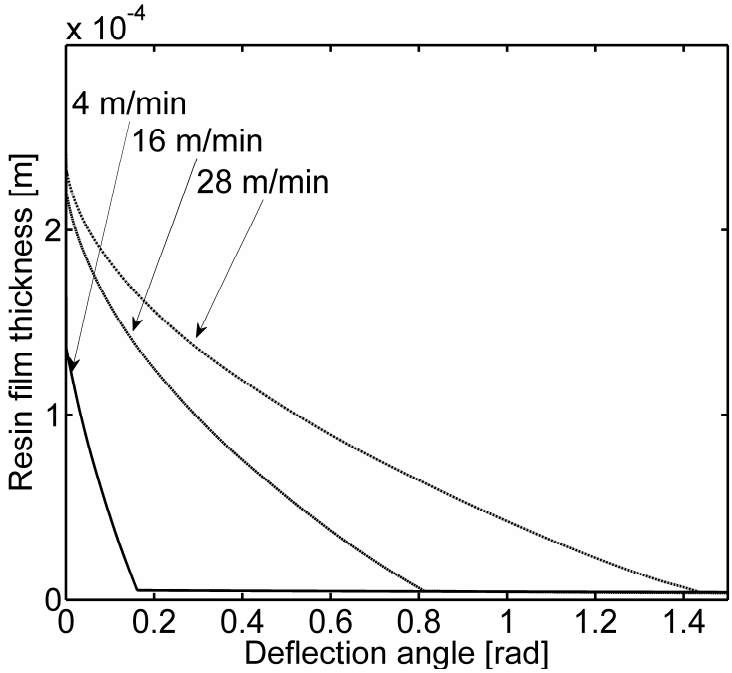

Figure 8.4: Resin film thickness vs. deflection angle. Target value of the resin weight fraction was set at 45%. Initial tension was set at 1 N.

The presence of the three different zones in the development of the tension can be explained by taking into account the diagram presented in Figure 8.4. The diagram presents the thickness of the resin film over the length of the impregnation unit. The

initial value of the film thickness is independent to the process speed. In this case and for a resin weight fraction of 45 % the film has an initial thickness of 0.244 mm.

As the process develops and the roving slides inside the unit the resin is absorbed and the film thickness decreases. The rate on which the resin film decreases is reversely proportional to the process speed. By comparing the two diagrams (Figure 8.3 and 8.4) it was found out that the tension transition zones are located in the region where the film thickness reaches its minimum value. Taking that into account one can make the following conclusions: At the beginning of the impregnation process the resin film thickness is relatively high resulting to low shear forces and thus to a moderate increase of the tension. Once the film has reached a critical thickness, shear forces start to develop and the transition zone is created. After the point that the film has reached the minimum value (s. Equation 4.24) the tension increases under a constant rate which can be affected only by the change of the compaction of the roving.

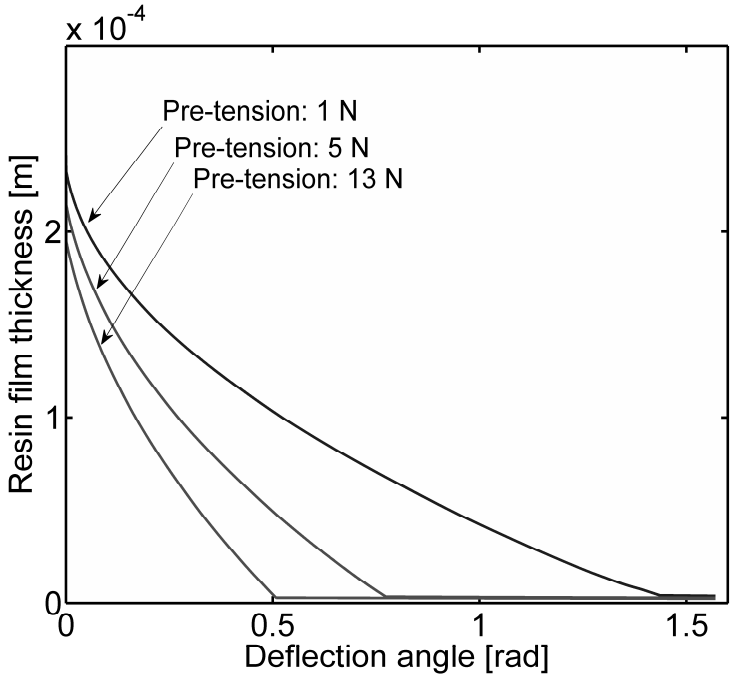

Figure 8.5: Resin film thickness vs. deflection angle. Target value of the resin weight fraction was set at 45 %. Roving speed was set at 28 m/min.

According to the above, the paradox of the lower tension values for higher processing speeds (Figure 8.2) can be explained by the different rates on the absorption

of the resin film. Under lower roving speeds the resin film is quickly absorbed but the shear rate is low due to the low speed. In average speed set-ups the film is relatively quickly absorbed and the higher shear rate leads to the maximization of the shear forces. On the other hand, on the even higher speed set-ups a thick resin film is present over the complete length of the impregnation unit resulting to low shear rates and forces. This phenomenon fades with the increase of the pre-tension since the higher initial tension leads to higher hydrostatic pressure and thus quicker impregnation and reduction of the length of the resin film (Figure 8.5).

8.1.2. Impregnation unit A2

Figure 8.6 presents the model predictions for the development of the roving tension in dependence on the roving speed for the impregnation unit A2. According to the diagram the model results come into agreement with the experimental measurements. The difference between model and experimental results for the case of high initial tension (14 N) and for speeds higher than 10 m/min are attributed to an underestimation of the roving's compaction. The model predicts low compaction and high permeation of the roving which leads to an overestimation of the generated tension.

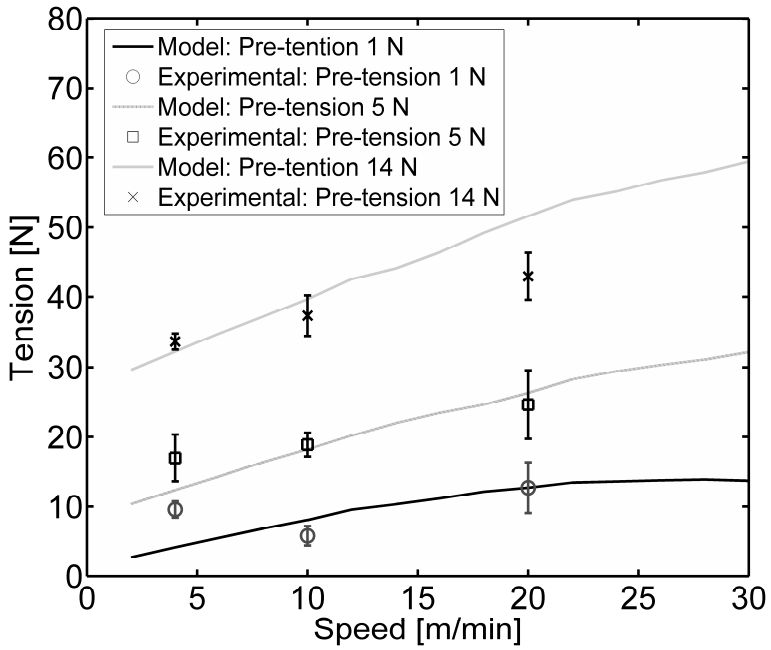

Figure 8.6: Roving tension vs. roving speed. Comparison between experimental and modeling results. Target value of the resin weight fraction was set at 45%.

The model predictions for pre-tension values of 1 N (Figure 8.6) show the same trend as in the case of the impregnation unit A1. Again the non-increase or the decrease of the roving tension at higher speeds is explained by the slower absorption of the resin film.

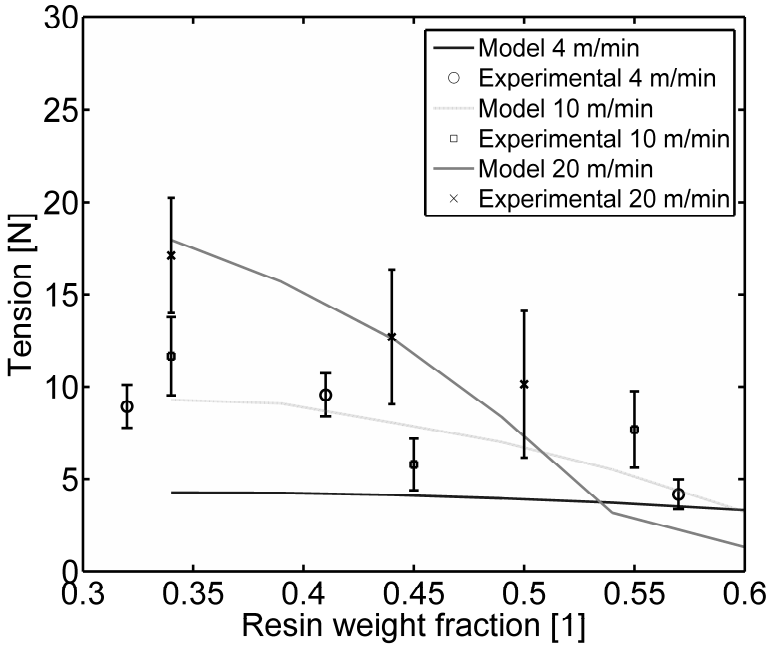

Figure 8.7: Roving tension vs. resin weight fraction. Comparison between experimental and modeling results. Initial tension (pre-tension) was set at 1 N (for detailed information about the resin metering s. Figure 7.4).

The resin weight fraction (RWF) is controlled directly by the resin dosing rate. In order to change the set value of the RWF, the volume of resin that enters the unit has to increase or decrease respectively. Figure 8.8 presents the effect of the variation of the RWF on the development of the resin film for a roving speed of 20 m/min. The initial thickness of the resin film increases proportionally to the resin dosing rate. For a given roving speed the roving needs a longer impregnation path in order to fully absorb a resin layer with higher thickness. This is the reason for the reduction of the generated tension with the increase of the dosed resin. According to the diagram presented in Figure 8.8 any set value of the RWF higher than 0.54 (target fiber volume fraction 0.35) would lead to an incomplete absorption of the resin film. This prediction of the model was experimentally confirmed by resin flowing out of the exit of the impregnation unit for the given processing parameters. The incomplete absorp-

tion of the resin film is responsible for the steep change of the 20 m/min tension curve in Figure 8.7. Since for RWF higher than 0.54 the fibers of the roving do not come into contact with the cavity of the impregnation unit the shear forces are on low range of magnitude and there is no development of coulomb friction.

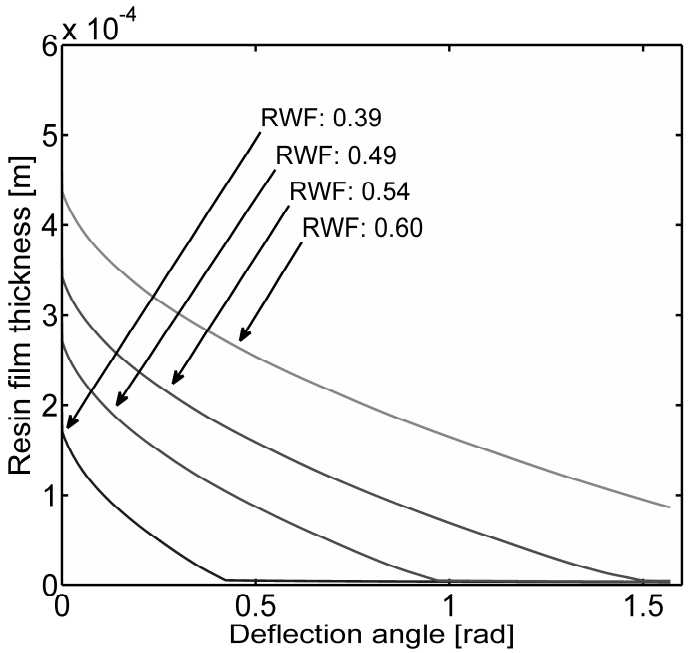

Figure 8.8: Resin film thickness vs. deflection angle. Roving speed was set at 20 m/min.

8.1.3. Comparison between impregnation unit A1 and A2

The impregnation units A1 and A2 have the same design. The only difference between the two units is the radius of the cavity. The modeling results have been compared in order to highlight the influence of the curve radius on the impregnation process. According to the Equation (4.8), the radius of the cavity and the roving tension force has a direct impact on the hydrostatic pressure in the resin underneath the roving. Figure 8.9 illustrates the development of tension and pressure inside the impregnation units A1 and A2. The boundary conditions (initial tension, speed and RWF) were kept the same for both units. According to the diagram, the impregnation unit A2, which has bigger curve radius than unit A1, generates a higher tension force for the same deflection angle. The effect of the curve radius and despite the higher tension force is that the developed pressure field inside the unit A2 is lower than this inside the unit A1. The magnitude of the pressure on the pressure film is determinant

of the resin flow through the roving.

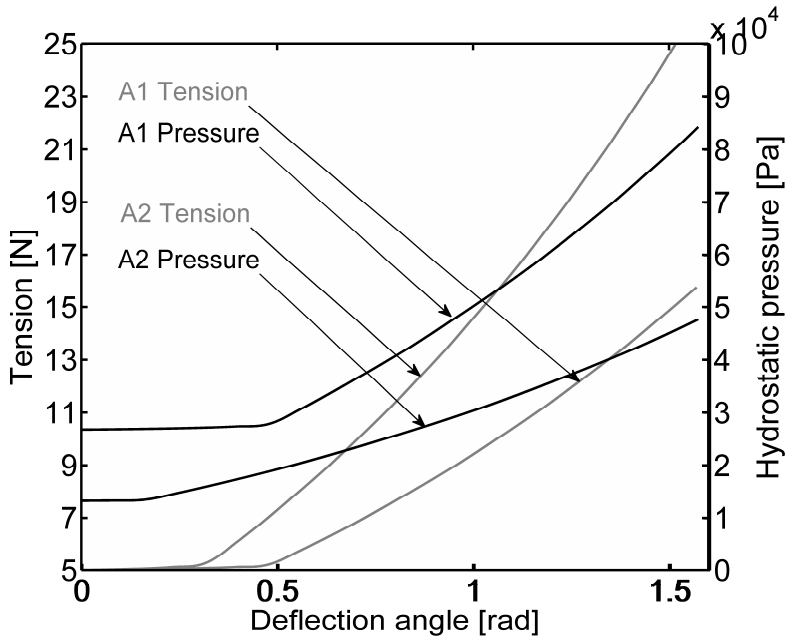

Figure 8.9: Development of the roving tension force and of the hydrostatic pressure over the deflection angle for the impregnation units A1 and A2. Roving speed was set at 20 m/min, initial roving tension at 5N and RWF at 0.45.

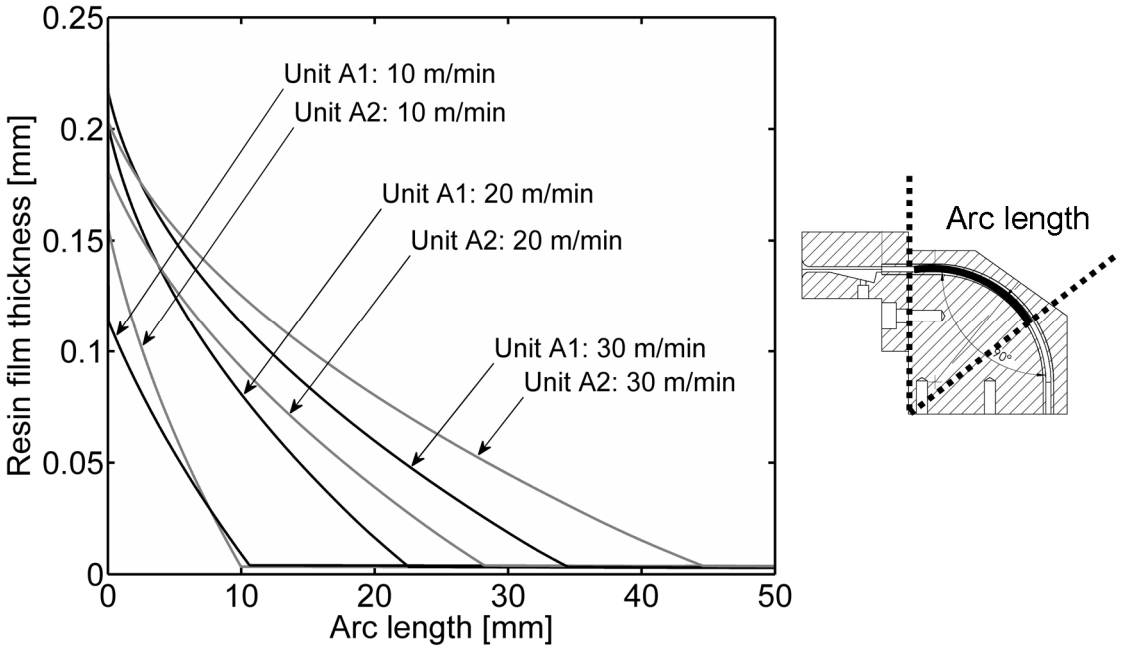

Figure 8.10: Resin film thickness vs. arc length. Initial tension was set at 5 N and RWF at 0.45.

Figure 8.10 presents the absorption of the resin film for three different roving speeds inside the two impregnation units. The model predicts that the roving, so as to completely absorb the resin film, needs a longer arc length inside the impregnation unit A2 than inside the unit A1. Moreover it was found that the difference between the two impregnation units concerning the required arc length increases respectively to the increase of the roving speed.

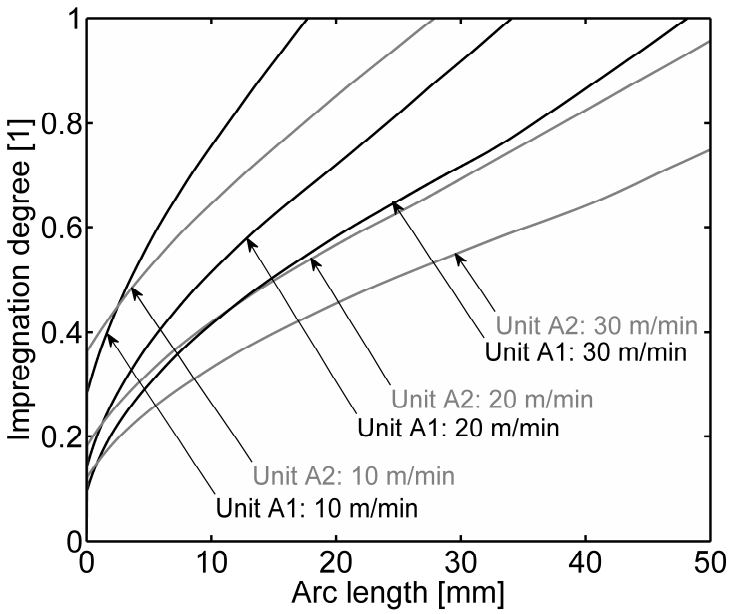

Figure 8.11: Impregnation degree vs. arc length. Initial tension was set at 5 N and RWF at 0.45.

Figure 8.11 illustrates another effect of the cavity radius. The diagram presents the increase of the impregnation degree of the roving over the length of the two impregnation units. The impregnation degree expresses the volumetric percentage of the roving which is completely filled with resin. In all cases it was found that the roving reaches a fully impregnated state faster inside the A1 than inside the A2. By comparing the diagrams of the Figures 8.11 and 8.12 it was established that the roving reaches the full impregnated state considerably after the point on which the resin film was fully absorbed. This phenomenon can be explained by taking into account the fact that the resin may has been completely absorbed but if the roving is not in a sufficient compacted state the absorbed resin will not be able to fill up the total free volume of the roving. In this case the roving can reach the complete impregnated state only if it is further compacted and get the set value of fiber volume fraction. That is a

so-call consolidation step.

Based on the above it can be concluded that the radius of the impregnation unit determines the efficiency of the impregnation process. The optimum for an impregnation process is to impregnate the roving in the smallest possible angle and with the minimum tension development. The factor X_{ef} (Equation (7.1)) is an evaluation factor for the design of an impregnation unit.

$$X_{ef} = \frac{1}{\left|\theta_i(r) - \lambda_i^2(r)\right|} \tag{7.1}$$

The value of the factor depends on the radius of the cavity (r). The term $\theta_i(r)$ stands for the normalized (to the maximum value) deflection angle on which the roving is fully impregnated for a certain speed and resin weight fraction. The term $\lambda_i(r)$ gives the normalized (to the maximum value) generated tension for the complete impregnation of the roving for a certain speed and resin weight fraction. The term $\lambda_i(r)$ was set on square since the deflection angle was considered as a more important design criterion than the lower tension development.

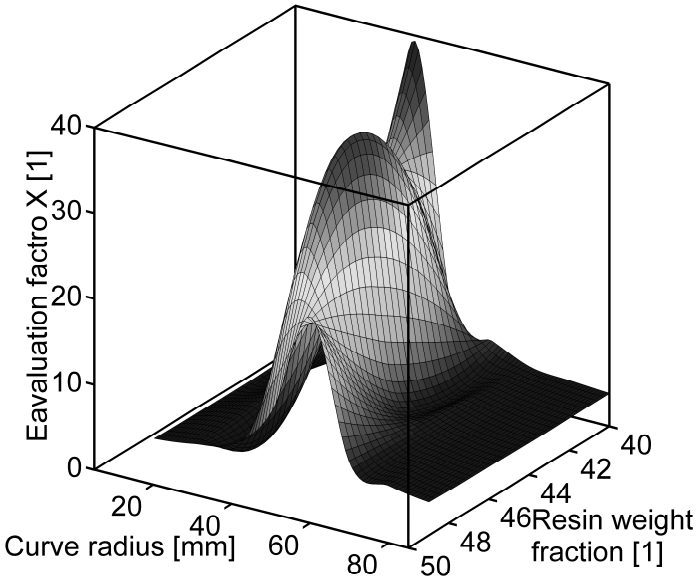

Figure 8.12: Design evaluation factor vs. cavity curve radius and resin weight fraction. The data is based on a process speed of 30 m/min initial tension of 5 N.

Based on Figure 8.12 it was found that for a process speed of 30 m/min the optimum radius of the impregnation unit would be in the order of 42 mm. According to the model such a curvature will fulfill the criteria of low deflection angle and minimum tension development on the most efficient way.

8.2. Double curve impregnation unit A3

The third impregnation unit used for the validation of the model was a unit with a cavity consisting of two curves. The lay-out of the unit A3 is presented in Figure 8.13. The curves of the cavity had a deflection angle of 45°. However, as shown by the dashed lines in Figure 8.13, the roving follows a tangential transition between the curves. Taking that into account, the effective arc length on which the roving lies on the cavity wall and hydrostatic pressure is developed is 32.86°. For the modeling of the impregnation process inside the unit A3 were taken into account only the areas where the roving is in contact with the cavity wall. The bottom sketch of Figure 8.13 shows the geometry of the impregnation unit as this was simulated by the developed software. In order to validate the results, the unit A3 has been implemented in the test rig presented in Figure 7.1 and an experimental campaign took place.

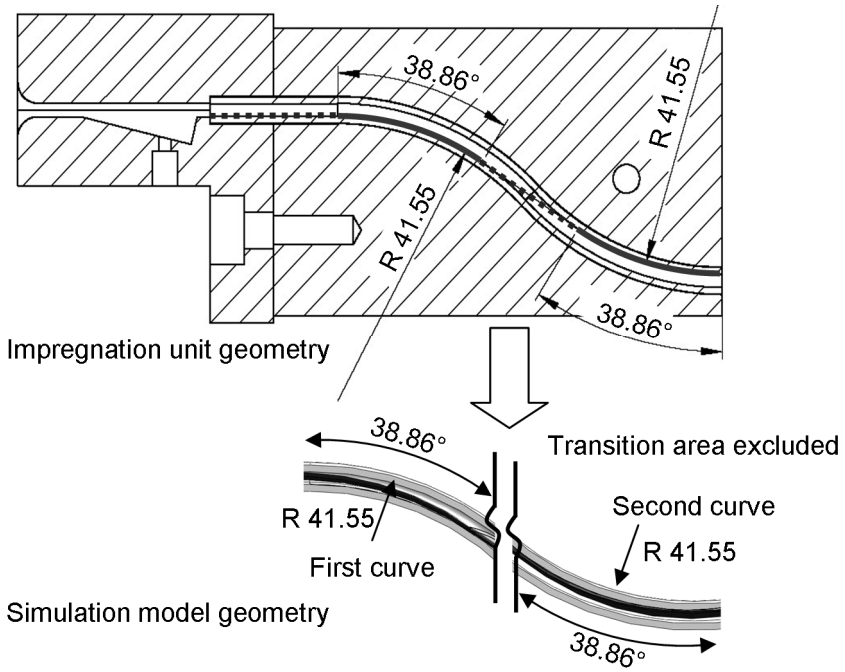

Figure 8.13: Section view of the impregnation unit A3 and schematic representation of the geometry used for the simulation of the impregnation process.

Figure 8.14: presents the predictions of the simulation tool. According to the diagram the software results follow the experimental data. The model predicts slight lower tension values compared to the experimental data. This phenomenon can be once again attributed to the fact that the software does not simulate the tension development taking place inside the injection box.

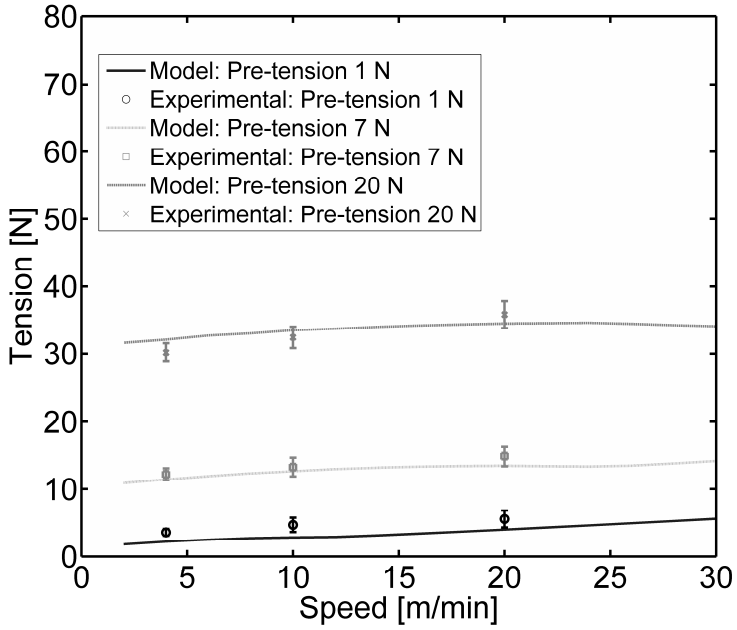

Figure 8.14: Roving tension vs. roving speed. Comparison between experimental and modeling results. Target value of the resin weight fraction was set at 45 %.

Figure 8.15 illustrates the development of the tension inside the unit A3 and in dependence to the roving speed. It was found that for higher processing speeds the rate of increase of the tension is not constant over the total length of the impregnation unit. Except to the initial entry region 0-0.2 rad in which the roving enters the cavity and the resin layer is thick there is another abrupt change in the tension development at about 0.6 rad. As highlighted by the Figure 8.15 this is associated with the transition of the roving between the two curves of the cavity. The roving passes from the first curve with the positive curvature to the second curve with the negative curvature. Due to this transition the boundary conditions which affect the generation of the tension force change significantly. The resin film that was present between cavity wall and roving over the first curve does not exist over the second curve. In the contrary the fibers come in direct contact with the cavity and therefore generate higher friction. Furthermore the resin film that is formulated on the surface of the second

curve has a minimum thickness which is described by the Equation (4.24). These new boundary conditions lead to the steep rise of the tension force over the second curve.

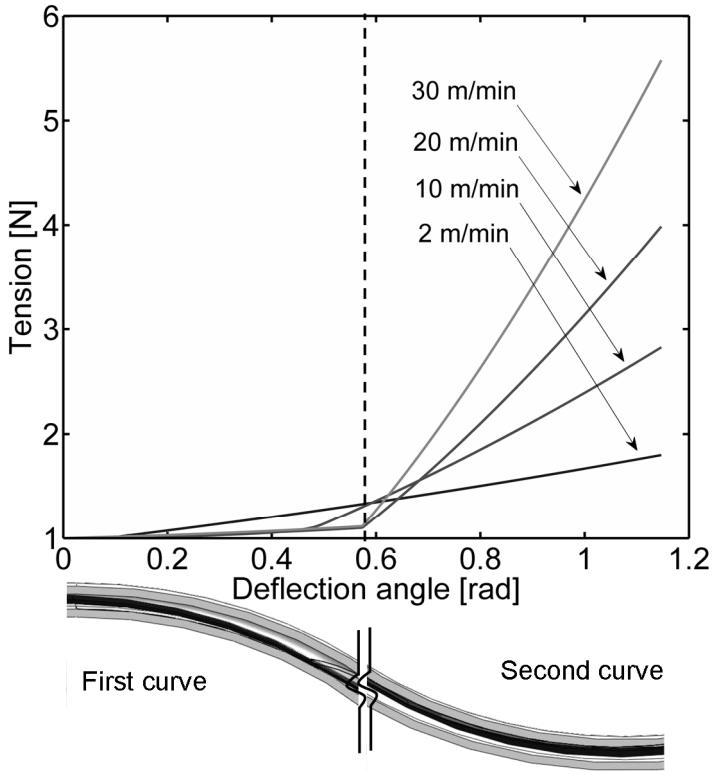

Figure 8.15: Tension development inside the impregnation unit A3. Initial tension was set at 1 N and RWF at 0.45.

Figure 8.16 presents the results concerning the absorption of the resin film and the evolution if the roving's impregnation degree inside the unit A3. According this diagram, for the applied processing parameters and for linear roving speeds up to 22 m/min, the entire volume of the resin film is absorbed over the first curve of the impregnation unit. As expected the impregnation degree increases proportionally to the resin film absorption. Nevertheless it was found again that the roving reaches the fully impregnated state after the point on which the resin film has been completely absorbed. The fact that the point where the roving is fully impregnated is not at the same point where the resin is fully absorbed can be explained by taking in to account the roving compaction. The resin is metered according to a certain volume fraction set point. If the roving has absorbed the total amount of resin, but the desired compaction has still not be reached, parts of the roving will be still not full of resin. These

will be eliminated only once the roving has reached the desired compaction grade.

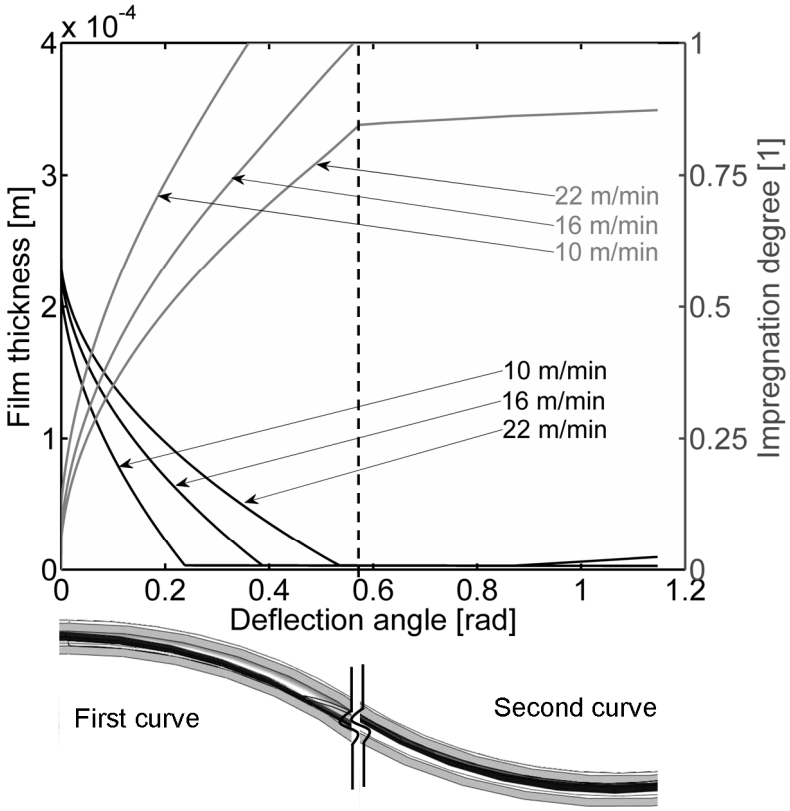

Figure 8.16: Film thickness and impregnation degree development inside the impregnation unit A3. Initial tension was set at 7 N and RWF at 0.45.

As shown in Figure 8.13 the second curve of the impregnation unit has a curvature opposite to the curvature of the first curve. That means that under ideal conditions this reversed curvature would initiate an opposite pressure field which could de-impregnate the roving. However this approach does not reflect the realistic processing conditions. In order to get a more realistic approximation on what really happens, the boundary conditions between roving and cavity wall have to be analyzed. In the case where the roving leaves the first curve in a not fully impregnated state, the roving will contact the second curve with dry fibers. Although that the tension force will generate a compaction pressure field on the fiber pack, the effect of the tension force on the resin pressure is assumed to be minimum. In this not fully impregnate state, the interface between cavity wall and roving will be rich of air pockets which will initially prevent the direct development of a hydrostatic pressure on the resin. Furthermore, even if the roving reaches the second curve fully impregnated it

is believed that the absence of a pre-formulated resin film will result to reduced pressure application. In order to represent these conditions the hydrostatic pressure acting of the resin was modeled as a fraction of the theoretically acting pressure which is given by the Equation (4.7).

Figure 8.17 illustrates the effect of the second curve on the impregnation degree of the roving in the case where the roving exits the first curve in not fully impregnated state. The increase on the resin film thickness over the second curve of the impregnation unit indicates that resin is squished out of the roving due to the reversed curvature. Nevertheless it was demonstrated that the impregnation degree of the roving increases over the second curve. This is caused by the further compaction of the roving over the second curve and by the action of the capillary forces which are still present and advance the flow front.

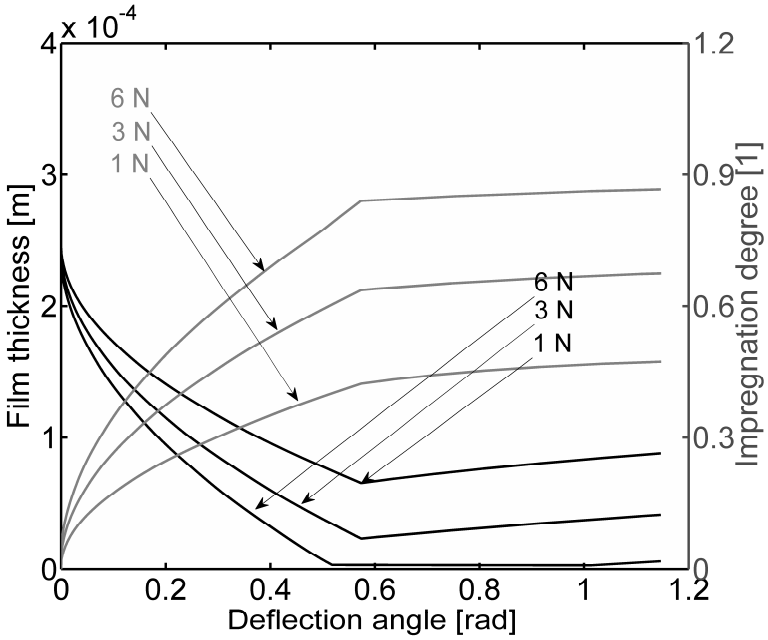

Figure 8.17: Film thickness and impregnation degree development over inside the impregnation unit A3 for different initial tensions. Roving speed was set at 10 m/min and RWF at 0.45.

8.3. Three curve impregnation unit A4 (siphon impregnation unit)

The fourth impregnation unit consisted of a cavity with three consequent curves and alternating curvature. The arc length of the first and third curve was 45° whereas the length of the second curve was 90°. The fact that roving follows a tangential transition between the curves results to an effective roving deflection angle of 32.86° for the first and the third curve and 65.73° for the second curve. The effective arc length is highlighted with continues lines in Figure 8.18. The radius of the cavity was kept at 41.55 mm for all three curves. This lay-out of the impregnation unit resulted to a coaxial entry and exit of the rovings. For the modeling of the impregnation process inside the unit A4 were taken into account only the areas where the roving is in contact with the cavity wall. Figure 8.18 presents the geometry of the impregnation unit and the geometry of the cavity as this was taken into account for the simulation.

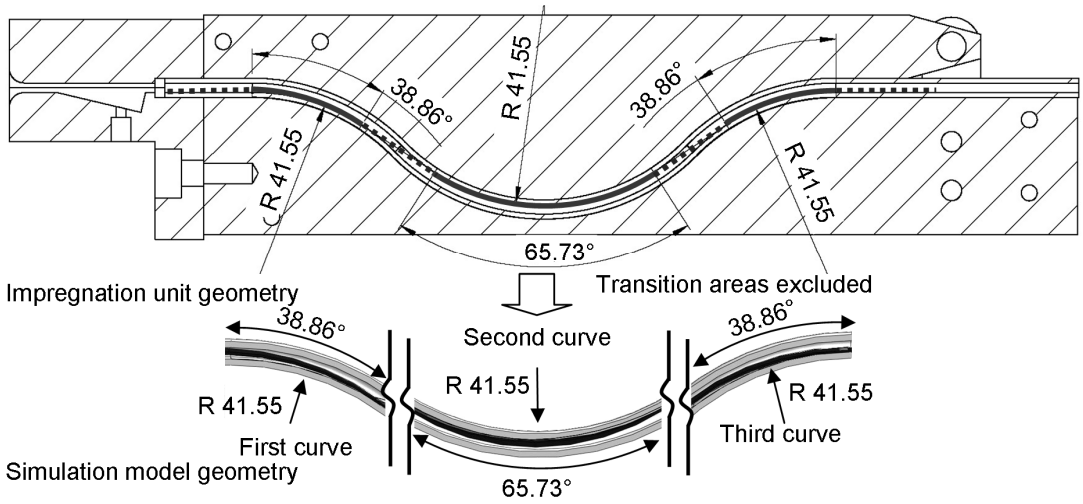

Figure 8.18: Section view of the impregnation unit A4 and schematic representation of the geometry used for the simulation of the impregnation process.

Figures 8.19 and 8.20 compare the experimental results with the predictions of the impregnation model. Figure 8.19 presents the dependence between roving tension and processing speed. According to the diagram the model predictions come into an agreement with the experimental results. The diagram in Figure 8.20 presents the correlation between resin weight fraction and tension. The trend of the diagram follows closely the experimental results. The decrease of the tension which was caused by the increase of the resin dosing can be explained in analogy to the findings of Figure 8.7.

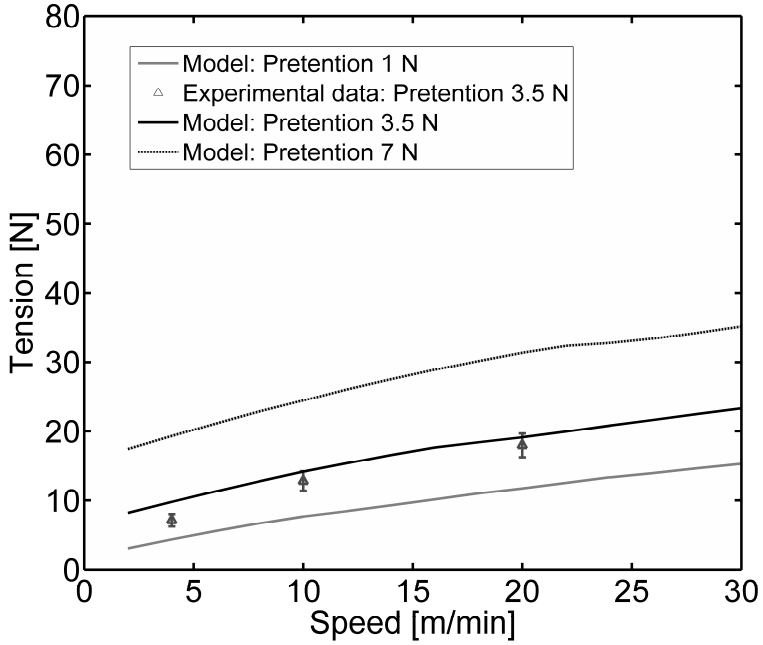

Figure 8.19: Roving speed vs. roving tension. Comparison between experimental and modeling results. Target value of the resin weight fraction was set at 45 % and initial tension at 1, 3.5, and 7 N.

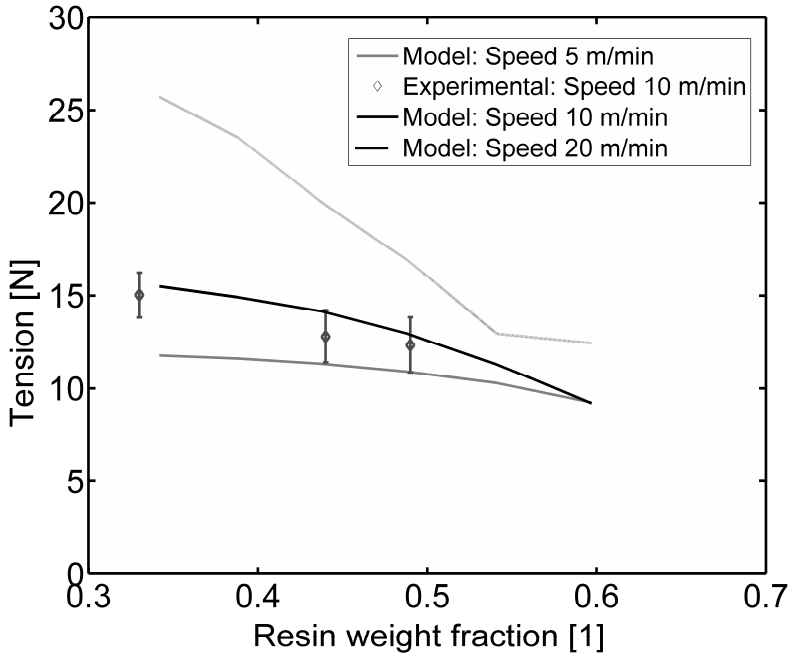

Figure 8.20: Resin weight fraction vs. Tension. Comparison between experimental and modeling results. Initial tension was set at 3,5 N and roving speed at 10 m/min.

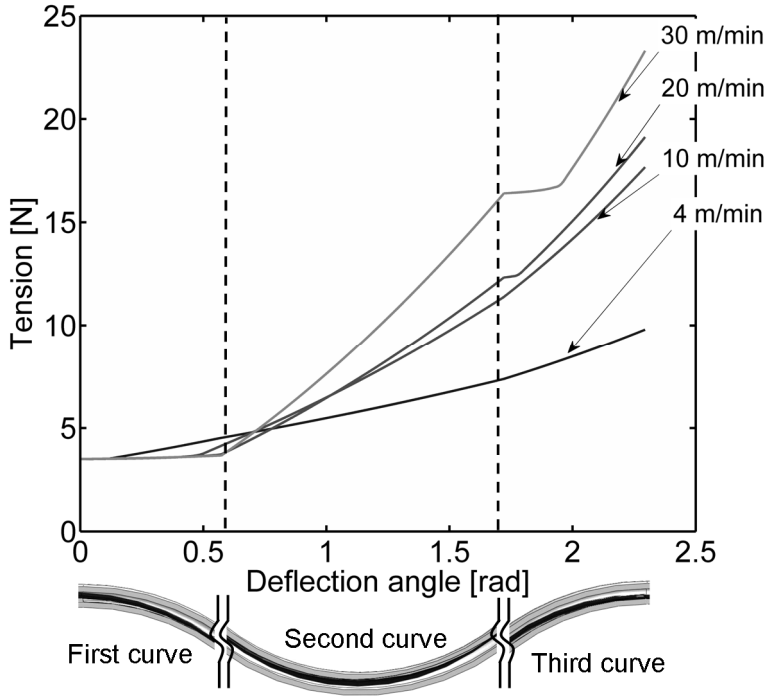

Figure 8.21: Development of the tension force acting on the roving inside the impregnation unit A4. Initial tension was set at 3.5 N and RWF at 0.45.

Figure 8.21 presents the development of the tension inside the impregnation unit A4. According to the diagram there is a uniform increase of the roving's tension for 4 and 10 m/min. In the case of 20 and 30 m/min at about 0.57 and 1.71 rad a steep change on the tension curve was observed. These two positions are the points where the transition of the roving from the one curve to the other takes place. The increase on the tension's derivative on the first transition point can be explained analogically to Figure 8.15. On the other hand at the second transition point there is a drastic decrease of tension. Initially that seems to be an awkward behavior. However Figure 8.22 gives the explanation of this behavior. The roving in the case of 20 and 30 m/min exits the first curve not fully impregnated. As explained in the previous chapter, the impregnation effect over the second curve is restricted due to the reversed curvature of the cavity. In this way by the time that the roving enters the third curve, a rich resin layer is formulated again between cavity wall and roving. The sliding conditions over this rich resin layer are significantly improved compared to the sliding conditions over the second curve where the fibers come in direct contact with the cavity wall and resin layer has a minimum value. Taking that into account, it can be concluded that the reformulation of a thicker resin film leads to moderate tension in-

crease on the front region of the third curve. As the roving absorbs again the resin film the shear forces become higher and the tension increase rate increases again.

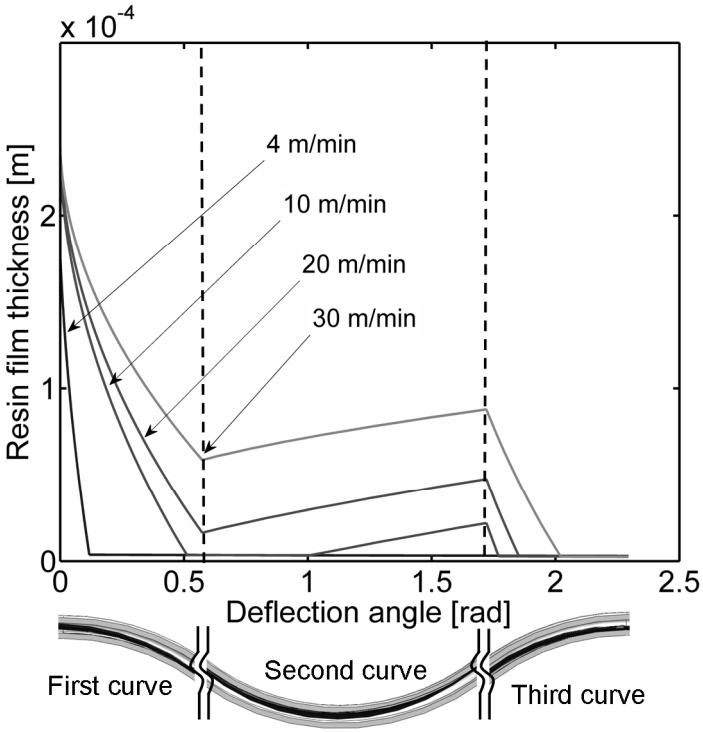

Figure 8.22: Resin film thickness vs. deflection angle inside the impregnation unit A4. RWF was set at 0.45 and initial tension at 3.5 N.

Figure 8.23 illustrates the absorption of the resin film thickness under real processing conditions. A specially designed impregnation unit with a transparent cover was implemented on a filament winding process. The cavity of the unit was similar to this of the unit A4. In order to allow the observation of the interactions between roving and resin there no PTFE tube was used (Figure 8.23a). The roving was pulled through the impregnation unit with speeds varying between 0 and 20 m/min. Figure 8.23b proves that for low processing speeds (0-10 m/min) the resin film was fully absorbed over the first curve of the impregnation unit. In Figure 8.23c it is highlighted that for higher processing speeds, the resin film absorption is not completed over the first curve and the remaining resin is transferred with the roving on the second curve. Figure 8.23d illustrates the reformulation of the film on the entrance of the third curve and the fully absorption of the resin until the exit of the impregnation unit. The snapshots presented in Figure 8.23 come in to full agreement with the modelling results of Figure 8.22 and confirm the validity of the calculations.

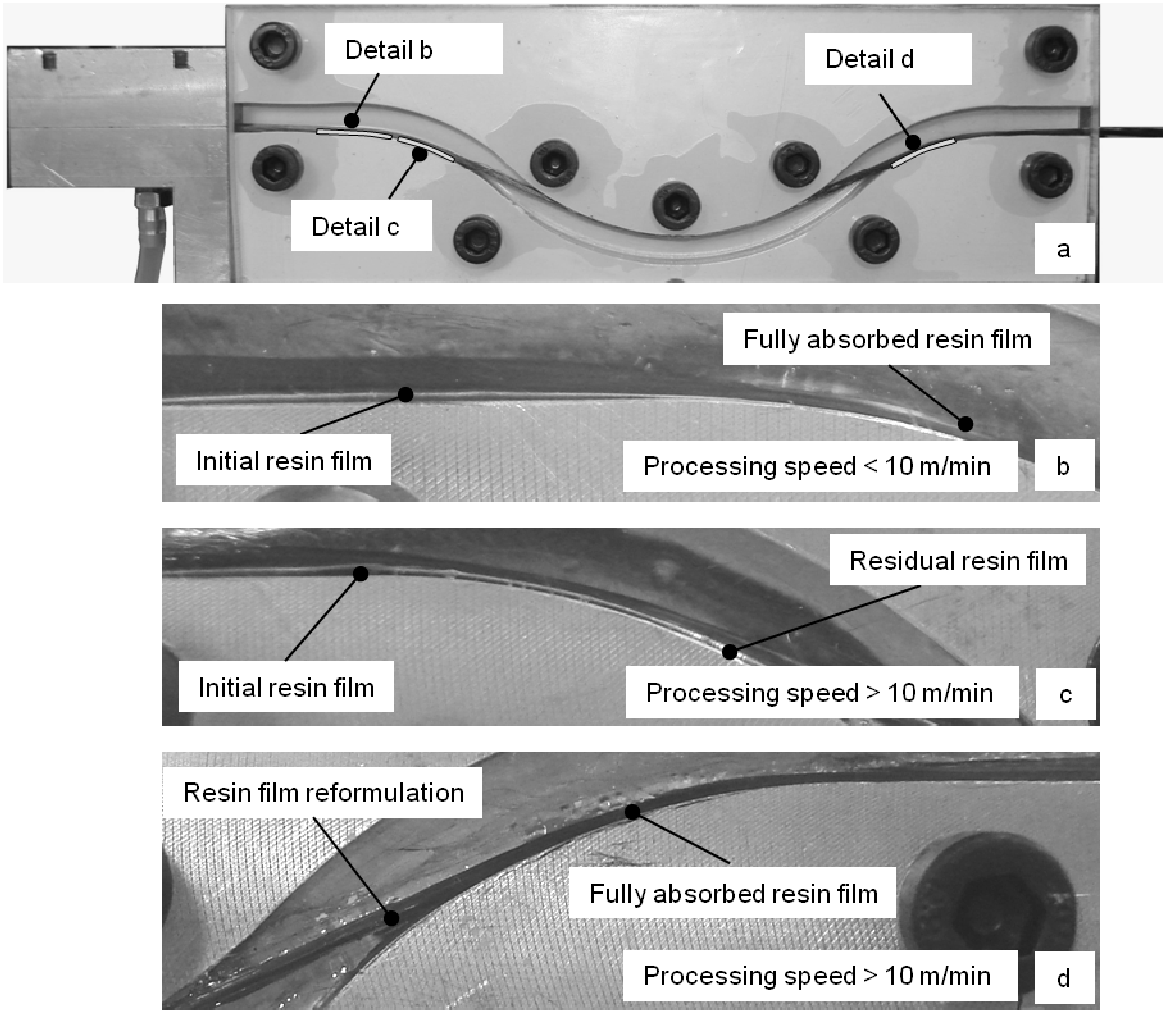

Figure 8.23: Snapshots of the resin film absorption during the impregnation process.

The diagram of Figure 8.24 presents the progress of the impregnation degree inside the unit A4. The impregnation degree was found to increase proportionally to the absorption of the resin film (Figure 8.22). According to the model the roving exits the impregnation unit in a fully impregnated state for processing speeds up to 30 m/min. This result is experimentally confirmed by the micrographs presented in Figure 8.25. The samples were produced on the winding mandrel shown in Figure 7.2 and reflect the state on which the roving exits the impregnation unit. After the impregnation unit there was no winding eye used in order not to distract the impregnation state of the roving. The examination of the samples produced with processing speeds between 1 and 30 m/min confirmed that the rovings were fully impregnated. In all cases the voids detected inside the roving were found to cover less than 2 % of the entire volume and were mainly located on the edges. This observation leads to the conclusion

that the pressure field on the corners of the cavity has a lower magnitude than the pressure developed on the middle due to the light oval cross section of the PTFE tube. On these regions the compaction of the roving is lower than expected resulting to a locally insufficient compaction of the roving which prevents the pressing out of the entrapped air in these regions of the roving. The smaller width of the sample produced under 30 m/min is attributed to the higher developed tension force.

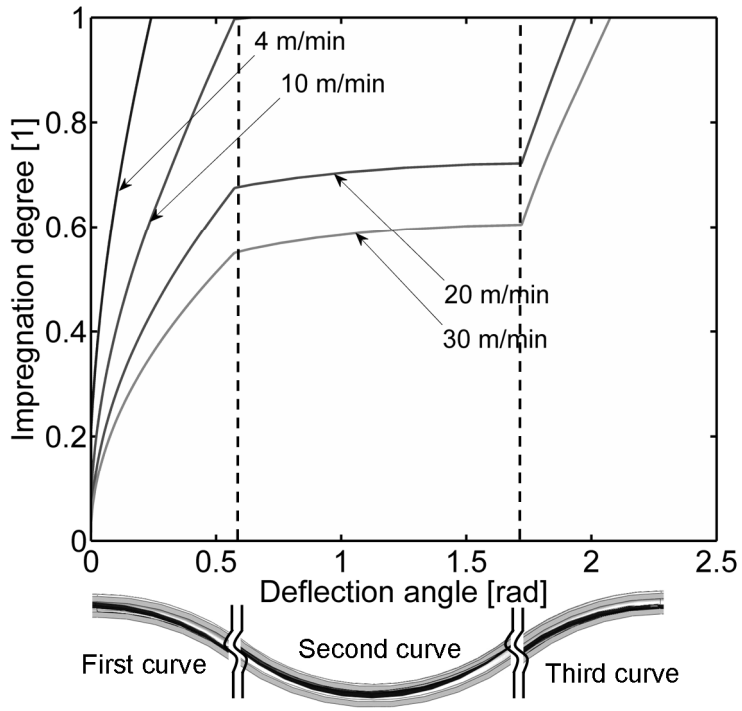

Figure 8.24: Development of the impregnation degree inside the unit A4. RWF was set at 0.45 and initial tension at 3.5 N.

Figure 8.26 presents the absorption of the resin film under different set values of the resin weight fraction (RWF) inside the impregnation unit A4. The diagram shows that the higher the amount of resin the longer it takes for the roving to fully absorb the resin film. According to the modeling results it was found that the impregnation unit A4 is able to impregnate a 24k roving under 10 m/min with a resin weight fraction up to 60 %. Although such a high resin ratio is not typical for most of the winding applications, it highlights the potential of the impregnation unit to work under a wide processing window.

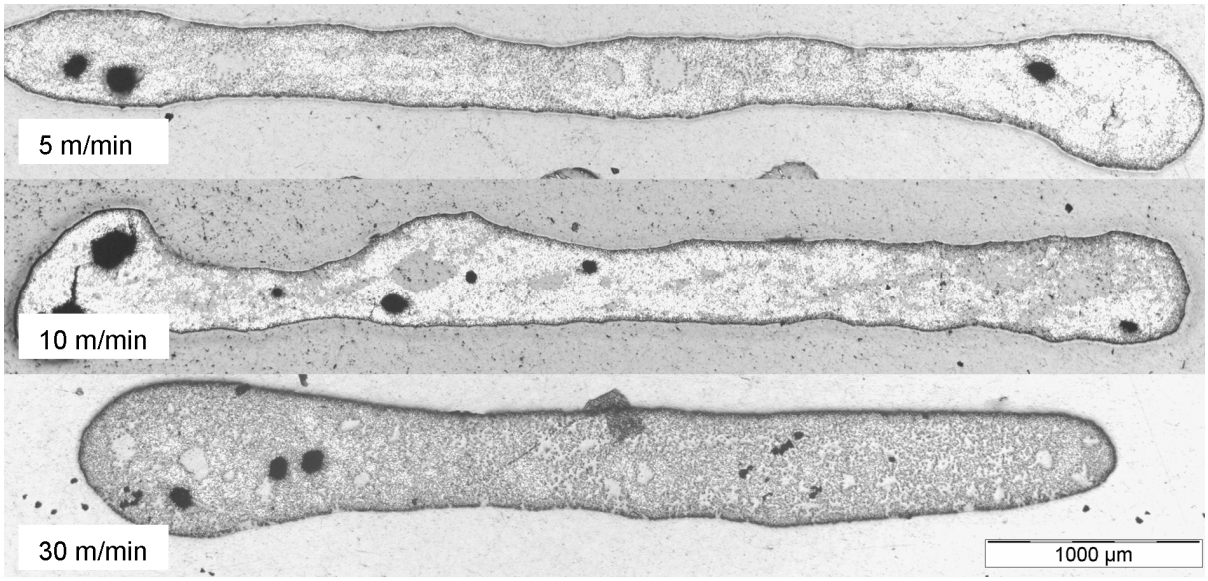

Figure 8.25: Micrographs of single rovings impregnated under different processing speeds. RWF was set at 0.45 and initial tension at 3.5 N.

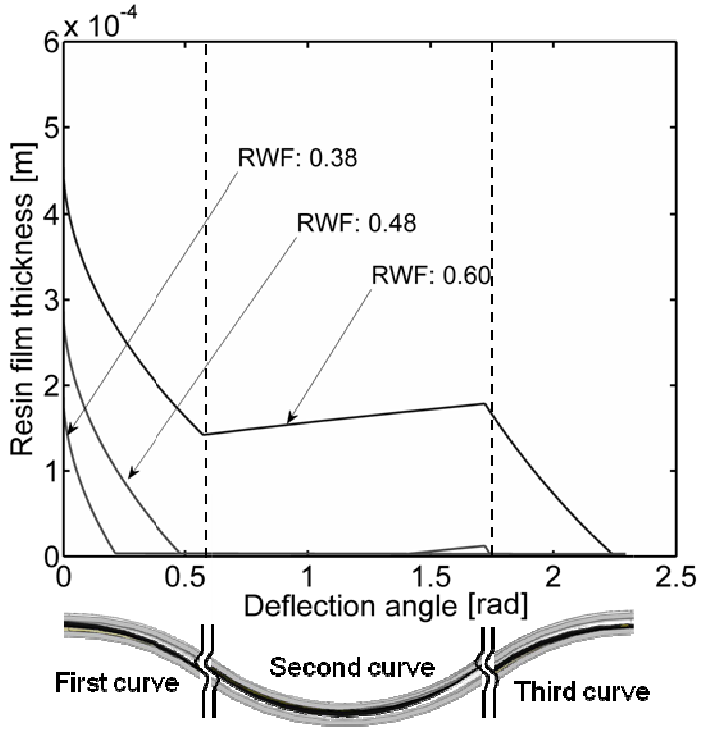

Figure 8.26: Resin film thickness vs deflection angle inside the impregnation unit A4. Roving speed was set at 10 m/min, and initial tension at 3.5 N.

Figure 8.27 presents two detailed micrographs from rovings impregnated with different resin dosing rates. During the experimental procedure the resin was dosed through the resin injection box under a pre-calculated volumetric flow. The figure il-

lustrates the micrographs for the case where the set value of the RWF was at 55 and 45 %. The examination of the samples under the optical microscope has revealed that the impregnation unit is able to precisely control the resin weight fraction of the roving. In both cases the difference between set- and measured value was lower than 2 %. This result further confirms that there is no resin gathering inside the impregnation unit since the entire volume of resin that has been dosed through the injection box was transferred on the roving.

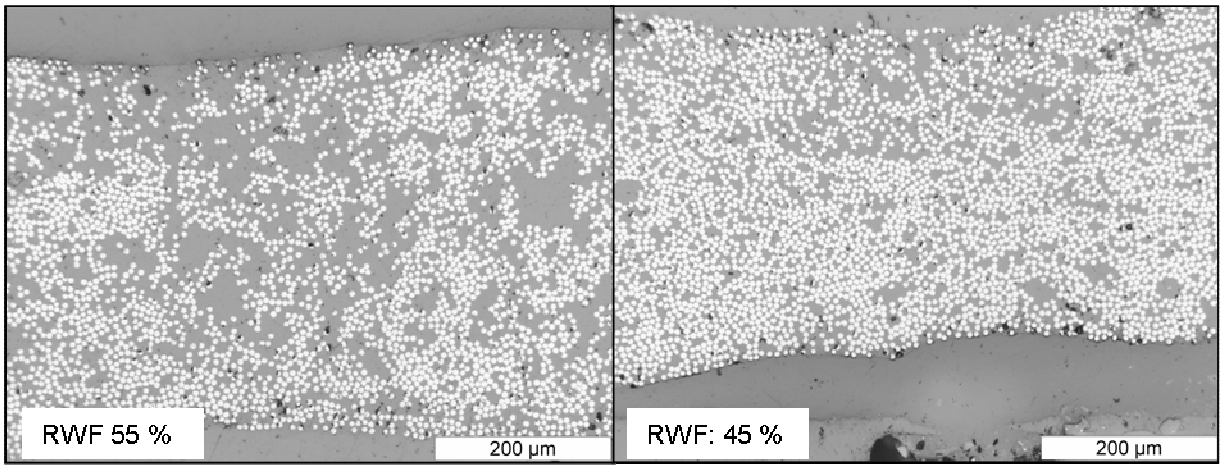

Figure 8.27: Micrographs of rovings impregnated with different resin dosing. Roving speed was set at 10 m/min and initial tension at 3.5 N.

8.4. Materials parameter study

The study presented in Chapters 7.1 – 7.3 has confirmed the validity of the simulation and gave a detailed characterization of the different phenomena that take place inside the impregnation unit. The following Chapter aims to highlight the influence of the different material properties on the performance of the impregnation process. Based on the geometry of the impregnation unit A4 the influence of parameters like the roving yield, filament diameter and resin viscosity will be examined.

The linear weight of the roving was the first parameter to be examined. The various state of the art carbon fiber rovings are produced in different sizes. The number of single filaments typically varies from 1000 (1K) up to 48000 (48K) which results to a linear weight per unit length (tex) of 400 up to 3200 g/km.

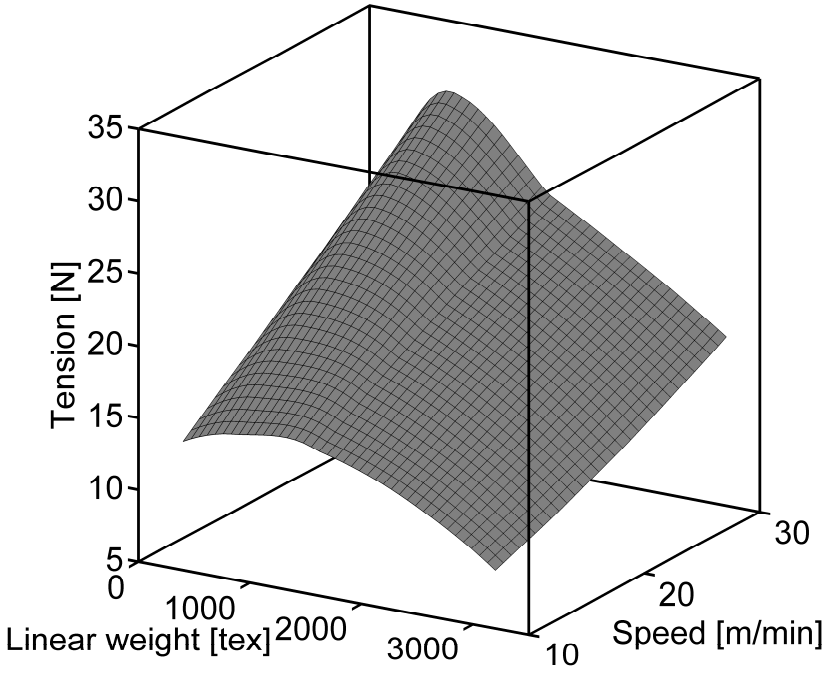

Figure 8.28: Influence of the roving's tex on the developed tension according to the process speed. RWF was set at 0.45 and initial tension at 3.5 N.

Figure 8.28 presents the effect of the roving's Tex on the tension force that develops during the impregnation process. According to the diagram, the increase of roving's yield leads to an increase of the roving's tension. This can be explained by taking into account the spreading behavior of the roving. Rovings with a higher number or monofilaments spread wider than rovings with a lower number of monofilaments. Taking into account the Equation (4.25) it can be understood that the bigger spreading width results to an increase of the developed tension. Nevertheless in the developed impregnation unit the roving runs inside a defined cavity. In this way the roving is restricted to spread up only to a certain width. Under the framework of the current study it was assumed that every roving having a tex higher than 800 will spread to the maximum width of 4.5 mm which is the groove inside the PTFE tube. On the other hand, the restriction of the spreading width influences directly the thickness of the fiber pack, and in an indirect way the absorption of the resin film.

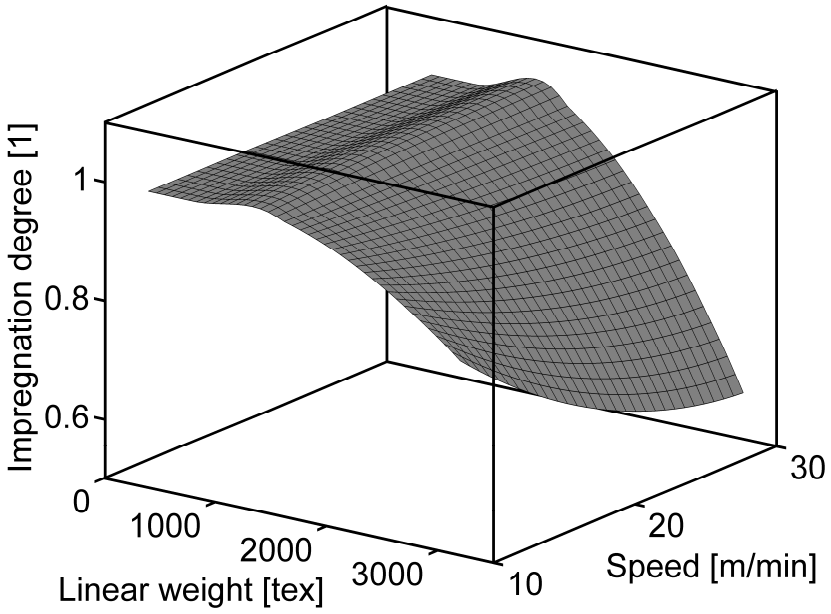

Figure 8.29: Influence of the roving's Tex on the roving's impregnation degree according to the process speed. RWF was set at 0.45 and initial tension at 3.5 N.

Figure 8.29 presents the impregnation degree of the roving at the exit of the unit A4 for various processing parameters. According to the modeling results it was found that up to a processing speed of 30 m/min the carbon fiber rovings with a tex of 1600 (CF 24k) exit the impregnation unit fully impregnated. A roving tex higher than 1600 does not allow a complete impregnation through the unit A4. In order to improve the impregnation state of the roving the initial tension can be increased. On the other hand, the simulation results have shown that even the increase of the initial tension up to 20 N is not efficient for a complete impregnation of the 48 k roving (Tex 3200 g/km) with a processing speed of 30 m/min inside the impregnation unit A4 with the given cavity width.

Concluding it can be stated that the increase of the roving's tex does not result to an increase of the generated tension. Rovings with a higher number of filaments need a cavity longer path or expanded width in order to fully absorb the resin film and reach the complete impregnated state.

The technical fibers used in the majority of composite applications are carbon, glass, aramid, or basalt fibers. All these types of fibers can be delivered in forms of continu-

ous untwisted rovings. The diameter of the mono filaments varies from 7 µm up to 20 µm according the type of fiber. Carbon fibers are the finest of all fibers with a diameter about 7 to 10 µm, the aramid and basalt fibers have a diameter about 13-15 µm, and the glass fibers are the ones with bigger diameter varing between 15-22 µm.

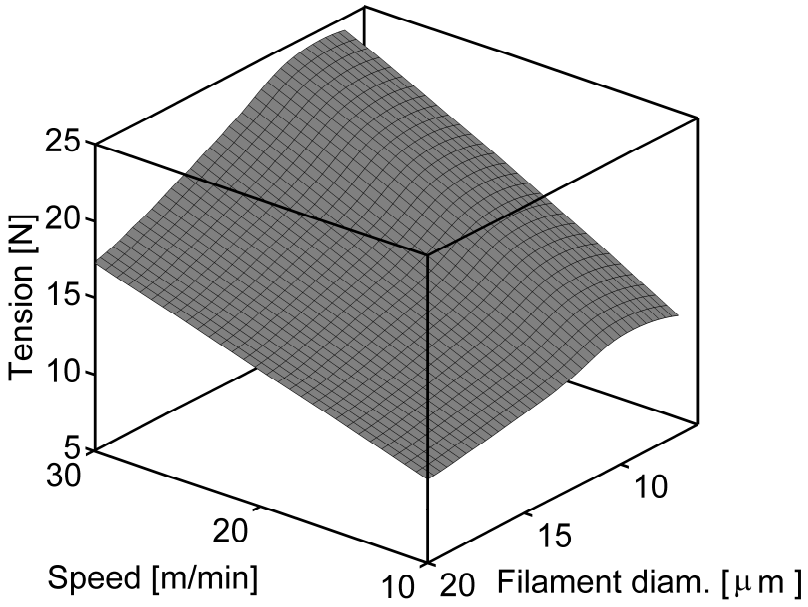

Figure 8.30: Influence of the mono filament's diameter on the roving's tension according to the process speed. RWF was set at 0.45 and initial tension at 3.5 N.

The model was used in order to theoretically investigate the influence of the mono filament's diameter on the impregnation process. Aim was to study the influence of the fiber diameter abstracting parameters like fiber compaction, fiber sizing, and fiber surface tension, which can change significantly between the different types of fibers. In fact the values used for the modelling of the 34-700 24K CF roving were used for all simulation trials. For all simulated cases the roving tex and the fiber density was kept constant. The mono filament diameter varied between 7 and 20 µm. The total number of fibers inside the roving was calculated in reverse proportion to the mono filament diameter and took values between 24000 and 2940 fibers per roving. Figure 8.30 presents the results of the study concerning the developed tension. It was found that the bigger the diameter of the mono filament the lower is the tension that develops during the impregnation process. This phenomenon can be explained by taking into account the Equations (4.4) and (4.17). The increase of the mono filament diam-

eter results to an increase the roving's permeability. Higher permeability causes lower shear of the resin film and thus lower tension.

Figure 8.31 presents the deflection angle which is required for a fully impregnation of the roving in dependence to the mono filament diameter. According to the diagram the bigger the filament diameter, the shorter is the required path inside the cavity for the fully impregnation of the roving. The easier impregnation for the materials with bigger monofilaments (GF/AF) can be explained by the higher permeability of these materials. As the diameter increases the permeability increases and the resin can flow quicker for a given hydrostatic pressure.

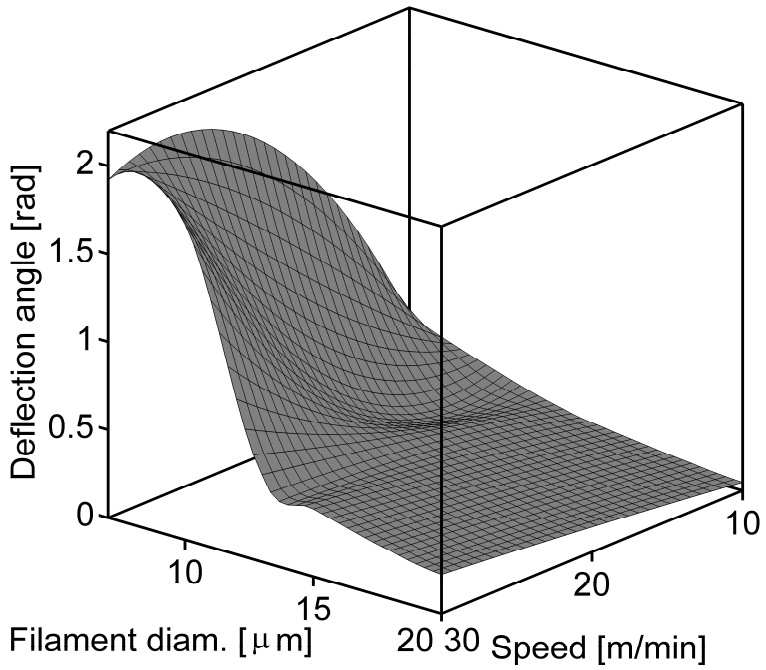

Figure 8.31: Influence of the mono filament's diameter on the needed deflection angle for fully impregnation according to the process speed. RWF was set at 0.45 and initial tension at 3.5 N.

Taking into account the above it can be concluded that fiber materials with a bigger mono filament diameter are easier to impregnate compared to materials with a smaller diameter. In all cases an increase of the filament diameter will result to a more compact impregnation unit and to a reduction of the tension which is generated by the impregnation process.

The options for a resin system suitable for the winding and pultrusion technology are

very wide. Depending on the type of the system (EP, UP, VE), and on the specific characteristics of its chemical formulation the mixture viscosity of the resin can vary significantly. Typical epoxy systems for industrial applications have viscosities in the range of 100-1000 mPa s. These values have been simulated with the developed tool and the results of the study are presented in the following figures. Figure 8.32 illustrates the dependence between developed tension and viscosity. As expected the increase of the viscosity results to the increase on the developed roving tension.

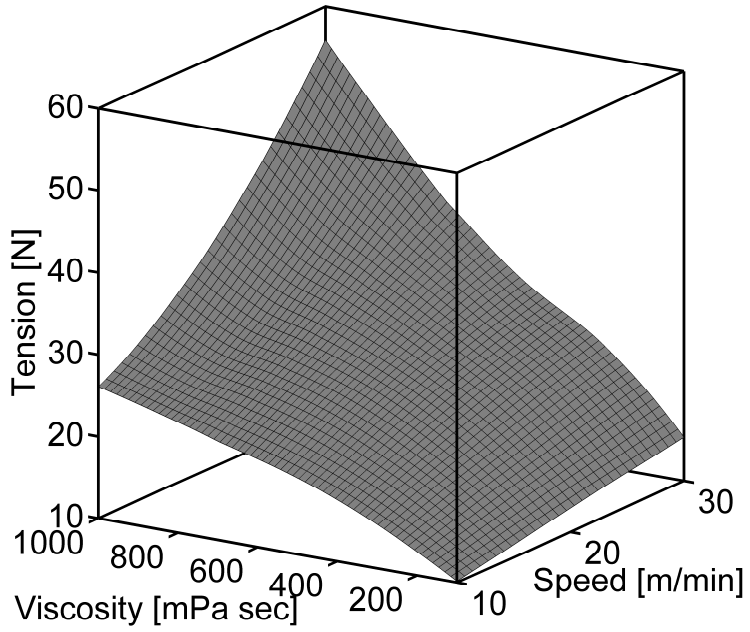

Figure 8.32: Influence of the resin's viscosity on the roving's tension according to the process speed. RWF was set at 0.45 and initial tension at 3.5 N.

Figure 8.33 presents the deflection angle which is required for a fully impregnation of the roving in dependence to the resin viscosity. According to the diagram the impregnation unit A4 is able to fully impregnate a 24k carbon fiber roving with a resin that has a viscosity up to 1000 mPa s. Although higher viscosity causes higher flow resistance, the simultaneous increase of the roving tension causes an increase on the hydrostatic pressure on the resin film. In this way, according to the modeling results, the cavity length which is required for a full impregnation is not in a linear relation with the viscosity of the resin.

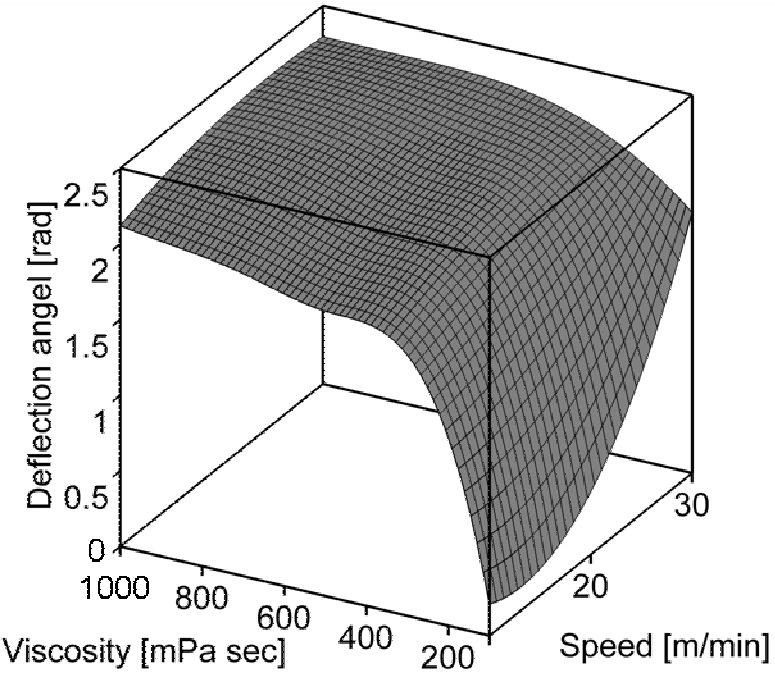

Figure 8.33: Influence of the resin viscosity on the needed deflection angle for fully impregnation according to the process speed. RWF was set at 0.45 and initial tension at 3.5 N.

8.5. Overview

The variable input parameters of the impregnation process can be classified in three groups. The values of these parameters depend on the choices made by the process operator. The parameters deal with the equipment set-up, the material choice, and the processing conditions. The values of these parameters define the values of the final roving tension and of the roving's impregnation degree. These are the most important process output parameters and the only ones that can be directly measured and logged by the operator.

The optimum output can only be achieved by setting the correct input variables. On the other hand, setting the ideal input variables is a trade off between process performance and costs. In this way it can be easily understood that the choice of the process variables is an optimization problem. The Table 8.1 gives an overview about the influence that every process variable has on the process output. The parameters are organized in the three categories. The result of the moderate increase of one of these parameters by keeping all the values of all the other constant is given by the

symbols +/-/o where:

- + or -describes a moderate increase or decrease
- o describes a imperceptible variation
- ++ or -- describes a big increase or decrease

Table 8.1: Correlation between input variables and process out parameters concerning the siphon impregnation unit.

		Roving tension	**Impregnation degree**
Equipment parameters			
Curve radius	↑	**++**	**+**
No. of curves	↑	**++**	**+**
Deflection angle	↑	**++**	**++**
Processing parameters			
Speed	↑	**+**	**--**
Resin weight fraction	↑	**-**	**o**
Initial tension	↑	**+**	**++**
Material parameters			
Roving size / tex	↑	**o**	**-**
Filament diameter	↑	**-**	**++**
Resin viscosity	↑	**++**	**-**

Concluding the results of Table 8.1 it can be stated that:

- The increase of the curve radius results to a considerable increase of the roving tension without an proportional increase of the impregnation quality
- The number of curves of the impregnation unit has a drastic influence on the developed roving tension but a limited effect on the impregnation degree. In this way the number of curves is a design criterion concerning more the roving

trajectory and less the impregnation quality.

- The total deflection angle affects significantly both the roving tension and the impregnation degree. The increase of the deflection angle results into a better impregnation.

- The increase of the processing speed is the aim of every manufacturer. However an increase of the roving's linear speed will result to an increase of the tension. It is also obvious that for a given cavity geometry, the continuous increase of the speed can result to incomplete impregnation.

- The direct adjustment of the resin weight fraction is one the most important advantages of the developed process. An increase of the resin weight fraction will result to a moderate decrease of the rovings tension without any significant effect on the impregnation quality.

- The initial tension can be adjusted by the operator. An increase of the initial tension will proportionally increase the final tension. Generally speaking the increase of the initial tension helps the impregnation process especially for rovings with high amount of fibers.

- The use of rovings with higher tex/yield is preferred in order to the increase the output of the process. The use of rovings with a higher tex results to a slight increase of the tension. On the other hand rovings with a bigger yield are a lot more difficult to impregnate and an enlarged cavity is required.

- The filament diameter depends on the material type. Materials with smaller fibers result to higher tension and are more difficult to impregnate.

- The increase of the resin's viscosity results into an increase of the roving tension and to a slight reduction of the degree of impregnation.

9. Industrial implementation of the developed type of impregnation process

Taking into account the results presented in Chapter 7 it was determined that the lay-out of the impregnation unit A4 is the most promising one. The cavity of the unit showed an excellent performance with the state of the art 24k rovings and according to the modeling results the unit is suitable for resin materials with a viscosity up to 600 mPa s. Another interesting characteristic of the impregnation unit A4 is the coaxial entry and exit of the rovings which makes it appropriate for adoption in already existing processes without the additional work of installing new roving guiding elements.

9.1. Impregnation unit design

The impregnation unit consists of the resin injection block and the impregnation cavity. Fibers and resin enter the impregnation unit under a predefined rate through the resin injection block. The main body of the impregnation unit is made of two parts and hosts the impregnation cavity with the PTFE tubes. The design of the unit prevents the contact of the rovings with any sharp edges in order to avoid any fiber damage. The design of the fiber path ensures that the transition between flat and curved region follows tangential trajectory. Currently the basic lay-out of the impregnation device consists of four independent parallel cavities. The present concept can be further upgraded for the parallel processing of more than four rovings according to the corresponding process demands.

During the development phase priority was given to the user friendly character of the design. The impregnation unit has to be robust, should be able to operate free of problems in continuous production conditions and the preparation and cleaning time has to be reduced to the minimum. The upper part of the main body and the injection box open in order to install and remove the PTFE- tubes. This operation was designed to be as quick and easy as possible without the use of any special tools. The simple design guaranties that in case of an unexpected failure, the system can be inspected, the defected part can be quickly replaced and the production can continue within few minutes.

Another function that has to be carried out by the unit is the forming of the PTFE tubes. The original round cross section of the PTFE tubes has to be pressed to an oval shape. In order to achieve this function, the main body is a stiff design machined out of a full aluminum block. The unit incorporates 2 latch clamps which help to compress the tubes which deform to a final flat-oval shape as the top part of the unit closes.

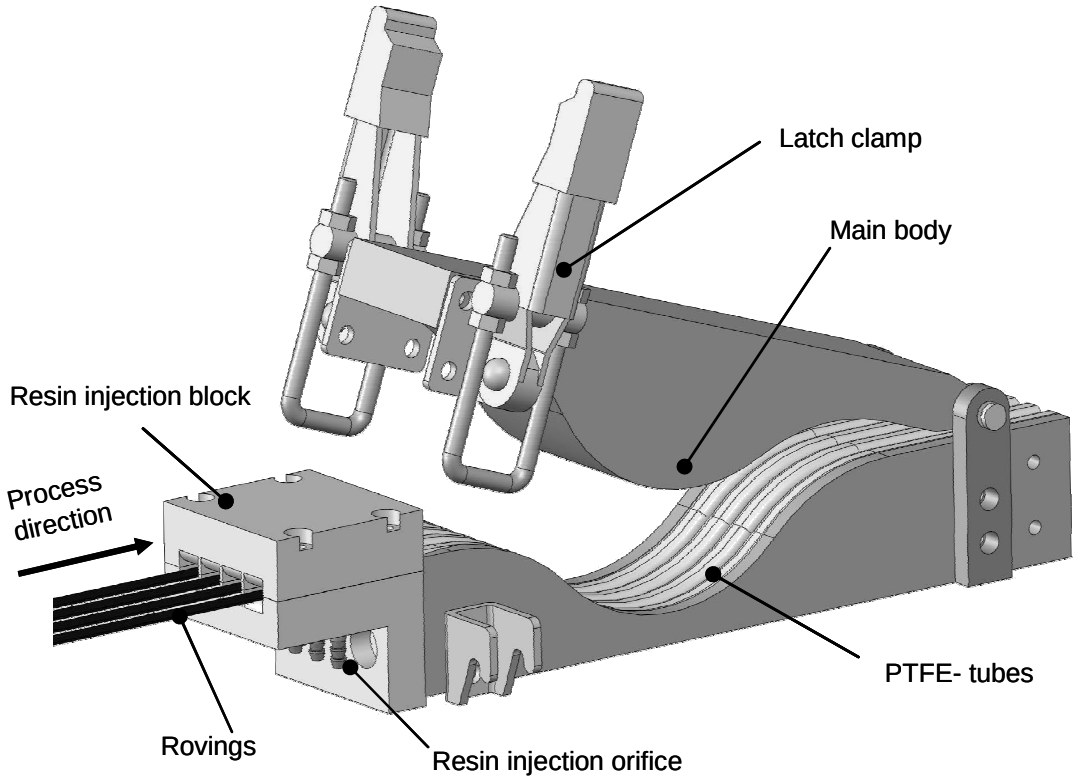

Figure 9.1: CAD representation of the basic lay-out of the developed impregnation unit.

Figure 9.1 presents the basic lay-out of the impregnation unit. The various parts of the unit as well as the entry ports for fibers and resin are highlighted. Figure 9.2 presents some details of the prototyped impregnation unit. The resin injection box, the interface to the tube-cavity, as well as the oval cross section of the tubes are highlighted. All these features were proven to work very reliably without any unexpected malfunctions.

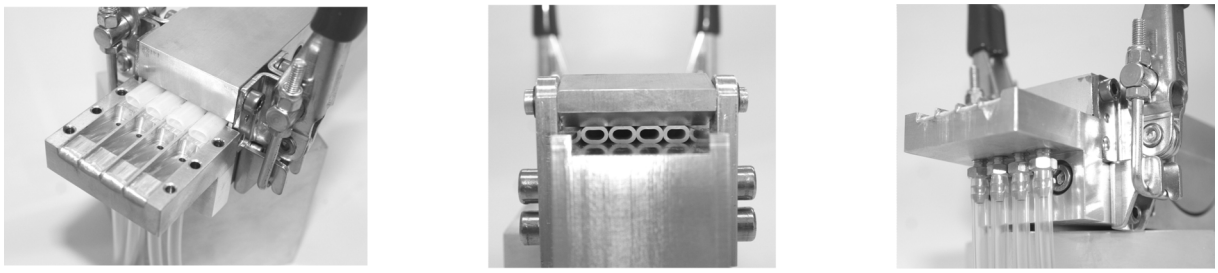

Figure 9.2: Details of the prototype impregnation unit.

Figure 9.3 illustrates the preparation steps of the impregnation unit. The impregnation unit is easy to handle. The preparation of a unit and the installation of the tubes do not take more than one minute and can be done by personnel without any special training or experience. After processing the disassembly and dispose of the tubes is a simple operation. The rest small quantities of resin which can be found in the injection box are removed with a brush wetted with acetone.

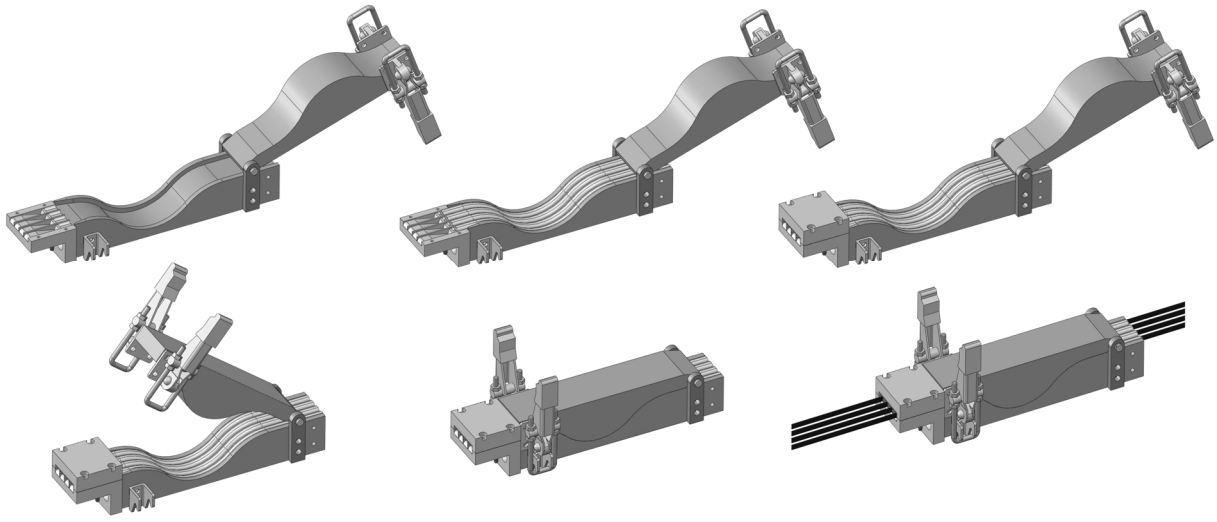

Figure 9.3: CAD representation of the installation of the PTFE- tubes inside the impregnation unit. Implementation in a winding process.

9.1.1. Ring winding head

The concept of the siphon impregnation unit as presented above is optimized for the use in a filament winding process. The studies [4, 5, 61, 62, 79] present the implementation of the impregnation unit in a multiple pay-out device (ring winding head) as well as in a state of the art filament winding machine.

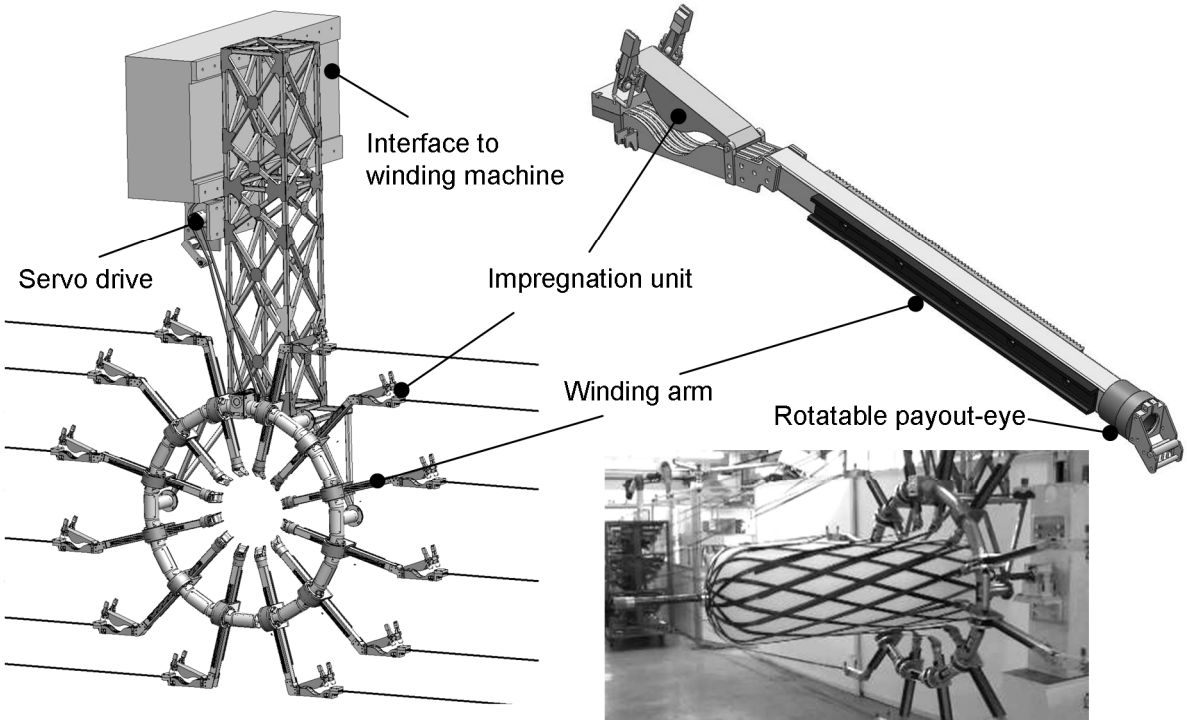

Figure 9.4: Ring winding head with the integrated impregnation unit.

The ring winding head (Figure 9.4) is a concept which aims to increase the efficiency of the manufacturing process of type III and type IV pressure vessels by multiplying the number of pay out eyes arranged circumferentially around the mandrel. This kind of pressure vessels are high-end structures with very demanding material properties which are used for CNG or H_2 storage in automotive applications. The design pressure of such vessels can be as high as 1500 bar. Depending on the volume of the vessel the laminate thickness can be up to 30 mm. The winding process of such a pressure vessel with a normal winding machine can last several hours. In order to reduce the production time of the vessels it is essential to increase the material lay-down rate. The ring winding head can be equipped with up to 12 radial movable feed-eyes placed around the circumference of the mandrel. An impregnation unit is integrated on every arm. The ring winding technology can achieve 5 times higher pro-

duction rates in comparison to the conventional winding techniques.

The concept of the ring winding head could not be feasible without the use of the siphon impregnation unit. The use of the impregnation unit allows the guidance of the dry rovings up to the head and their impregnation close to the delivery head. The siphon impregnation unit allows stable and exact process conditions as well as continuous production without interruptions. The functionality of the ring winding head has been extensively tested. Several type III and type IV pressure vessels have been wound with two prototype ring winding heads. The testing of the cylinders has proved that the quality of the produced parts fulfills the design standards. Burst, as long as cycle testing has shown that, the performance of the cylinders is at the same level as the ones produced with the standard winding machines with conversional resin baths.

Figure 9.5: Type III pressure vessel produced with the ring winding head.

9.1.2. Standard winding machine

The designed impregnation unit can be easily implemented to any standard winding machine. Due to its small volume, the unit can be directly installed on the carriage module (Y-axis) of the filament winding machine. In the case of a winding machine with more than one winding spindle the design on the impregnation unit allows the option of one dedicated impregnation unit per winding spindle. Since there is no stagnated resin inside the impregnation unit, the dynamic movement of the carriage module has no influence on the impregnation process. The direct mounting of the impregnation unit on the machine frame enables the rearrangement of the machine park and the saving on valuable area used for production.

9.1.3. Alternative winding modules

Except the standard winding machines or the ring winding machine, the impregnation unit is also suitable for the development of alternative winding equipment. For example the unit is an ideal solution for the development of winding industrial robotic systems. The impregnation unit due to the compact form, the simplicity of the design and the clean operation, can be integrated directly on a winding head which will be moved by a standard industrial robot.

9.2. Resin metering equipment

Chapter 7 has highlighted the influence of the resin metering on the processing parameters as well as on the impregnation quality. The assurance of stable impregnation conditions implies the on-line mixing of the different resin components and the precise volumetric control of the resin flow into the impregnation unit. These functions can be performed by a resin metering apparatus which is implemented in the filament winding production rig.

There are several types of resin dosing and mixing systems available on industrial scale. Most of them are developed and optimized to cover the needs of the various resin injection processes. Nevertheless a filament winding application is very different from a standard RTM application. In the case of the impregnation unit, the resin has to be delivered under very ow pressure. Since the winding speed is not constant, the system has to deliver the resin under permanently changing dosing rates. The resin dosing rate has to be proportional to linear speed of the roving. The user should be able to adjust the volumetric dosing rate in accordance to the roving tex and the set value of the fiber volume fraction. Another special characteristic of the winding applications is that for example in the case of the ring winding head or a multiple spindle filament winding machine the resin has to be delivered with the same rate on all impregnation units which are placed on different levels.

The most widespread types of metering systems which are typical used for LCM applications are currently two. The first type is based on piston type pump systems. The concept is based on a cylinder-piston system which is filled with the resin components. Because of the act of force on the piston, usually by a pneumatic, hydraulic or electric servo drive the piston moves and presses the material out of the cylinder.

The second type is the geared pump system. As the gears rotate they separate on the inlet of the pump, creating a void and suction which is filled by the resin material. The material is carried by the gears to the discharge side of the pump, where the meshing of the gears displaces the fluid.

Both systems are suitable for the metering of resin systems. Nevertheless the demand of delivering the resin material at multiple levels with the same precision cannot be covered by any of the above described standard solutions without using multiple parallel driven units. Furthermore the synchronization of 12 pumps driven by 12 independent motor is a complex and expensive task. In order to fulfill this specification, a prototype dosing machine based on planetary gear pumps was developed. This type pumps are used in various fiber spinning applications and allow the metering of equal amount of material out of a variable number of discharge ports.

Figure 9.6 illustrates the control diagram of the developed resin dosing system. The control is based on a programmable logic controller (PLC). The user gives information about the set point of the resin weight fraction and the resin mix ratio. The current winding speed is measured by an incremental encoder mounted on the spool creel. These information are processed by the control algorithm and based on the theoretical output of the pumps the set-point of the motor speed is calculated. The servo control units drive the two motors and respectively the pumps. The resin and hardener delivered by the pumps are mixed through a mixing head which is directly connected to the impregnation unit.

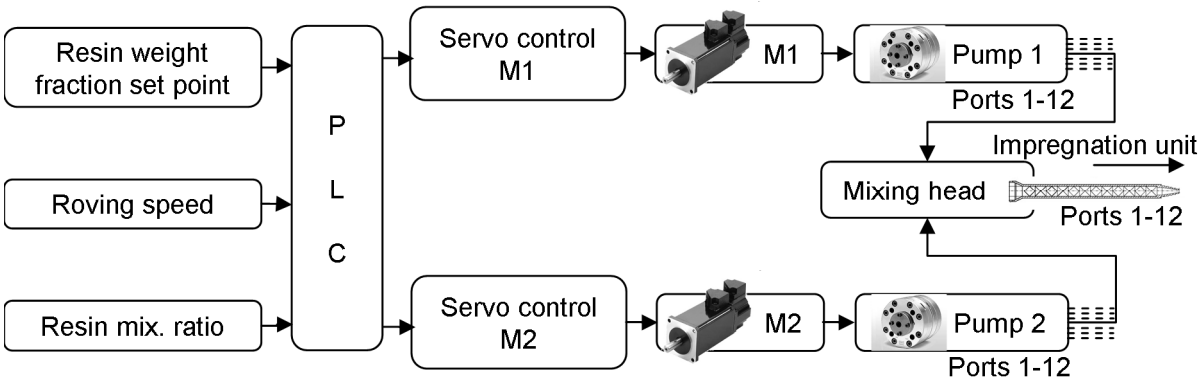

Figure 9.6: Block diagram of the resin dosing-mixing control system.

Figure 9.7 presents the physical lay out of the resin dosing-mixing system. The sys-

tem is built as a stand-alone device. Since there is no data interface with the winder the device can cooperate with any type of filament winding equipment or other application (e.g. pultrusion, towpreg ect.). The equipment was implemented both in a typical filament winding apparatus, and in the ring winding head. In all cases the system has performed according to the expectations. The testing has proved that an exact dosing is possible independent to the winding speed. The system operated harmoniously with the impregnation unit and despite the changes of the winding speed there was no resin back flow or resin over-dosing even when the machine stopped.

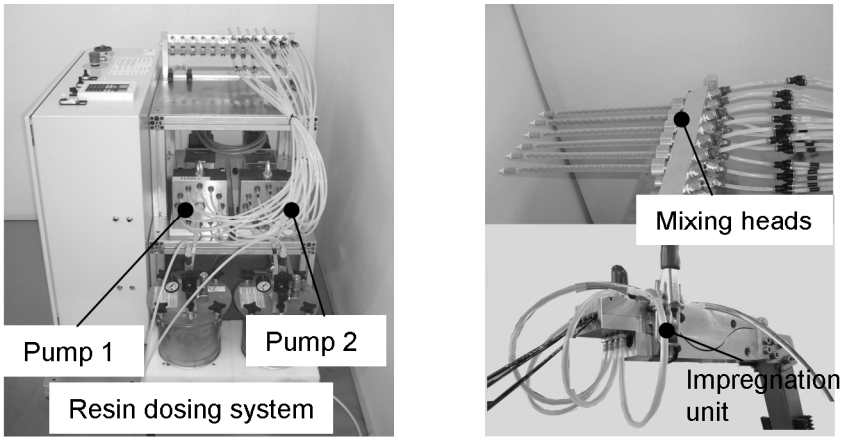

Figure 9.7: Lay-out of the developed resin dosing apparatus.

9.3. Comparison to the drum bath impregnators

In Chapter 2 the state of the art impregnation systems have been intensively discussed. The drum bath impregnator is the mostly used system for the fiber impregnation in the filament winding industry. The presence of voids inside a wound laminate is directly affected by the quality of the impregnation (void content of the saturated roving after the resin bath), the winding pattern, and the roving tension. Various studies have analyzed the presence of voids in filament wound laminates. The authors of [63] associate the working principle of the bath systems with poor impregnation of the roving and unsatisfying high void content in the wound laminates. According to their findings the bath systems face problems to control the resin weight fraction stable for different winding speed. Moreover the circulation and the stripping of the resin cause foaming of the resin. The presence of entrapped air in the resin decreases the quality of the impregnation. According to [64], the typical filament wound parts have higher void content than parts made by autoclave or compression molding. As reported the

typical void content inside high-end wound structures such as rocket motor cases can be up to 5% or in the worst case even 10%. In contrary to pressure cured laminates (autoclave) which are rejected if the void fraction overcomes the 2% these structures are qualified for use [64]. The difference in the acceptance criteria can be explained by the loading conditions of the parts. Usually the filament wound parts are subjected to in-plane tensile loads where the fiber dominated properties are most important. On the other hand, the laminate void content affects significantly properties which are influenced by the matrix material. These are the transverse shear strength, in plane compressive strength, transverse tensile strength, etc. Moreover the void fraction reduces the expected fatigue life of a component [65, 66] since the voids act as crack initiators.

Several studies have examined the quality of filament wound structures. Rousseau et al. in [70] reports void fraction in glass wound tubes between 2 and 2.5 %. He associates the presence of the voids to the bad impregnation of the prepreg and to the winding pattern. In [71] the authors report for GF/EP tubes porosities between 3 and 7 % depending on the winding angle. In [72] the measured void fraction is between 4 and 6 %. Cohen in [73] presented a study concerning the manufacturing parameters of filament wound CF/EP cylinders. According to the winding set-up he reports of void fractions in a range of 1.97 and 3.93 %.

In order to evaluate the performance of the developed impregnation unit under realistic processing conditions an experimental set-up was built. The impregnation unit was implemented on a filament winding machine and connected to the resin dosing equipment. A band of 4 rovings was wound on a steel mandrel with a diameter of 164 mm. The winding speed was set at 5, 10 and 15 m/min. Initial tension of 3.5 ± 1N was applied on every roving spool on the creel. Fiber orientation of approximately 90° was chosen in order to minimize the influence of the winding pattern on the creation of voids. Hoop wound tubes having a length of 120 mm and a thickness of 12 layers were produced under 4 different winding speeds. At the end of the winding process, a peel ply tape was applied on the samples. The samples were cured in an oven for 4 hours at 100 ℃. The same procedure was followed using a standard drum bath impregnator. Figure 9.8 presents the equipment used for the fabrication of the samples. After curing the rings were extracted from the mandrel and samples for micro-

graphs and apparent interlaminar strength testing were cut out of the rings.

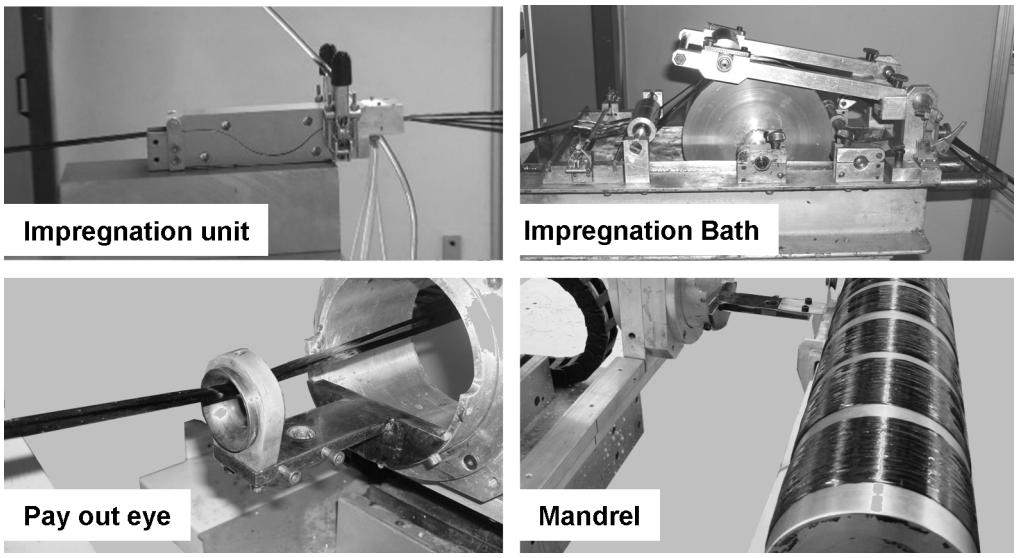

Figure 9.8: Details of the equipment used for the production of hoop wound samples.

During the winding trails with the siphon impregnation unit, the resin weight fraction was adjusted by the resin dosing equipment and set to 0.35. The exact resin dosing resulted to a clear winding without any resin misapplication. By observing the samples during the process, the operator gained the impression of a fully wet laminate but without any excess resin. The appearance of the produced samples remained constant for all winding speeds. After the application of the peel ply tape a moderated flow of resin on the glass cloth has been observed. On the other hand the performance of the impregnation bath varied with the process speed. During the low speed trials (5 m/min) the bath applied the right amount of resin. As the winding speed increased the resin weight fraction was increased. This phenomenon can be partially attributed to the bad performance of the resin strippers. The higher resin faction resulted to the creation of a rich resin layer on the surface of the samples on the end of the winding process. Moreover the operation of the resin bath under 10 and 15 m/min resulted to the extensive creation of a bubbly foam layer on the surface of the resin inside the resin tab. During the application of the peel ply tape the excess resin flew through the glass cloth.

The diagram of Figure 9.9 illustrates the dependence between winding tension and winding speed. The tension values were measured during the winding process using a hand tensionmeter. The values correspond to the winding tension acting on every single roving.

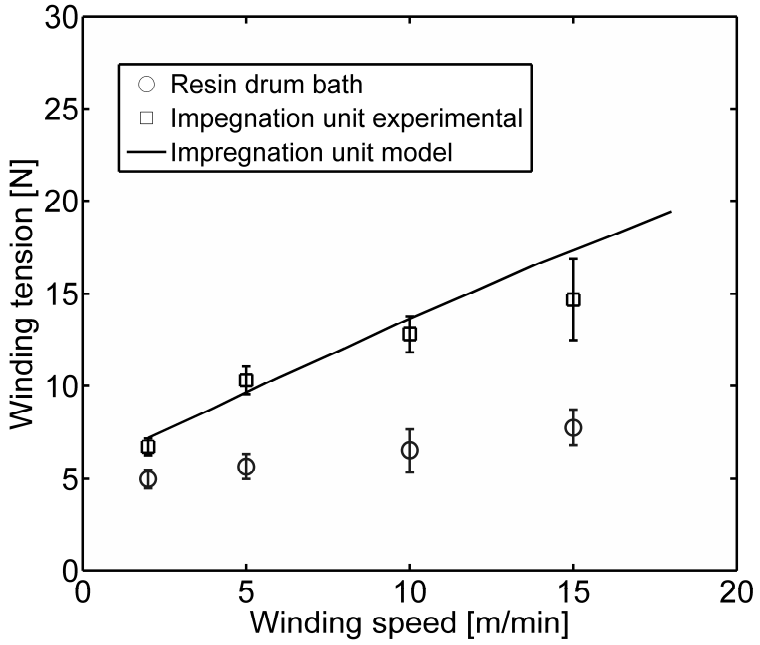

Figure 9.9: Winding tension over speed for a typical resin bath and the developed impregnation unit.

According to the above diagram, the resin bath which was used for this particular study generates lower tension than the new siphon impregnation unit. The tension produced by the resin bath increases with the winding speed but in a lower rate compared to the impregnation unit. This effect can be attributed to the small surface of the resin stripers inside the bath and to the fact that the resin level inside the resin tank dropped continuously during the experimental procedure. On the other hand the impregnation unit generated higher tension as the processing speed increased. This phenomenon has been extensively discussed in Chapter 7. Nevertheless as shown in the diagram, the developed impregnation model is able to predict precisely the magnitude of the winding tension over the complete processing window.

After curing, the wound laminates were cut to 12 mm wide rings. Samples were cut out of the rings and embedded in stereolithography potting resin for polishing microscopical analysis.

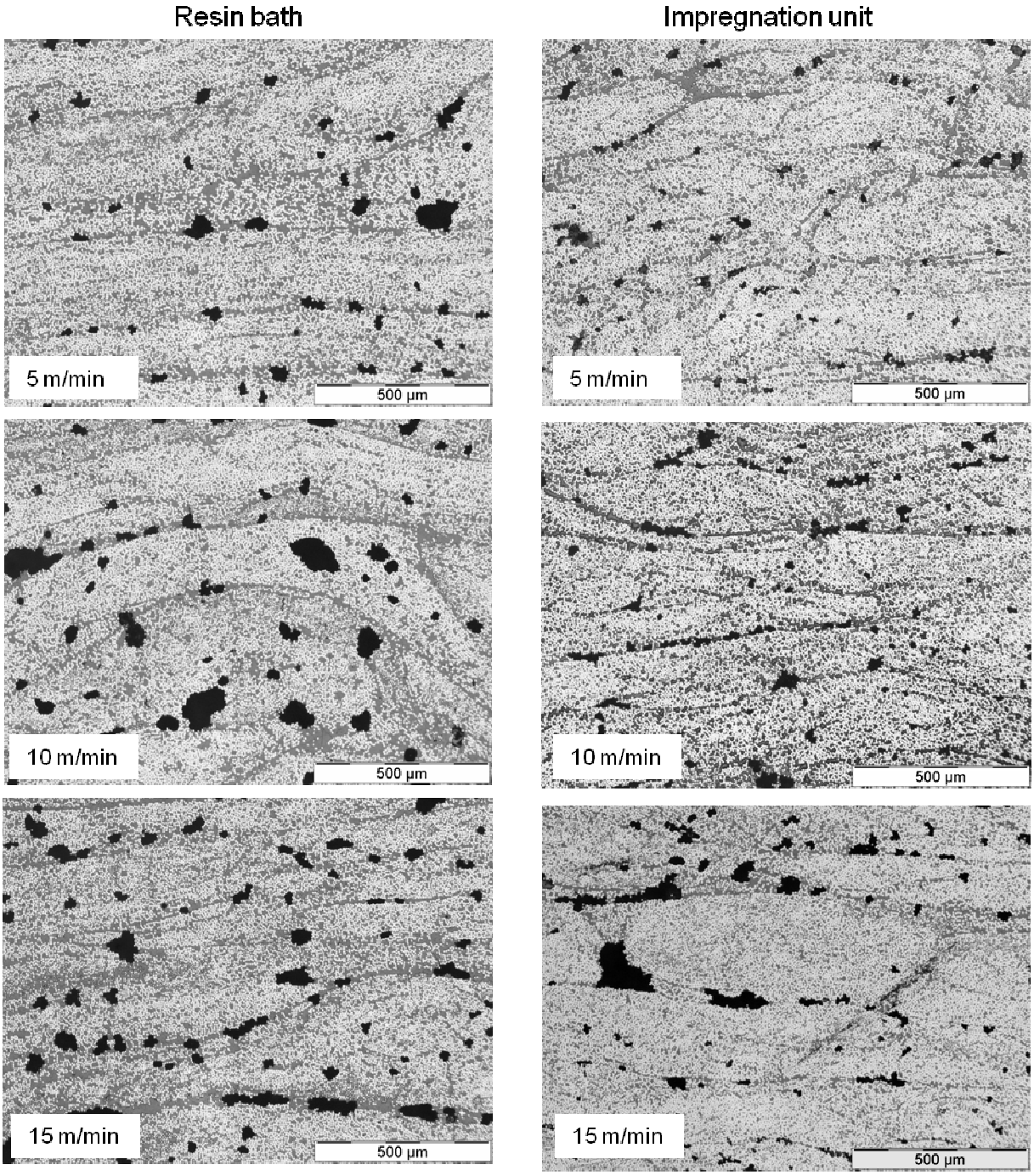

Figure 9.10: Micrographs of the wound samples with a conventional resin bath and the developed impregnation unit.

Figure 9.10 presents an overview of the micrographs extracted from the wound samples. The micrographs were taken at an optical microscope with a 50x magnification in order to give a wider overview of the laminate quality. By analyzing the results with an image processing software it was found that the void fraction at the samples im-

pregnated with the siphon impregnation system exhibit lower void and higher fiber volume fraction. The diagram of Figure 9.11 compares the void fraction values between the two processes. By observing the micrographs it was found that the majority of the voids were detected at the interface between the single rovings. Taking into account the fact that the rovings were laid on the mandrel fully impregnated it can be concluded that the voids they have been created during the lay down process. The grounds for the creation of the voids can be associated to the irregular Still for the case of the resin bath by increasing the winding speed more voids were detected in the intra roving region. Generally speaking the higher percentage of voids inside the resin bath laminate were attributed except to the lower tension values, to the fact that the resin weight fraction varies with the process speed and the process dependent impregnation conditions.

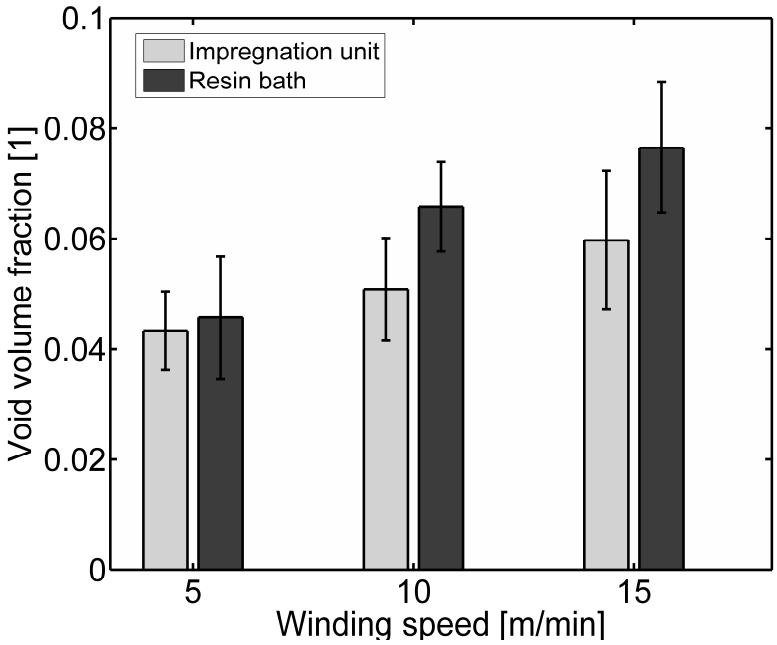

Figure 9.11:Void fraction inside the filament wound samples.

It was found that the laminates which were wound with the resin bath had a lower fiber volume fraction compared to the laminates which were wound with the impregnation unit. This was caused by the resin overflow and probably by the lower level of the generated tension. The diagram of Figure 9.12 presents the measured fiber volume fraction of the specimens in dependence to the winding speed. Combining the data of Figure 9.12 with the data of Figure 9.9 it can be concluded that the fiber vol-

ume fraction on the wound body is not controlled only by the resin content of the roving but also by the winding tension. This has also been verified by the studies of Gutowski et al. and Springer et al. [40 41].

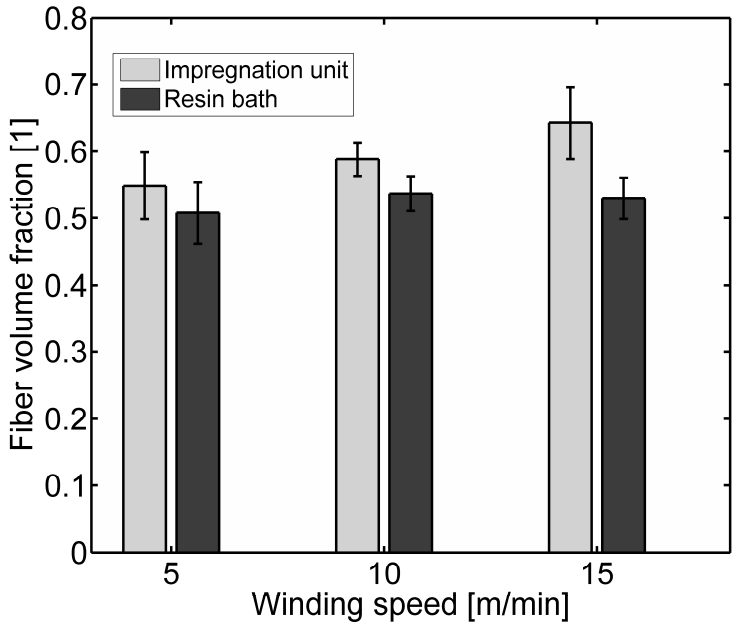

Figure 9.12: Fiber fraction inside the filament wound samples.

The ASTM test standard D 2344/D 2344M describes a 3-point bending test method for the short beam strength of polymer matrix composites. The test is applicable for wound laminates. According to the test standard the short beam strength is dominated by resin and interlaminar properties. As mentioned in the manuscript of the standard, the test can be used for quality control and specification purposes but it doesn't give any design values like mechanical properties.

Figure 9.13 presents the results of the short beam strength for the two different impregnation methods. According to the diagram, the samples which were produced with the use of the impregnation unit exhibit lower levels of short beam strength. Nevertheless the level of the reached stress stays constant over the tested parameter window. In the case of the resin bath the short beam strength values are higher compared to the impregnation unit but drop as a function of the winding speed.

The variation of the strength values can be attributed to the differences in the void concentration and to the fluctuation of the fiber volume fraction. The studies in [67–69] report that an increase of the void content leads to a decrease of the interlaminar

shear strength. On the other hand the research works in [76-78] associate a decrease of the short beam strength with a corresponding increase of the fiber volume fraction.

In order to explain the trend of the measured values, it can be supposed that the higher values of the resin bath are attributed to the significantly lower fiber volume fraction whereas the fluctuation in the values is a result of the increasing void fraction. Furthermore it was found that for the case of the impregnation unit the values are constant and independent to the processing parameters. In the case of 15 m/min it can be seen that impregnation unit and resin bath are on the same order of magnitude. Nevertheless the goal to maximize the interlaminar strength of the wound laminate overcomes the aims of this study.

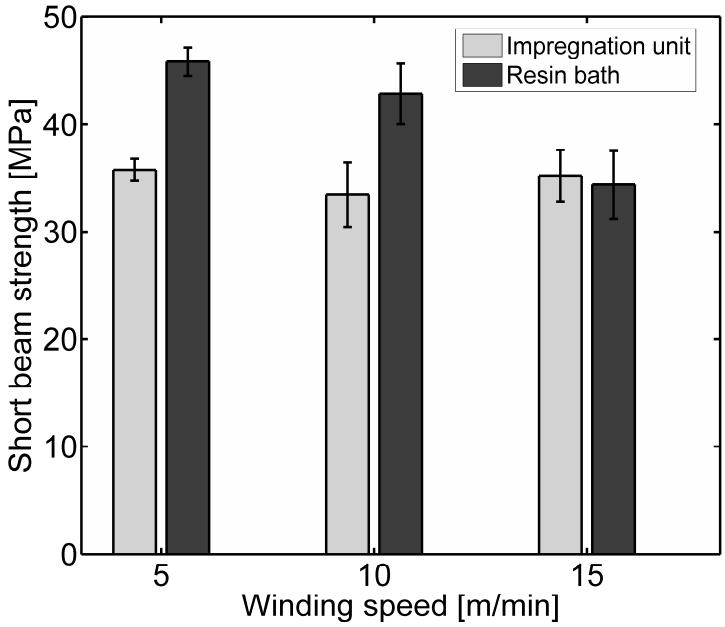

Figure 9.13: Short beam strength values of filament wound samples.

9.4. Techno economical aspects

Chapters 1 and 2 gave an overview about the motivation of the present work. Except the quality assurance and the better impregnation quality one of the most important aims that motivated the development of the impregnation unit is the reduction of the manufacturing costs. DuVall in [74] presented a model that calculated the costs for the manufacturing of type II and type IV pressure vessels by a filament winding process. DuVall in his model suggested that the impregnation process is a central point

that has a major effect on the costs and the productivity. In this paper, he gives the basic cost drivers for the filament winding process. He concludes that using towpregs instead of online impregnated roving wound result to higher unit costs but to an increased profit due to the increased output. However this study only took into account an impregnation process using traditional bath impregnators.

A techno-economical model was build in order to prove the economic advantages of the developed impregnation method. The model takes into account a typical filament winding process and a process using the developed impregnation system. Figure 9.14 presents the flow chart of a pressure vessel production line. The flow chart reveals that the winding process can be stopped by two events. The first event is that the fiber spools are empty and they have to be replaced whereas the second one is that the resin level inside the resin bath is low. In this case the winder has two options. The first one is to refill the bath and the second one is to remove it, clean it from the old resin, and fill it up with fresh resin again if the resin has reached a critical reaction level. In the present study it has been supposed that after a 3rd refill of the resin bath the remaining resin has to be completely removed. According to DuVall it's a common practice among the winders to perform the cleaning of the resin bath in a parallel station whereas the original bath is being replaced by a second unit. Although a quick replacement of the resin bath can be performed within a few minutes the cleaning of the bath demands labor and extensive use of solvents. DuVall estimated that about 200 l of acetone are needed for the production of 50 vessels (43 L Ø240 mm L1050mm). Moreover he made the hypothesis that the amount of chemical waste produced equals to the 1/3 of the used solvent.

The use of the bath impregnators is also associated with a series of other problems. The bath systems are not able to direct control the resin fraction (s. Chapter 8.4). This causes resin overflow which is squeezed off and has to be removed at the end of the winding process. The amount of resin wastage including the resin which is lost during the bath changing and resin mixing is considered to be about 35% more than the resin which is applied on the wound structure. Furthermore the inaccurate resin application results to a relatively high scrap rate. If the resin content of the final part is under or over the low and high weight specifications respectively then the component will not pas the quality control and it will have to be rejected. According to [74] the

scrap rate for the case of the traditional impregnation techniques is at 10%.

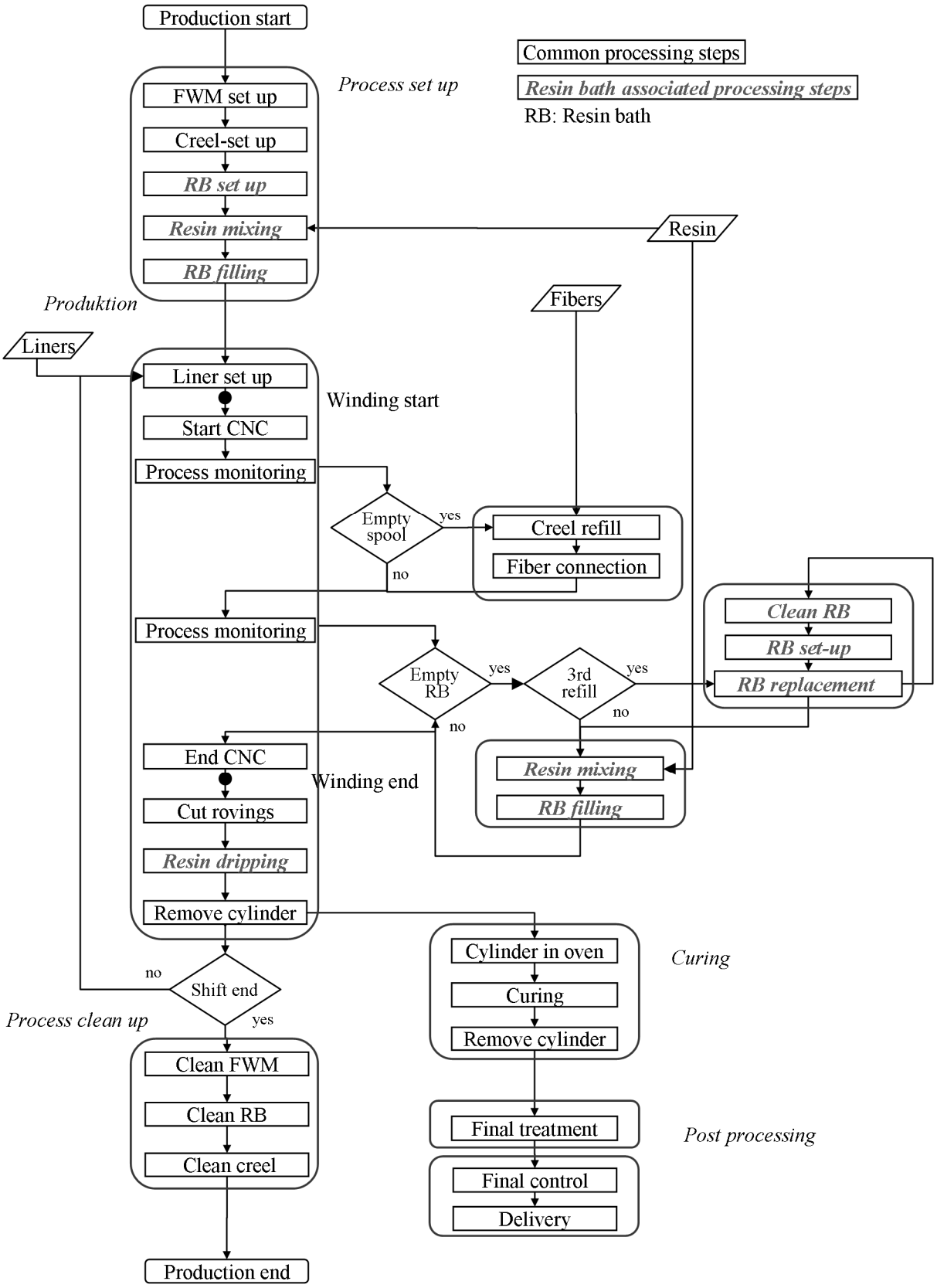

Figure 9.14: Flow chart of a typical winding process.

By using the developed siphon impregnation system some of the processing steps presented in Figure 9.14 are eliminated. During the preproduction phase, the set up of the resin bath is replaced by the set up of the impregnation unit and the set up of the dosing equipment. The winding process is at no time interrupted by the impregnation process. Because of the adjustment of the fiber volume fraction it is expected that the resin wastage will be minimized. The use of disposable parts minimizes the use of solvents. On the other hand the disposable resin static mixer, the tubes that formulate the impregnation cavity and the resin line that connects dosing systems and siphon have to be calculated in the costs.

The labor demands are different between the 2 processes. Although the winding process runs automatically the constant refill and cleaning of the resin baths consume a lot of work hours. Nevertheless the labor demand cannot be fully eliminated. Personnel are needed to monitor the process, mount and demount the liners and replace the empty spools.

The production costs for the production of a typical type III pressure vessel with a volume of 45 l and a working pressure of 350 bar working pressure were calculated. The cost calculations were based on the Activity Based Costing (ABC) method [75]. The ABC methodology is carried out by the following steps:

a) Identification of activities or transactions that generate costs during product development (sub-processes and main processes)

b) Identification of cost drivers associated with each sub-process

c) Assignment of costs to each sub-process via the creation of the Cost Estimation Relationships (CERs), and finally

d) Summation of the costs of sub-processes that occur to ‘make’ a product.

Since the present study focuses on the analysis of the impregnation process, the cost calculation was only restricted to the actual filament winding process. Costs dealing with the curing, the testing, and the quality assurance of the pressure vessel as well with the liner were not taken into account. It should be pointed out, that the investment and the depreciation costs associated with the acquisition of the impreg-

nation system were excluded from the calculation. These costs are considered to be for both impregnation methods neglectable small in comparison to the total investment costs for the installation of a pressure vessel production line.

Table 9.1 presents the unit costs of the basic cost drivers. The values given to every cost driver are representative of the current market values. Table 9.2 gives details about the winding process simulated by the costing model. The total fiber mass that is wound on the liner is assumed to be 7.5 kg. For the winding are used 4x 24k rovings with 1600 tex. Taking into account an average winding speed of 15 m/min a clear winding time of 78.13 min has been calculated. It was assumed that the winding takes place with a 3 spindle winding machine. The size of the resin bath was set at 3.5 kg. That means as soon as 3.5 kg resin are consumed, the resin bath has to be refilled or replaced. The duration of the production time was set at 16 h.

Table 9.2 presents the time consumed by the different activities during the winding process for the two different processes. If a time is no given then that means that the activity is not applicable for the particular process

By analyzing the activities it was made clear that a winding cell using a standard resin bath needs at least 2 workers. The first one should be an experienced winding technician who controls the processes and an additional assistance that overtakes the work of the resin bath refill and replacement. By analyzing the workflow it was found that the experienced winder has to supervise full time a single winding station whereas the assistance can serve 2 winding stations in parallel. On the other hand for the case on the winding process that used the impregnation unit, it was calculated that a single technician wound be enough to overtake the work load of one winding station.

Table 9.3 gives details about the winding process simulated by the costing model. The total fiber mass that is wound on the liner is assumed to be 7.5 Kg. For the winding are used 4x 24k rovings which have a yield of 1600 tex. Taking into account an average winding speed of 15 m/min a clear winding time of 78.13 min has been calculated. It was assumed that the winding takes place with a 3 spindle winding machine. The size of the resin bath was set at 3.5 kg. That means as soon as 3.5 kg resin are consumed, the resin bath has to be refilled or replaced. The duration of the

production time was set at 16 h.

Table 9.1: Unit costs of the basic cost drivers.

Materials	
Fibers	20.00 €/kg
Resin	8.00 €/kg
Resin waste	8.00 €/kg
Cleaning agents	
Acetone	2.00 €/l
Chemical waste	3.00 €/l
Consumables	
PTFE Tube	5.20 €/m
Static Mixer	2.50 €/pc.
Disposable resin line	1.25 €/m
Labor costs	
Wage rate skilled winder	40.00 €/h
Wage rate assistant winder	30.00 €/h

Table 9.2: Work steps time estimation.

	Resin bath	**Impregnation unit**
Set up		
FMA set-up	15.00 min	15.00 min
Creel set-up	7.00 min	7.00 min
RB set-up	5.00 min	-
Initial resin mix	15.00 min	-
RB fill up	5.00 min	-
Impregnation unit set-up	-	5.00 min/spindle
Dosing system set-up	-	10.00 min
Production		
Liner set-up	3.00 min/spindle	3.00 min/spindle
CNT start	1.00 min	1.00 min
Spool change	1.00 min/spool	1.00 min/spool
RB replacement	5.00 min	-
Rb cleaning	20.00 min	-
RB set-up	5.00 min	
Initial resin mix	15.00 min	-
RB refill	5.00 min	-
Resin dripping	5.00 min/spindle	2.00 min/spindle
Liner demount	3.00 min/spindle	3.00 min/spindle
Clean up		
FMA cleaning	10.00 min	10.00 min
Rb cleaning	20.00 min	-

Creel cleaning	10.00 min	10.00 min
Impregnation unit cleaning	-	5.00 min/spindle
Dosing system cleaning	-	10.00 min

Table 9.3: Winding scenario.

Cylinder fiber weight	7.50 Kg
Roving tex	1600
Spool size	5.00 Kg
RB size	3.50 Kg
Average winding speed	15.00 m/min
No. Of Rovings	4
Winding time	78.13 min
No of Spindles	3
Shift	16.00 h

Figure 9.15 illustrates the costs of the winding process for the two cases. It was found out that the total costs in the case of the resin bath are 222.3 € whereas in the case of the impregnation unit are 199.6 €, meaning that they are reduced by 10.2%. This is attributed both to the reduction of the material costs as well as to the reduction of the labor hours. Although the cylinders are considered to be identical, the reduced material costs are about 4 %. This is because of the lower resin wastage and to reduced generation of chemical waste and thus chemical waste disposal. This difference would be even higher but the relative high costs of the PTFE tubes and static mixers used in the impregnation unit balance out the result. On the other hand the labor costs are reduced about 36 %. The absence of the second assistant who is responsible for the resin refill is the main reason for that.

Figure 9.16 illustrates the effect of the impregnation method on the daily productivity. The diagram reveals that the daily production of a winding cell that works in a 16 hour shift would increase 14 %. This is due to the reduction of the process interruption for refilling and cleaning the resin bath. Moreover the time on the end of every winding circle that is required for removing the excess resin form the produced cylinder is minimized.

The reduced costs as well as the increased productivity will have a positive impact on the profit of a winding company. Providing the fact that the market needs consume the total production and there is a sufficient profit on the selling price of the vessel,

150 € for the conventionally manufactured cylinder, the total profitability of the company will be increased more than 30 % only by the use of the developed impregnation system.

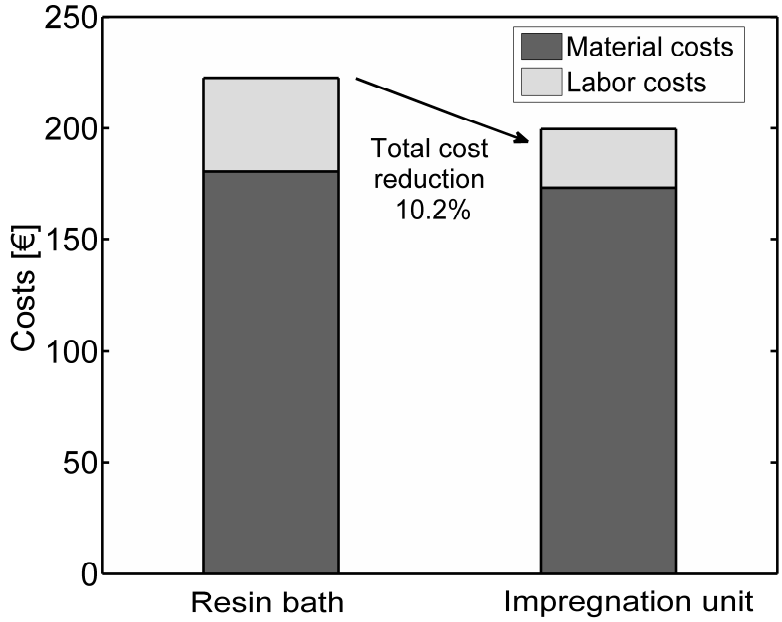

Figure 9.15: Apparent winding costs.

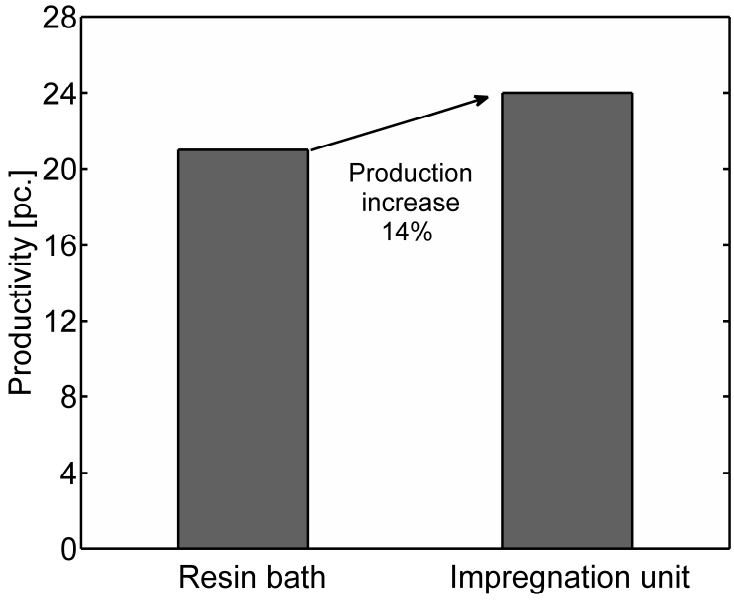

.

Figure 9.16: Daily productivity of a 3 spindle winding machine in 16h shift.

9.5. Further industrial applications

The impregnation system as described above can be used with light modifications in a series of other manufacturing processes.

The idea to impregnate fibers by means of a sinusoidal cavity can be adopted in a pultrusion process. In this case the process designer has the possibility either to use one single impregnation cavity for every yarn or, to guide multiple yarns through an impregnation unit with the appropriate cavity. Figure 9.17 illustrates a test pultrusion set-up with an integrated siphon impregnation unit. The die was designed for the manufacturing of round profiles made of glass fibers and thermoset quick reacting resin material. In this test 18 glass rovings (1600 Tex) which resulted to a fiber volume fraction of 0.55 were pulled though a single impregnation unit. Micrographic analysis (s. Figure 9.17) prooved that the pultruded profile was fully impregnated and free of voids.

Figure 9.17: Left: Pultrusion die with integrated impregnation unit. Middle: build impregnation unit module. Right: Micrograph of the cross section of the pultruded profile.

A further application of the developed technology could be the application of resin at a tow-preg process. This process is very similar to the online impregnation of the rovings during the filament winding process. In this case the impregnated rovings are not wound on a mandrel but they are wound on a spool which can be unwound later on. Moreover in the towpreg production, the process runs at a constant speed which allows very constant processing conditions.

According to the resin formula, the range of the mixture viscosity can vary from 10^1 up to 10^3 mPa s. it is a common industrial practice to heat up the viscous components in order to drop the mixture viscosity and be able to impregnate the fibers.

Nevertheless the heating up of a resin bath shortens the pot life of the resin and increases the possibility of an unexpected and uncontrolled exothermic reaction. In the same way, the process designer can add a tempering system in the impregnation unit and in the metering equipment in order to decrease the resin viscosity and allow a better impregnation. In contrary to the resin baths, since the volume of resin is restricted inside the impregnation unit and the resin components are online mixed by the metering-mxing equipment, the danger of an unexpected reaction does not exist. Moreover due to the continuous resin flow the shortage of the pot life by the elevated temperature does not restrict the process efficiency. The diagram of Figure 9.18 illustrates the possible implementation of the developed impregnation unit at a towpreg production line. In this case the biggest advantage of the impregnation unit is the ability to precisely control the resin content.

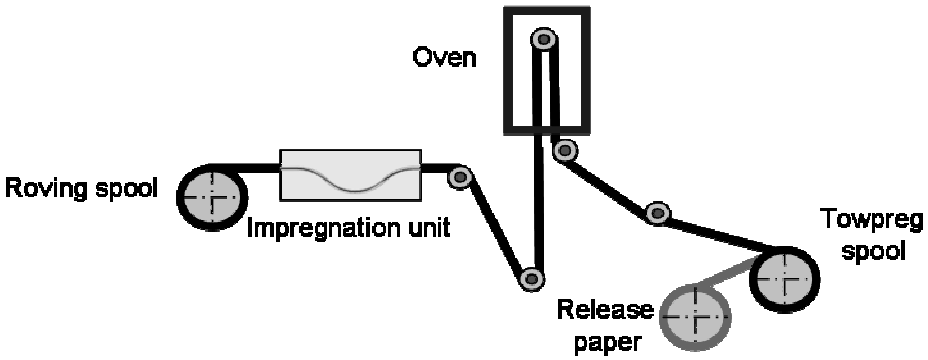

Figure 9.18: Schematic diagram of a possible towpreg line using the siphon impregnation unit.

Except the production of towpregs, the system is suitable for the application of different kinds of sizing on various types of fibers. It is often required that a functionalizer should be applied on the surface of the fibers. The functionalizers are chemical solutions that advance the properties of the fiber interface and improve the properties of the composite. In this case the developed impregnation unit can be used to carry out this task. The functionalizers could be applied either in their original form or solved in a solution depending on the set value of the weight content. Again in this application the strongest advantage of the impregnation unit is the ability to precisely control the process as well as the closed cavity that restricts the volcanic emissions.

The concept of the impregnation unit that was presented in the previous chapters

was mainly based on the use of PTFE tubes for the formulation of the impregnation cavity. This concept has a series of advantages since the tubes offer low friction coefficient, do not damage the fibers or cause fiber fuzzle, they are used as disposable parts which do not require cleaning or any kind of maintenance. Nevertheless the developed know how is applicable for the design of impregnation units with sinusoidal cavities that are not based on disposable PTFE tubes. Alternative to the tubes and depending to the given process specifications solutions like metal polished cavity, or ceramic coated surfaces can be used without deviating from the developed impregnation concept.

10. Summary and conclusions

The presented study describes the development of a novel method for the continuous impregnation of endless carbon fiber rovings. The various steps of the development included the review of the state of the art, the development of a simulation tool, the performance of parameter studies, the design of an optimum impregnation unit, the implementation of the unit in a filament winding process and the evaluation of the economic impact of the process.

The review of the state of the art has revealed that the established impregnation methods which have not further developed since their initial development during the 60's they still face the problem of resin advance that leads to instable processing conditions. Furthermore the exposure of resin's surface to the open air results to high VOC and ODC emissions. Although a series of research works have tried to face these problems none of the developed solutions has made it possible to fully replace the bath systems in the praxis.

A new impregnation method has been introduced. The method is based on a closed design exhibiting a sinusoidal cavity. Fibers and resin enter the impregnation unit and due to the special design of the die a low hydrostatic pressure is being developed on the resin film. This hydrostatic pressure together with the capillary action is forcing the impregnation.

A methodical discretization of the physical phenomena that occur during the impregnation of an endless CF roving has led to the identification of the physical laws that are critical for the description of the process. Under the framework of the presented study the mathematical expressions concerning the capillary action and the viscous drag of the roving have been experimentally verified. The results have shown that these laws can be applied to describe phenomena that occur during the manufacturing of composite materials.

An algorithm has been developed in order to simulate the evolution of the impregnation process. The algorithm implements all the identified physical laws. Based on this algorithm a mathematical simulation tool which uses the MATLAB® computing environment has been built. The simulation tool has a GUI interface that allows the user

to input all relevant data and extract valued information.

The performed parameter study has revealed the importance of the various processing parameters and has validated the simulation tool. According to the findings of the study, the design of the cavity (number of curves, radius, and deflection angle) are critical for the development of the impregnation process. The tension that develops during the process affects the compaction of the roving and controls the impregnation pressure. The resin dosing rate sets the resin weight fraction and affects the development of the viscous drag.

The outcome of the above tasks was the design of an optimized siphon impregnation unit. The device is able to impregnate 24k CF rovings under linear speeds of 30 m/min. A specially designed resin dosing apparatus has been build and commissioned together with the impregnation unit. The system has been successfully implemented into a filament winding process. Different wound parts under variable processing conditions have been produced. The inspection of the samples has revealed that the developed impregnation system is able to provide advanced and stable laminate quality independent to the processing conditions.

The use of the developed impregnation system in a filament winding production cell will lead to a more efficient use of the raw materials and to the reduction of labour. According to the performed techno economical evaluation the manufacturing costs will decrease. The absence of process stops caused by the impregnation process will further increase the productivity of the winding unit. The reduced costs combined with the increased productivity will maximize the profit of the cell. The system was successfully used for the winding of type III and type IV pressure vessels and the testing results showed that the produced parts fulfill the design specifications.

Concluding, the presented work based on the scientific analysis of the impregnation process developed a complete know-how packet which can be used by the state of the art processing of unidirectional composites. The developed impregnation method not only advances the impregnation quality but has a major economic as well as environmental impact.

11. References

[1] Neitzel, M.; Mitschang, P.: Handbuch Verbundwerkstoffe. Werkstoffe, Verarbeitung, Anwendung. München: Hanser, 2004.

[2] Witten, E.; Schuster, A.: Composites Marktbericht: Marktenentwicklungen, Herauforderungen und Chancen. Frankurt: AVK, 2011.

[3] Ahn, K. J.; Seferis, J. C.: Prepreg Processing Science and Engineering. Polymer Engineering and Science Vol. 33, Part 18 (1993), pp. 1177–88.

[4] Paessler, M.; Schledjewski, R.: Thermoset Filament Winding with High Efficiency. In: 9. Internationale AVK Tagung. Essen, Germany, 2006.

[5] Paessler, M.; Schledjewski, R.: Manufacturing of Pressure Vessels for Hydrogen Storage in Automotive Applications. In: SAMPE Europe 28th International Conference. Paris, France, 2007.

[6] EHA Composite Machinery GmbH: Photo Galery. URL: http://www.eha.run-web.de (1.10.2011).

[7] Fibrolux GmbH: Photo Galery. URL: http://fibrolux.com (5.10.2011).

[8] Jones, R. T.: Method of Impregnation Permantent form to Resin Impregnated Webbing (1959). Patent No.: US 3,091,547.

[9] Mc Larty, J. L.: Device for Coating a Strand with a Binding Material (1973). Patent No.: Part US 3,874,329.

[10] Mc Clean Anderson: Phot Galery. URL: http://www.mccleananderson.com/auxiliary%20equipment/resin%20baths.html (14.10.2011) .

[11] Kellogg, C. W.: Winding Apparatus for the Manufacture of Filament-wound, Reinforced Resinous Products (1979). Patent No.: US 4,267,007.

[12] Rolston, J. A.: Resin-stripping Die (1987). Patent No.: US 4,775,434.

[13] Gehard, D.; Walter, G.; Eberherd, j.; Erwin, M.; Richard, W.: Thermoplastic

resin Paste Impregnated Substrates (1981). Patent No.: US 4,464,432.

[14] Furbeck, W.: Method and apparatus for impregnating and drying material in a fibrous web (1969). Patent No.: US 3,553,845.

[15] CTM GmbH - Composite Technologie & Material: Photo Galery. URL: http://www.ctmat.de (14.10.2011).

[16] COATEMA Coating Machinery GmbH: Photo Galery. URL: http://www.coatema.de (18.10.2011).

[17] Voorakaranam, S.; Joseph, B.; Kardos, J. L.: Modeling and Control of an Injection Pultrusion Process. Journal of Composite Materials Vol. 33, Part 13 (1999), pp. 1173–204.

[18] Rahatekar, S. S.; Roux, J. A.: Numerical Simulation of Pressure Variation and Resin Flow in Injection Pultrusion. Journal of Composite Materials Vol. 37, Part 12 (2003), pp. 1067–82.

[19] Jeswani, A.; Roux, J.; Vaughan, J.: Multiple Injection Ports and Part Thickness Impact on Wetout of High Pull Speed Resin Injection Pultrusion. Journal of Composite Materials Vol. 43, Part 19 (2009), pp. 1991–2009.

[20] Gauchel , J.; Lehman, R.: Apparatus for Resin Impregnated Pultrusion (1995). Patent No.: US 5,747,075.

[21] Beall, F.; Koppernaes, J.: Pultrusion Method for Condensation Resin Injection (1990). Patent No.: US 5,176,865.

[22] Packer, B.; Rhodes, M.; Montgomery, R.; Holstein, R.: Apparatus for Fiber Impregnation (1996). Patent No.: US 5,766,357.

[23] Glemet, M.; Gourdon, B.; Lottiau, M.: Process for Producing Thermoplastic Resins Reinforced with Long Fibers (1988). Patent No.: US 4,937,028.

[24] Marttila, P.: Method and Apparatus for Impregnating a Continuous Fiber Bundle Wherein a Nozzle Impinges on the Fiber Bundle in a Chamber (1990). Patent No.: US 5,084,305.

[25] Custer, M.; Vicknair , K.; Sherwood , W.: Method and Apparatus for Impregnating fibers with Highly Viscous Materials and Article Made Therewith (1990). Patent No.: US 5,573,813.

[26] Unger, M.: Method and Apparatus for Manufacturing Fibre-reinforcing Material (1990). Patent No.: US 5,158,806.

[27] Azari, A.: Process for Using an Extruder Die Assembly for the Production of Fiber Reinforced Thermoplastic Pellets, Tapes and Similar Products (1991). Patent No.: US 5,268,050.

[28] Britton , A.; Smith , J.; Davis , R.; Page , J.: Application of Liquid Material to Webs (1978). Patent No.: US 4,259,379.

[29] Connolly, M.; King, J.; Shidaker, T.; Duncan, A.: Pultruding Polyurethane Composite Profiles: Practical Guidelines for Injection Box Design, Component Metering Equipment and Processing. In: COMPOSITES 2005 Convention and Trade Show. Columbus, Ohio, 2005.

[30] Chandler, H. W.; Delvin, B. J.; Gibson, A. G.: A Model for the Continuous Impregnation of Fibre Tows in Resin Baths With Pins. Plastics Rubber and Composites Processing and Applications Vol. 4, Part 18 (1992), pp. 215–20.

[31] Scheidegger, A. E.: The Physics of Flow Through Porous Media, 3d. Toronto, Buffalo [N.Y.]: University of Toronto Press, 1974.

[32] Cai, Z.; Gutowski, T. G.: The 3-D Deformation Behavior of a Lubricated Fiber Bundle. Journal of Composite Materials Vol. 26, Part 8 (1992), pp. 1207–37.

[33] Gutowski, T. G.; Dillon, G.: The Elastic Deformation of Lubricated Carbon Fiber Bundles: Comparison of Theory and Experiments. Journal of Composite Materials Vol. 26, Part 16 (1992), pp. 2330–47.

[34] Darcy, H.: Les Fontaines Publiques de la Ville de Dijon. Paris: Dalmont, 1856.

[35] Carman, P. C.: Fluid Flow Through Granular Beds. Trans. Inst. Chem. Eng. Vol. 15 (1937), pp. 150–66.

[36] Gutowski, T. G.; Cai, Z.; Bauer, S.; Boucher, D.; Kingery, J.; Wineman, S.: Consolidation Experiments for Laminate Composites. Journal of Composite Materials Vol. 21, Part 7 (1987), pp. 650–69.

[37] Skartsis, L.; Kardos, J. L.; Khomami, B.: Resin Flow Through Fiber Beds During Composite Manufacturing Processes. Part I: Review of Newtonian Flow Through Fiber Beds. Polymer Engineering and Science Vol. 32, Part 4 (1992), pp. 221–30.

[38] Gutowski, T. G.; Morigaki, T.; Zhong Cai: The Consolidation of Laminate Composites. Journal of Composite Materials Vol. 21, Part 2 (1987), pp. 172–88.

[39] Gebart, B.: Permeability of Unidirectional Reinforcements for RTM. Journal of Composite Materials Vol. 26, Part 8 (1992), pp. 1100–33.

[40] Cai, Z.; Gutowski, T.; Allen, S.: Winding and Consolidation Analysis for Cylindrical Composite Structures. Journal of Composite Materials Vol. 26, Part 9 (1992), pp. 1374–99.

[41] Lee, S.-Y.; Springer, G. S.: Filament Winding Cylinders: I. Process Model. Journal of Composite Materials Vol. 24, Part 12 (1990), pp. 1270–98.

[42] Bates, P. J.; Kendall, J.; Taylor, D.; Cunningham, M.: Pressure Build-up During Melt Impregnation. Composites Science and Technology Vol. 62, Part 3 (/2), pp. 379–84.

[43] Gaymans, R. J.; Wevers, E.: Impregnation of a Glass Fibre Roving with a Polypropylene Melt in a Pin Assisted Process. Composites Part A: Applied Science and Manufacturing Vol. 29, Part 5-6 (1998), pp. 663–70.

[44] Rebouillat, S.; Letellier, B.; Steffenino, B.: Wettability of Single Fibres - Beyond the Contact Angle Approach. International Journal of Adhesion and Adhesives Vol. 19, Part 4 (1999), pp. 303–14.

[45] Hayes, B. S.; Seferis, J. C.: The Effect of Fabric Tension and the Number of Impregnation Rollers on Woven Fabric Prepreg Quality and Cured Laminates. Composites Part A: Applied Science and Manufacturing Vol. 28, Part 9-10 (1997), pp. 791–99.

[46] Bates, P. J.; Charrier, J. M.: Pulling Tension Monitoring During the Melt Impregnation of Glass Roving. Polymer Composites Vol. 21, Part 1 (2000), pp. 104–13.

[47] Giordano, M.; Nicolais, L.: Resin Flow in a Pultrusion Process. Polymer Composites Vol. 18, Part 6 (1997), pp. 681–86.

[48] James, D. F.; Davis, A. M. J.: Flow at the Interface of a Model Fibrous Porous Medium. Journal of Fluid Mechanics Vol. 426 (2001), pp. 47–72.

[49] Gibson, A. G.: Modification of Darcy's Law to Model Mould Interface Effects in Composites Processing. Composites Manufacturing Vol. 3, Part 2 (1992), pp. 113–18.

[50] Ochoa-Tapia, J. A.; Whitaker, S.: Momentum Transfer at the Boundary Between a Porous Medium and a Homogeneous Fluid--I. Theoretical Development. International Journal of Heat and Mass Transfer Vol. 38, Part 14 (1995), pp. 2635–46.

[51] Le Bars, M.; Worster, M. G.: Interfacial Conditions Between a Pure Fluid and a Porous Medium: iImplications for Binary Alloy Solidification. Journal of Fluid Mechanics Vol. 550 Part -1 (2006), pp. 149.

[52] Kissinger, C.; Mitschang, P.; Neitzel, M.; Roder, G.; Haberland, R.: Continuous on-line Permeability Measurement of Textile Structures.In: Loud, S. (Hrsg.): Bridging the Centuries with SAMPE's Materials and Processes Technology. Long Beach Convention Center, Long Beach California, May 21-25, 2000. Covina, Calif 2000.

[53] Rieber, G.; Mitschang, P.: 2D Permeability Changes Due to Stitching Seams. Special Issue: Flow Processes in Composite Materials. Composites Part A: Applied Science and Manufacturing Vol. 41, Part 1 (2010), pp 2–7.

[54] Stoeven, T.; Weyrauch, F.; Mitschang, P.; Neitzel, M.: Continuous Monitoring of Three-dimensional Resin Flow Through a Fibre Preform. ICMAC 2001 - International Conference for Manufacturing of Advanced Composites. Composites Part A: Applied Science and Manufacturing Vol. 34, Part 6 (2003), pp. 475–80.

[55] Stalder, A. F.; Melchior, T.; Mueller, M.; Sage, D.; Blu, T.; Unser, M.: Low-bond Axisymmetric Drop Shape Analysis for Surface Tension and Contact Angle

Measurements of Sessile Drops. Colloids and Surfaces A: Physicochemical and Engineering Aspects Vol. 364, Part 1-3 (2010), pp. 72–81.

[56] Batch, G. L.; Chen, Y.-T.; Macoskot, C. W.: Capillary Impregnation of Aligned Fibrous Beds: Experiments and Model. Journal of Reinforced Plastics and Composites Vol. 15, Part 10 (1996), pp. 1027–51.

[57] Szekely, J.; Neumann, A. W.; Chuang, Y. K.: The Rate of Capillary Penetration and the Applicability of the Washburn Equation. Journal of Colloid and Interface Science Vol. 35, Part 2 (1971), pp. 273–78.

[58] Washburn, E. W.: The Dynamics of Capillary Flow. American Physics Society: 374 Part 17 (1921), pp. 374.

[59] Amico, S.; Lekakou, C.: An Experimental Study of the Permeability and Capillary Pressure in Resin-transfer Moulding. Composites Science and Technology Vol. 61, Part 13 (2001), pp. 1945–59.

[60] Ahn, K. J.; Seferis, J. C.; Berg, J. C.: Simultaneous measurements of permeability and Capillary Pressure of Thermosetting Matrices in Woven Fabric Reinforcements. Polymer Composites Vol. 12, Part 3 (1991), pp. 146–52.

[61] Miaris, A.; Paessler, M.; Lichtner, J.; Schledjewski, R.: “Siphon impregnation”: The Development of a New Method for Impregnation During Filament Winding. In: 17th International Conference on Composite Materials. Endiburgh, UK, 2009.

[62] Miaris, A.; Päßler M., P.; Schledjewski, R.: Effects of the Impregnation Die Geometry on the Roving Tension and Laminate Quality During Filament Winding. In: 14th European Conference on Composite Materials. Budapest ,Hungary, 2010.

[63] Deckers, M. E.; Dainton, R. L.; Adkinson, W. R.: Improved Process for Fabrication of Composite Flextensional Shells. Orlando, Florida, US, 1988.

[64] Peters, S. T.; Humphrey, W. D.; Foral, R. F.: Filament winding. Composite structure fabrication. Covina, CA: Society for the Advancement of Material and Process Engineering, 1991.

[65] Greszczuk, L.: Compressive Strength and Failure Modes of Unidirectional Composites. Analysis of the Test Methods for High Modulus Fibers and Composites, ASTM STP-521 (1973), pp. 192–217.

[66] Kunz, S.; Beaumont, P. W. R.: Microcrack Growth in Graphite Fiber-Epoxy Resin Systems during Compressive Fatigue. Fatigue of Composite Materials, ASTM STP-569 (1975), pp. 71–91.

[67] Bowles, K. J.; Frimpong, S.: Void Effects on the Interlaminar Shear Strength of Unidirectional Graphite-Fiber-Reinforced Composites. Journal of Composite Materials Vol. 26, Part 10 (1992), pp. 1487–509.

[68] Hancox, N. L.: The Effects of Flaws and Voids on the Shear Properties of CFRP. Journal of Materials Science Vol. 12, Part 5 (1977), pp. 884–92.

[69] Yoshida, H.; Ogasa, T.; Hayashi, R.: Statistical Approach to the Relationship Between ILSS and Void Content of CFRP. Composites Science and Technology Vol. 25, Part 1 (1986), pp. 3–18.

[70] Rousseau, J.; Perreux, D.; Verdière, N.: The Influence of Winding Patterns on the Damage Behaviour of Filament-Wound Pipes. Composites Science and Technology Vol. 59, Part 9 (1999), pp. 1439–49.

[71] Bai, J.; Seeleuthner, P.; Bompard, P.: Mechanical Behaviour of ± 55 ° Filament-wound Glass-Fibre/Epoxy-Resin Tubes: I. Microstructural Analyses, Mechanical Behaviour and Damage Mechanisms of Composite Tubes Under Pure Tensile loading, Pure Internal Pressure, and Combined Loading. Composites Science and Technology Vol. 57, Part 2 (1997), pp. 141–53.

[72] Stecenko, T.; Piggott, M. R.: Fiber Waviness and Other Mesostructures in Filament Wound Materials. Journal of Reinforced Plastics and Composites Vol. 16, Part 18 (1997), pp. 1659–74.

[73] Cohen, D.: Influence of Filament Winding Parameters on Composite Vessel Puality and Strength. Composites Part A: Applied Science and Manufacturing Vol. 28, Part 12 (1997), pp. 1035–47.

[74] DuVall, F. W.: Cost Comparisons of Wet Filament Winding Versus Prepreg Filament Winding for Type ii and Type iv CNG Cylinders. SAMPE Journal Vol. 37, Part 1 (2001).

[75] O'Guin, M. C.: The Complete Guide to Activity-Based Costing. Englewood Cliffs, N.J: Prentice Hall 1991.

[76] Wisnom, M. R.; Reynolds, T.; Gwilliam, N.: Reduction in Interlaminar Shear Strength by Discrete and Distributed Voids. Composites Science and Technology Vol. 56 Part 1 (1996), pp. 93–101.

[77] Davies, P.; Casari, P.; Carlsson, L.: Influence of fibre Volume Fraction on mode II Interlaminar Fracture Thoughness of Glass/Epoxy Using the 4ENF Specimen. Composites Science and Technology Vol. 65, Part 2 (2005), pp. 295–300.

[78] Woods, D. W.; Ward, I. M.: Study of the Interlaminar Shear Strength of Unidirectional High-Modulus Polyethylene Fibre Composites. Journal of Materials Science Vol. 29, Part 10 (1994), pp. 2572–78.

[79] Päßler, M.; Miaris, A.; Schledjewski, R.; Mitschang, P.: Ring Winding Technology – Increased Process Efficiency and Effects on the Mechanical Properties of Ring Specimens In: Proc. of the ASME 2011 Pressure Vessels and Piping Conference (PVP 2011). Baltimore, MD, USA, 2011.

[80] Grafil inc.: Data Sheet: Carbon Fiber Roving Grafil 34-700, 2011. Sacramento, USA.

[81] Huntsman LLC.: Data Sheet: Warm Curing Epoxy System Based on Araldite LY 564 / Hardener XB 3486, 2011. Basel, Switzerland.

List of the supervised student thesis and internships

Estevez, X.: Design and modelling of an injection box for polyurethane pultrusion. Internship report 2008.

Picot, G.: Beschreibung der Hauptparameter in die Duroplast-Pultrusion von 2-Komponenten Polyurethan und E-Glasfaser FEM Modellierung des Temperaturverlaufs. Studienarbeit 2008.

Degel, J.: Erweiterung eines Prüfstandes um die Aufhängung eines Lasermoduls als Heizquelle für die Online-Konsolidierung von kohlenstoffaserverstärkten Thermoplasttapes. Studienarbeit 2008.

Philippsen, M.: Entwicklung eines Systems zur Temperierung einer Konsolidierungsrolle mit Druckluft für den Tapelegeprozess. Studienarbeit 2009.

Roddriguez, M.: Capillary Impregnation of Fiber Rovings. Internship report 2009.

Adams, B.; Maier, B: Entwicklung einer adaptiven, außengekühlten Konsolidierungsrolle für den Bindertapelegeprozess. Studienarbeit 2010.

Mack, J.: Experimentelle Untersuchung der Einflussfaktoren für die Qualitätssicherung des Thermoplast-Tapeherstellungs-prozesses. Diplomarbeit 2010.

O'Donoghue, R.: Determination of the capillary effect during impregnation of single rovings. Internship report 2010.

Bolz, K.: „Vergleich von ungesättigten Polyesterharzen und Polyurethanharzen zur Herstellung von Faserverbunden". Seminararbeit 2010.

Tapeinos, I.: Techno economic study of the Ring Winding Technology with integrated closed type impregnation unit. Internship report 2010.

Publications list

Miaris, A.; Paessler, M.; Schledjewski, R.; Mitschang, P.: Modeling the Impregnation Process of a Siphon Impregnation System during Filament Winding. In: Proc. of the ASME 2011 Pressure Vessels and Piping Conference (PVP 2011). Baltimore, MD, USA, 2011

Päßler, M.; Miaris, A.; Schledjewski, R.; Mitschang, P.: Ring winding technology – increased process efficiency and effects on the mechanical properties of ring specimens . - in: Proc. of the ASME 2011 Pressure Vessels and Piping Conference (PVP 2011). Baltimore, MD, USA, 2011

Miaris, A.; Schledjewksi, R.: Spontaneous Impregnation and Capillary Phenomena in Carbon Fiber Rovings. In: Proc. of the 7th Asian Conference on Composite Materials (ACCM 7). Taipei, Taiwan, 2010

Miaris, A.; Päßler, M.; Schledjewski, R.: Effects of the impregnation die geometry on the roving tension and laminate quality during filament winding In: Proc. of the 14th European Conference on Composite Materials (ECCM 14). Budapest ,Hungary, 2010

Miaris, A.; Paessler, M.; Lichtner, J.; Schledjewski, R.: “Siphon impregnation”: The development of a new method for impregnation during filament winding. In: Proc. of the 17th International Conference on Composite Materials (ICCM 17). Edinburgh, UK, 2009

Schledjewksi, R.; Miaris, A.: Thermoplastic Tape Placement by Means of Diode Laser Heating. - in: Proc. of SAMPE 2009 International Conference. Baltimore, MD, USA, 2009

Tsotra, P.; Karappapas, P.; Vavouliotis, A.; Loutas, T.; Miaris, A.; Tsantzallis, S.; Kostopoulos, V.: On the improvement of the fracture behaviour of the unidirectional CFRP laminates by the use of multi-wall CNTs as matrix dopants. – in Proc of the 12th European Conference on Composite Materials (ECCM 12). Biarritz, France, 2006

Vavouliotis, A.; Karappapas P.; Tsotra, P.; Miaris, A.; Nikolaou, N.; Kostopoulos,

V.: Mwcnt-modified fiber reinforced composites with nano-sensing capabilities: a way towards the development of the new functional materials. –in Proc. of the 57th International Astronautical Congress (IAC). Valencia, Spain, 2006

Vavouliotis, A.; Miaris, A.; Patricio, R.; Kruijff, M.; Kostopoulos, V.: Thermal modelling of ESA Second Young Engineers Satellite. –in Proc. of the 57th International Astronautical Congress (IAC). Valencia, Spain, 2006

Tsotra, P.; Kostopoulos, V.; Vavouliotis, A.; Kapappas, P.; Miaris, A.; Nikolaou, N.: On the use of Carbon NanoFibers for the preparation of antistatic epoxy-based nanocomposites Journal of Nanostructured Polymers and Nanocomposites, Vol. 2 (2006), pp. 61-65

Menon, C.; Kruijff, M.; Vavouliotis, A.; Miaris, A.; Kostopoulos V.; Angrilli, F; European Barberpole Mechanism for Space Tether Deployment. - in: Proc. of the AIAA, 56th International Astronautical Congress. Fukuoka, Japan, 2005